ULTRA HIGH QUALITY FACTOR MICROTOROIDAL OPTICAL RESONATORS IN LABEL - FREE BIOSENSING APPLICATIONS WITH HIGH SENSITIVITY AND SELECTIVITY

A DISSERTATION SUBMITTED TO

THE GRADUATE SCHOOL OF ENGINEERING AND SCIENCE

OF BILKENT UNIVERSITY

IN PARTIAL FULFILLMENT OF THE REQUIREMENTS FOR

THE DEGREE OF

DOCTOR OF PHILOSOPHY

IN

MATERIALS SCIENCE AND NANOTECHNOLOGY

By

Pelin TÖREN

November 2016

ULTRA HIGH QUALITY FACTOR MICROTOROIDAL OPTICAL RESONATORS in LABEL - FREE BIOSENSING APPLICATIONS with HIGH SENSITIVITY and SELECTIVITY
By Pelin TÖREN
November 2016

We certify that we have read this dissertation and that in our opinion it is fully adequate, in scope and in quality, as a dissertation for the degree of Doctor of Philosophy.

Bülend ORTAÇ(Advisor)

Mehmet BAYINDIR(Co-Advisor)

Mehmet Fatih DANIŞMAN

Hasan Tarık BAYTEKİN

Hakan ALTAN

Çağlar ELBÜKEN

Approved for the Graduate School of Engineering and Science:

Ezhan KARAŞAN
Director of the Graduate School

ABSTRACT

ULTRA HIGH QUALITY FACTOR MICROTOROIDAL OPTICAL RESONATORS IN LABEL - FREE BIOSENSING APPLICATIONS WITH HIGH SENSITIVITY AND SELECTIVITY

Pelin TÖREN
Ph.D. in Materials Science and Nanotechnology
Advisor: Bülend ORTAÇ
November 2016

Whispering - Gallery - Mode type microresonators provide great opportunities for label - free biosensing, allowing detections down to single - molecule levels. Microtoroids as optical resonators are quite sensitive and preferable biosensors due to their high quality factors. However, their surface design should be carefully considered for a selective biodetection. For this purpose, studies on WGM type biosensing for DNA, RNA and protein detections using various surface modifications are herein summarized. Over and above, this thesis mainly focuses on the microfabrication and surface modification of the microtoroids for various selective biosensing purposes such as antigen detection in complex media or detecting single base pair DNA alterations in buffer. With this regard, the developed microtoroid surface modification for dual characteristics (anti - fouling property and bioconjugability) is described in detail. The dual surface approach, used for selective Interleukin - 2 and Exotoxin - A detections in complex media, is applied to the microtoroids. Biosensing in complex media is a challeging task to perform unless the calibration approach is used. To overcome this challenge the suggested surface modification approach for nano - molar level detections is explained in detail. Besides, a novel surface modification approach for a selective single - stranded DNA detection based on discriminating single base pairs is portrayed as well.

Keywords: Optical Resonator, Microtoroid, Ultra - high Q, Whispering - Gallery - Mode, Label - free, Biosensing.

ÖZET

ÇOK YÜKSEK KALİTE FAKTÖRLÜ MİKROTOROİDAL OPTİK REZONATÖRLER İLE YÜKSEK HASSASİYET VE SEÇİCİLİKTE ETİKETSİZ BİYOLOJİK ALGILAMA UYGULAMALARI

Pelin TÖREN
Malzeme Bilimi ve Nanoteknoloji, Doktora
Tez Danışmanı: Bülend ORTAÇ
Kasım 2016

Fısıldayan Galeri Modu tipi mikro - rezonatörler, tek molekül seviyesine kadar tespit sağlayabilen etiketsiz biyoalgılamalar için büyük fırsatlar sunmaktadırlar. Optik rezonatör olarak mikrotoroidler, yüksek kalite faktörlerine sahip olmaları nedeniyle oldukça hassas olduklarından tercih edilen biyoalgılayıcılardır. Ancak; seçici bir biyoalgılama için mikrotoroid yüzey tasarımı dikkatle uygulanmalıdır. Bu amaçla, çeşitli yüzey modifikasyonları kullanılarak DNA, RNA ve protein algılamaları için bugüne kadar yapılan WGM tipi biyoalgılama çalışmaları özetlenmiştir. Ancak en önemlisi, bu tez esas olarak karmaşık ortam içinde antijen tespiti ve çözelti içinde tek baz DNA ayrımı gibi çeşitli seçici biyoalgılamalar için mikrotoroidlerin mikrofabrikasyonu ve yüzey modifikasyonu üzerine yoğunlaşmıştır. Bu bağlamda, ikili yüzey özelligi (protein direnci ve biyo - bağlama) için geliştirilmiş mikrotoroid yüzey modifikasyonu ayrıntılı olarak tarif edilmiştir. Geliştirilmiş bu ikili yüzey yaklaşımı, karmaşık ortam içinde İnterlökin - 2 ve Ekzotoksin - A moleküllerinin seçici tespiti için uygulanmıştır. Karmaşık ortam içinde biyoalgılama, kalibrasyon yaklaşımı kullanılmadığı sürece, zorlu bir görevdir. Bu zorlu görevi aşmak için, geliştirilen mikrotoroid yüzey yaklaşımının nano molar mertebedeki biyoalgılama uygulamaları detaylı olarak açıklanmıştır. Ayrıca, tek bir baz çifti değişikliklerine dayalı tek sarmal DNA molekülünün seçici tespiti için yeni bir mikrotoroid yüzey modifikasyonu yaklaşımı da gösterilmiştir.

Anahtar sözcükler: Optik Rezonatör, Mikrotoroid, Çok Yüksek Q, Fısıldayan Galeri Modu, Etiketsiz, Biyolojik Algılama.

Acknowledgement

I would like to present my acknowledgements to Prof. Mehmet Bayındır for his endless faith in my scientific potential, his supports in every step of my PhD studies and expanding my knowledge in materials science by meeting me with the optical resonators.

Secondly, I would like to acknowledge The Scientific and Technological Research Council of Turkey (TÜBİTAK) for supporting my PhD studies with "TÜBİTAK - 2211 Domestic Doctorate Fellowship Program" and also partly supporting my studies with Project No: 112T612.

I also would like to acknowledge Assist. Prof. Bülend Ortaç, Assist. Prof. Aykutlu Dâna, Assoc. Prof. Mehmet Fatih Danışman, Assist. Prof. Ali Kemal Okyay, Assoc. Prof. Gökçen Birlik Demirel and Prof. Osama Tobail for guiding scientific discussions on my PhD studies.

Most significantly, I would like to thank my dearest and precious parents: Canan Tören and Yakup Ergin Tören, who always be there whenever I crumble on the challenging life way to stand me up. My father, an extra - ordinary engineer and the smartest person I ever met, had been my first teacher in engineering, taught me the power of imagining and taught me how to not fear to carry out my wishes. My mother, a very clever and very beautiful lady, taught me the value of exertion and hard work in this life. Yet, most importantly, I would like to present my acknowledgements to my mother for giving me never - ending affection and being my mother in this life.

Besides, I would like to thank from the bottom of my heart to my dearest grandparents: Aysel Turan and Memduh Turan, both for being such a wonderful grandmother and grandfather, giving me limitless fondness, giving me unforgettable childhood memories and all the time supporting me during the PhD journey.

With all my heart, I also would like to thank my beloved, late grandparents: Sebahât Tören and Ali Tören for always loving me, always thinking of me and being proud of me.

Moreover, I am full of gratitude and thankful to my love: Dr. Ege Özgün, a remarkable physicist, a gifted, natural - born musician, a very talented writer, a very talented interpreter, an intelligent gentlemen and a wonderful person, for

coloring my life, loving me, always being my best supporter and always giving scientific guidance during my PhD studies.

Additionally, I would like to thank my dear friend: Emel Gürbüz, a smart, promising physicist and a lady with a golden heart, for giving me the chance to be her friend, showing me her kindness and supporting me. In addition, I would like to thank my colleague, Pınar Beyazkılıç, a naive lady, a brilliant chemical engineer and materials scientist, for her all supports. Withal, I owe a dept of gratitude to Dilara Öksüz Yeni, Ersin Hüseyinoğlu, Dr. Ozan Aktaş, Dr. Berna Şentürk, Berrin Şentürk and Ayşe Özhan for all their supports and friendship. Furthermore, I would like to thank two skilled UNAM coordinators: Neşe Özgür and Ayşegül Torun for all their kind helps during my PhD. Also, I would like to thank all Bayındır Research Group members for sharing nice memories.

Besides, I would like to thank my dearest cat: Leo, for being a well - behaved cat while I was writing my PhD thesis.

Lastly, I would like to thank all scientists around the world who work day and night to make prominent contributions to the sea of knowledge by giving hope to our universe.

Contents

List of Figures

List of Tables

Chapter 1

Introduction to Biosensing Using Microresonators

1.1 Optical Resonators Used in Biosensing

Biosensing covers all the analytical methods used to detect the presence of the biological entities within a media, and the interactions among them, using various equipments and methodologies. Besides its indispensable everyday applications, biosensing is also a prominent research field since there is a huge demand for label - free, ultra - sensitive, scaled down and robust biosensors in basic research, as well as food, environmental, biomedical, and pharmaceutical technologies. For this purpose, during the last decades, a significant number of methods with novel alternative strategies[1, 2, 3] have been suggested.

Biosensors are the analytical devices specialized for detection of a certain biological species. Similar to signal transduction pathways in cellular biology, biosensors consist of 2 basic parts: receptor and transducer. The receptor recognizes the target, while the transducer converts the receptor - target interaction into a measurable signal. In biosensors, several transduction mechanisms exist, which can be categorized under main titles including mechanical[4], acoustic[5], electrical[6]

and optical[7].

The optical sensors, among the most investigated biosensing tools, particularly provide opportunities for label - free, highly sensitive sensing capabilities with small working volumes, easy on - chip integrations, and fast and multiple read - outs. They are also quite suitable platforms for investigating light - matter interactions. Since such interactions can be mathematically described using 2 parameters, refractive index (n) and extinction coefficient (k), these parameters also define the characteristics of materials in terms of optical properties. Therefore, a considerable amount of research has been devoted to deciphering and engineering the optical characteristics of materials. One of the important branches, which sprouted out of optical engineering, is detecting the presence of various interactions between materials by exploiting the changes in the measured optical characteristics.[8] Among different applications of optical detectors, one of the most practical applications is biological sensing, where optics provides invaluable opportunities.[9]

Most biological entities and biological interactions occur within the nanometer scale. This makes their direct visualization impossible without causing them serious harm. Labelling biological samples with fluorophores is a limited solution with several issues to consider such as adverse interaction of the label with the sample and difficulty in real - time observation.[10] Therefore, label - free biosensors enabling detection of biological materials and their interactions are essential for a better comprehension of all biological phenomena. There are various methods for label - free biodetection[11, 12] all employing indirect methods for realizing their purpose. Electrochemical sensors[13], for instance, can measure a change in electrical impedance, conductivity or electric potential caused by the interaction of an analyte with the biosensor. The optical biosensors, on the other hand, provide this information by taking into account the changes in n and k using various strategies. Different types of biosensors possess distinct comparative advantages and deficiencies. These criteria directly influence their applicability over various biosensing issues. The most important characteristics determining the applicability of a biosensor are sensitivity, selectivity, dynamic range, robustness, and cost. These parameters are all intertwined, imposing strict

compromises among each other.

Optical biosensors, compared to their mainstream biochemical or electrochemical counterparts such as Enzyme - Linked Immunosorbent Assay (ELISA)[14] or blood glucose sensors[15], have a limited use in biosensing, particularly due to their generally complex operation and relatively higher performance and maintenance cost. On the other hand, there are certain potentials yet to be realized, motivating researchers to devote considerable effort in order to devise novel optical biosensors. The main reasons for pursuing optical sensors for the detection of biomolecular species and interactions are the possibility of ultimate, i.e. single entity, detection[16], the potential of fabrication from well - defined materials[17], and the maturity in methods for appropriate functionalization of particularly Si - based optical biodetection.[18]

Among various methods of optical biosensing, resonators of Whispering - Gallery - Mode (WGM) type solely have the potential for ultimate sensitivity.[16] The figure of merit of these WGM microresonators is the quality factor (Q - factor), which is the ratio of the total optical power accumulated within the microresonator to the power dissipated with various mechanisms such as absorption, scattering or coupling.[19] The higher the Q - factor of a microresonator, the sharper the resonant mode becomes due to the fact that the time each photon travels within the microresonator also increases while the circumference remains constant; thus, more strict measures apply for a photon to satisfy the resonance condition in terms of wavelength.[19] This positively affects the WGM biosensors in terms of sensitivity in 2 aspects, sharper resonances, which provide easier WGM shift tracking, and longer photon - analyte interaction times, thus increasing the efficiency. The latter one leads to one of the critical advantages of WGM biosensing, paving the way for single biological entity detection.[19] The only alternative to this strategy is reducing the mode volume, i.e. the volume in which light is confined drastically, such as in the case of plasmonic nanoparticles, where even alterations caused by single molecules become detectable.[20] Yet, compared to WGM biosensors, this is a relatively recent technology requiring a specialized set - up for dark - field imaging with high sensitivity. The WGM microresonators have been recently demonstrated to be even capable of single molecule detection

by exploiting the plasmonic enhancement.[21]

The WGM biosensors form a suitable platform for biodetection in which light interacts with the analyte in the vicinity of the microresonator. In order to perform biosensing, light must be coupled to the microcavity during its travel. The most efficient method for coupling light by satisfying resonance conditions and observing a shift in the tracked resonance mode simultaneously is using a tunable laser with a narrow linewidth. External cavity lasers[22] or distributed feedback lasers[23] are generally used for this purpose.

Current laser systems provide tunability with sub - picometer resolution. A significant part of biodetection using the WGM microresonators is the detection of the optical signal. On this side, blind photodetectors connected to a power-meter or directly to an oscilloscope could be effectively used.[24] The rest of the measurement is basically signal acquisition and processing, where an oscilloscope and a computer are required. A schematic description of the WGM biosensing is given in Figure 1.1.

WGM biosensors are mostly fabricated using standard micro - processing materials, i.e. Si and SiO_2, via various microfabrication techniques. For producing some of the types including microtoroids, a post - fabrication process is required, in which surface roughness is significantly decreased by thermal treatment, resulting in ultrahigh Q microresonators, where energy dissipation primarily occurs due to optical absorption of the material from which the resonator is produced. These microcavities are referred to as surface tension induced microcavities (STIMs).[26] They have quite low surface roughness values, reducing scattering losses virtually down to zero. On the other hand, it is extremely cumbersome, if not impossible, to provide a robust on - chip waveguide integration with the STIM microresonators, except for some rare examples.[27] The light is commonly coupled to the STIMs either via tapered fibers or via prism couplers. However, these light coupling approaches require precise alignment and are inconvenient to integrate with microfluidic systems, particularly for the tapered fiber coupling. Non - STIM microcavities, on the other hand, can be fabricated with on - chip waveguides. However, they have at least 2 orders of magnitude lower Q values, preventing

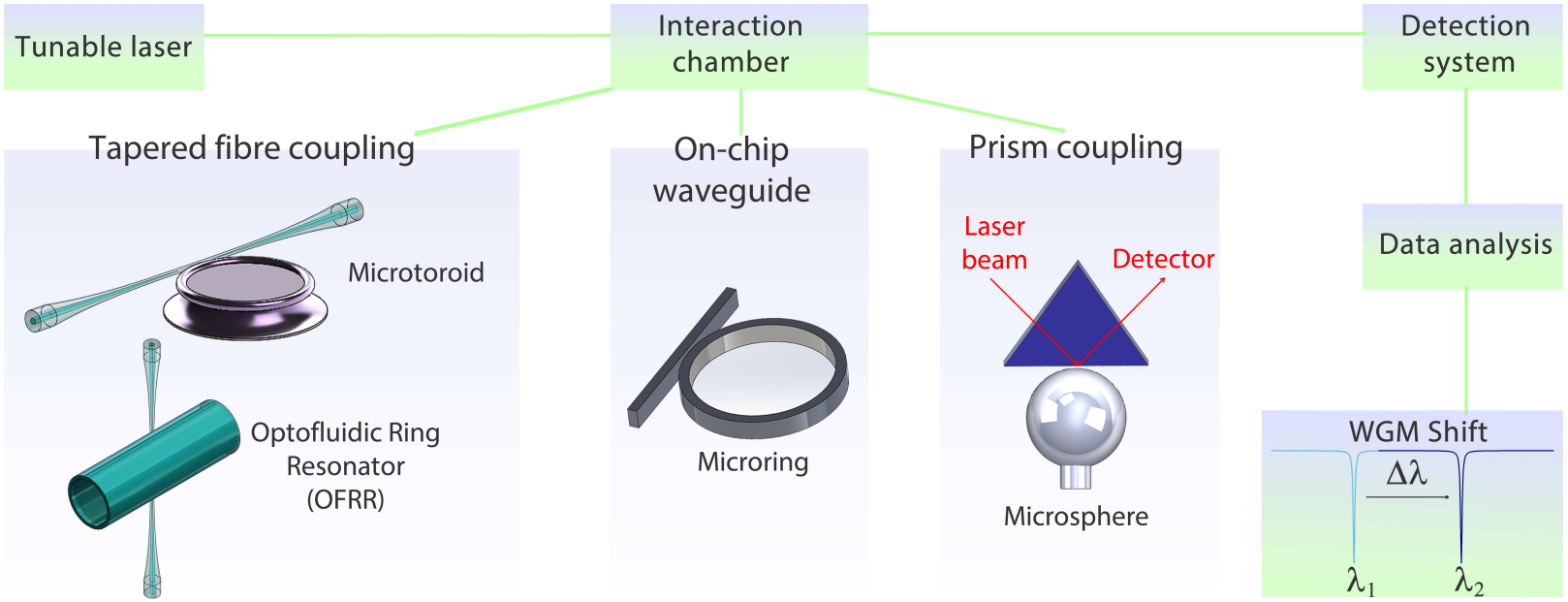

Figure 1.1: Schematic diagram summarizing the WGM based biosensing approaches using various optical resonators (microtoroids, optofluidic ring resonators (OFRRs), microrings and microspheres). Light incoming from a continuously sweeping laser source is coupled to an optical resonator via a tapered fiber, an on - chip waveguide or a prism coupler. The intensity of the transmitted light is traced using a detection system. The resonance wavelength shift (from λ_1 to λ_2) of the traced WGM is analyzed. The biosensing module, in which coupling and analyte infusion through the surface modified resonator occur, can be either a microfluidic or a flow system.[25]

their use in single molecule biodetection.[19] Nevertheless, the non - STIM microresonators, particularly microrings, are significantly advantageous especially in multiplexed detection because tens of microrings can be fabricated and utilized in a parallel manner, and this is unique to the microring resonators.

Biosensing heavily depends on the sensitive and selective target detection capability of the biosensor. For this issue, the approach used in surface modification for conjugating probe molecules is crucial. In order to perform feasible biosensing, the surface of the biosensor should be engineered elaborately. Entities for molecular recognition, which are generally referred to as probe molecules, are a must for biodetection. The first prerequisite of the surface modification is covalent or non - covalent attachment of the probe molecules onto the biosensor surface. However, many parameters should be individually considered besides probe conjugation for an enhanced sensitive and selective biodetection. The approach used in probe conjugation can be considered adequate for a reliable biosensing to some extent; however, for most cases, additional surface chemistry is required, especially for biosensing in a complex medium.[24] A myriad of different strategies exist for biosensor surface modification, where different problems demand different solutions.[18] Yet, some of these solutions are inevitably more effective than those of their counterparts in terms of efficiency and reliability. Here, it is important to mention that silane - based surface modification is dominant in optical biosensors, since silane molecules enable covalent attachment on Si / SiO_2 - based surfaces, which constitute the vast majority of the WGM biosensors. On the surface of a WGM biosensor, various functional groups can be obtained using silane chemistry. Each functional group provides a distinct characteristic to the biosensing system.

Biomolecular interactions (such as antibody antigen) occur within an aqueous medium. This fact compromises the use of the WGM type of microcavities regarding several aspects. The first issue that needs to be considered is the wavelength to be used. Although the optimum wavelengths in SiO_2 structures are 1310 and 1550 nm, which are also referred to as telecommunication wavelengths for the minimum loss of SiO_2, at these wavelengths there is considerable water absorption.[28] Therefore, visible and near - infrared wavelengths, such as 670 nm, are shown to

be more effective in optical biosensing.[28] Also, another important concern is optical coupling in aqueous media. Especially, tapered fiber coupling suffers heavily from mechanical perturbations occurring within the environment[29], particularly by the presence of a fluid flow.

This thesis includes different biosensing strategies used to detect antigens in complex media and single DNA base pair alterations in a buffer solution, performed using microtoroids as the WGM type optical resonators.

1.2 Deoxyribonucleic Acid (DNA) Detection Using Optical Resonators

1.2.1 DNA Amplification and Detecting Genetic Alterations

Polymerase Chain Reaction (PCR)[30] is the most commonly used nucleic acid amplification technique. However, recombinase polymerase amplification (RPA) is an alternative method to the PCR, which enables DNA amplifications at a low and constant temperature ($\sim 37\,^{\circ}\mathrm{C}$)[31, 32] contrariwise to the PCR. This isothermal method provides enzyme - oriented synthesis[33] of the DNA molecules. Also, undesired side products of the PCR, such as primer dimers, can be reduced by using the RPA technique.[34] In a consecutive manner, the RPA process is performed by three enzymes: recombinase, ss - DNA[1] binding protein and polymerase. The recombinase forms a complex in between a template ds - DNA[2] and its opposing primer parts and expedites the strand exchange at cognate sites. Stabilization of the structures is done by the ss - DNA binding proteins which prevent branch migration.[31] Lastly, DNA elongation is performed by the strand displacing polymerase to end the RPA process.

[1]Single stranded DNA.
[2]Double stranded DNA.

Combining the RPA technique in the solid - phase with an optical microresonator having a biosensor array is an emerging field, which enables real - time and specific DNA detection by providing rapid DNA amplification in a small working volume. For this purpose, J. S. del Rio and co - workers[35] developed a biosensor platform consisting of arrays of label - free microrings to perform solid - phase RPA (SP - RPA) of the DNA molecules. To functionalize the surface, covalent conjugation of hexynyl terminated ss - DNA probes to ABCR modified microrings was achieved via a click chemistry reaction. Detection of pathogen *Francisella tularensis* related ds - DNA was done with the microrings having *F. tularensis* forward primers. Withal, the method suggested a rapid DNA amplification time (40 mins) with a low limit - of - detection (LOD) (2 fg.μl^{-1}) level while the LODs in the standard RPA and the conventional / real - time PCR techniques were reported in the order of pg.μl^{-1} levels.[34, 35]

Y. Shin and co - workers[34] suggested a label - free, multiplexed DNA amplification platform with faster times (20 - 30 mins) as compared to the above study. In order to detect single point mutations in the *Harvey RAS* (*HRAS*) gene, they fabricated an isothermal solid - phase amplification / detection (ISAD) device consisting of APTES / GAD chemistry applied microrings. The LOD was reported as 500 fg.μl^{-1} for this study.

1.2.2 Detecting Methylated DNA and its Oxidized Derivative

DNA methylation is an epigenetic modification which results in a 5 - methylcytosine (5mC) molecule via covalent modification of the 5^{th} carbon in the DNA base cytosine.[36] The DNA methylation can be presented in $\mathcal{C}$G, $\mathcal{C}$HG and $\mathcal{C}$HH sequences where H can be A, T or $\mathcal{C}$.[37]

Without any sequence change, via a chemical modification, DNA methylation can alter the function of the DNA molecule. For instance, it has been revealed that DNA methylation plays essential roles in various cellular processes[38] such

as development and regulation in gene expression (i.e., gene silencing in eukaryotic cells).[37, 39, 40, 41, 42] Expectedly, abnormal methylation processes occurring in the chemical structure of the DNA molecule have a relationship with numerous diseases.[39, 43] Recent studies have also shown that oxidation of the 5mCs by enzymes like human ten - eleven translocation 1 ($TET1$)[44]leads to 5mC derivatives such as 5 - hydroxymethylcytosine (5hmC) which was first found in mammalian genomic DNA[45] in 1972.[46] Like the 5mCs, the 5hmCs are also known to be involved in embryonic development as well as many diseases.[42]

Bisulfite sequencing is the most widely used method for analyzing DNA methylation by converting non - methylated cytosines to uracils selectively while keeping methylated cytosines unchanged.[47, 48, 49] Among techniques based on bisulfite conversion for methylated DNA detection, methylation specific (MS) PCR[50] is the most commonly used method.[51] Despite the fact that MS PCR is widely used, alternative detection techniques have also been suggested due to the complexity and long analysis time of the MS PCR.[47, 51] For instance, Y. Shin and co - workers[52] showed the detection of some DNA methylation biomarkers since their included DNA methylation patterns are well known in human diseases. Microring arrays, each containing 4 rings (3 measurement rings and 1 reference ring to control thermal drifts), were fabricated for this purpose. Probes having either methylated cytosine or unmethylated thymine were covalently conjugated to APTES / GAD chemistry applied microrings. Using the surface modified microresonators provided real - time analysis and discrimination of methylated and unmethylated DNA targets following the bisulfite conversion of the targets. However, as the authors also indicated, for such an approach, a compact biosensor chip having microfluidic channels and sequential process steps were required to reduce the process time.

Later on, J. Yoon and co - workers[51] suggested a practical on - chip platform to analyze the methylation status of DNA in real - time based on the former approach.[52] The methylation status of DNA, obtained from an epithelial cell line ($RAR\beta$ 93,95 gene as a common human DNA methylation biomarker), was detected by methyl - specific or unmethyl - specific primers conjugated to biosensor chips following the bisulfite conversion of the DNA targets. The suggested

idea provided amplification of the methylated DNA strands and specific detection down to 0 % in terms of target concentration in a mixture containing methylated and unmethylated DNA strands.

As a similar approach to the former work[51], T. Y. Lee and co - workers[47] developed a flexible and on - chip biosensing platform for detection of the methylation status of the $RAR\beta$[53, 54, 55] or $HAAO$ (3 - hydroxyanthranilate - 3, 4 - dioxygenase)[56] genes as other biomarkers within 65 mins. In this work, instead of the bisulfite conversion methylation specific endonuclease digestion[230] was used. Additionally, the fabricated biosensor chip consisted of 2 parts: a modification module in which cleavage of the appropriate sequence sites ($\mathcal{CC}$GG) by the enzymes occurred, and a detection module to understand the methylation status of the targets.

In order to detect the oxidized derivative (5hmC) of the 5mC molecule, R. M. Hawk and co - workers[57] used microtoroids for selective detection of 5mC and 5hmC molecules. In this regard, the anti - 5hmCs were covalently conjugated to a GPTMS - coated microtoroid. The measurements were taken in a sample chamber having a microtoroid and a tapered SiO_2 fiber (765 nm) in 100 μl of PBS as the measurement solution. The LOD for this study was reported as 4.2 x 10^{-13} M with a detection of the 5hmC signal, which was twice that of the 5mC signal.

Furthermore, the OFRRs are also functional platforms for the DNA methylation analyses because they provide fluidic integrations. J. D. Suter and co - workers[58] used methyl binding protein (MBD - 2) and 5 - methylcytidine antibody as probe molecules to detect artificially methylated ss - DNA and ds - DNA molecules by the OFRRs coupled to tapered fibers (1550 nm). Either the MBD- 2 or the anti - 5 - methylcytidine probes was covalently conjugated to a 3 - APS coated inner biosensor surface via DNA as a bifunctional linker. The suggested system was able to discriminate methylated and unmethylated DNA strands. They also reported strong binding affinities of ds - DNA and ss - DNA to the MBD - 2 and the 5 - methylcytidine antibody, respectively.

1.3 Ribonucleic Acid (RNA) Detection Using Optical Resonators

1.3.1 Multiplexed MicroRNA (miRNA) Detection and Quantification

miRNA, which is a small RNA molecule (containing 19 - 24 nucleotides[59]) that does not encode proteins,[60] had been first identified as *lin* - 4[61]in 1993. However, the function of the miRNAs as regulators was discovered in the early 2000s.[62, 63, 64] These tiny RNA molecules, since then, have been known to possess transcriptional and post - transcriptional roles in gene expression.[65] The discovery of the regulatory function of the miRNAs has led the way to gathering further knowledge on their roles in biological processes. For instance, miRNAs are known to play profound roles in cellular processes (such as proliferation[66], apoptosis[67] and development[68]). Additionally, they also take part in various diseases such as diabetes[69], and cardiovascular[70], autoimmune[71] and neurodegenerative[72] diseases. Thus, they are excellent biomarkers for the early detection, diagnosis and prognosis of a disease. Increased or decreased levels of miRNAs in cells can be indicators of many diseases.[73] Conventional techniques for miRNA detection can be listed as cloning[74], Northern blotting[75], reverse transcription polymerase chain reaction (RT - PCR)[76] and microarray[76, 77] analyses. However, many of these techniques require a large amount of samples46 and suffer from complexities.[77, 78]F. Porichis and co - workers[79] demonstrated miRNA detection using fluorescence in situ hybridisation (FISH) technique combined with flow cytometry. Recently, among label - free techniques[80], electrical detection techniques[81] based on detecting a change in current due to hybridization between miRNA and probe, and optical detection techniques[81] (label, label - free, spectroscopy and refractive index based) have been suggested to increase the sensitivity of the miRNA detection.

Among optical techniques, the detection of miRNAs using on - chip integrated microring optical resonators provides rapid, robust and multiplexed detections[82]

with considerably high miRNA sensitivities. There are 2 noteworthy examples[59, 78] of miRNA detection which used microring optical resonators. A. J. Qavi and R. C. Bailey[59] reported a multiplexed miRNA detection platform using Si photonic microring resonators. For this purpose, they fabricated sensor chips each containing 32 individual microrings including reference microrings having 30 μm diameter with its adjacent linear waveguide. This biosensing platform possessing multiple microrings with several unmodified microrings, which serve as references, is quite advantageous in terms of data corrections for undesired non - specific interactions and shifts due to thermal and instrumental fluctuations.

For surface modification, the sensor chips were exposed to S - HyNic solution following APTES solution. ss - DNA probes (22 - mer nucleotides), which reacted with the S - 4FB heterobifunctional crosslinker previously, were conjugated covalently to the modified sensor chip surface. A tunable laser, centred at 1560 nm, was coupled to the linear, on - chip waveguides and a resonance wavelength was tracked. Target miRNA infusions to the sensor chips were performed in microfluidic flow channels. 4 sets of microrings were functionalized with 4 different fully complementary ss - DNA probes, individually. Each modified microring showed a dramatic response to its corresponding target miRNA during the sequential introduction miRNA targets ($miR-133b$, $miR-21$, $miR-24-1$ and $let-7c$) through the microfluidic system. In this study, a detection limit of 150 fmol of miRNA was reported and the suggested biosensing mechanism provided a multiplexed quantification of the 4 aforementioned miRNAs. Moreover, an isothermal method was suggested to discriminate single base differences by performing hybridization in 50 v/v % formamide solution. Since detecting single base pair variations in an oligonucleotide is a challenging task, the demonstrated miRNA biosensing platform suggests a highly sensitive and selective miRNA detection approach.

Another example of the multiplexed detection of miRNA is the other work of A. J. Qavi and co - workers[78]. They fabricated sensor substrates each containing 32 addressable microring resonators in the same manner as that in the previous works[59, 78, 82] and S - 4FB modified ss - DNA probes (22 - mer nucleotides) were covalently conjugated to Hy - Nic silane coated sensor substrates. An external

cavity laser was used to trace the resonance wavelength. They fabricated laser etched microfluidic channels for analyte infusion. Subsequently, antibody S9.6 (anti - DNA) was harvested from a mouse hybridoma cell line that was able to recognize the formed DNA - RNA heteroduplexes on the surface and was introduced to the system following blocking of the microring surface to avoid non - specific interactions. Since anti - DNA binding response was higher than that of the bound miRNAs to the surface, the system provided an enhanced miRNA detection limit down to 350 amol (10 pM), which is lower than the detection limit reported in the previous study.[59] In order to investigate antibody (S9.6) binding kinetics, antibody solutions having the same concentration (2 μg.ml^{-1} were infused to the microrings with varied capture probe densities following the miRNA infusions at the same concentration (40 nM). The elicited response due to antibody binding increased as the surface probe density increased. On the other hand, as the authors also indicated, after a certain surface probe density this increasing behaviour was not observed since possibly occurring steric effects due to probe crowding on the resonator surface resulted in a decrease in the antibody - binding rate. The study demonstrated a simple miRNA sensing platform, which enabled real - time and multiple read - out measurements.

1.3.2 Messenger RNA (mRNA) Detection

mRNA is a single - stranded RNA intermediate (between 500 and 10,000 bases), which possesses the complementary sequence of a DNA strand for representing a protein during the transcription process.[83] Studies have revealed a relationship between some mRNA expression levels (or mRNA abundance) and diseases[84], Hence, as one of the transcriptomic biomarkers, detection of the mRNA molecules is quite critical for the diagnosis, treatment and determination of the stage of different types of diseases.[85, 86, 87, 88]

So far, bulk mRNA detection has commonly been done via microarray[89, 90] and real - time RT - PCR[91, 92] analyses. Also, a label - free cantilever - array sensor[93] was suggested as an mRNA detection platform. However, to detect

cell - to - cell mRNA variations[94] which can be observed in heterogeneous diseases, nanoflares[95] and core - shell nanocomposites[87] were used rather than the aforementioned bulk mRNA detection techniques, which were reported to be incapable of detecting the alterations.[87, 95] In fixed or living cells, the mRNA levels were obtained using molecular beacons.[96, 97] Withal, imaging of individual mRNA molecules in fixed cells was achieved using labeled probes.[98] In another study[79], at the single cell level mRNA detection, the FISH technique combined with flow cytometry was used. Also, electrochemical - based biodetection techniques[99, 100, 101, 102] can be used for the mRNA detection.

Several optical biodetection[103, 104] techniques can provide rapid and label - free quantification of the mRNA molecules. As an optical detection technique, J. T. Kindt and co - workers[105] suggested Si photonic microrings as optical microresonators for full - length mRNA quantification in a multiplexed manner with a 512 amol limit of mRNA detection. The S - 4FB modified ss - DNAs as probe molecules were tethered to the microring surface covalently. Also, the resonance wavelength shift was enhanced by adding short DNA chaperones and submicrometer beads, which improve hybridization kinetics between the ssDNA probes and the target mRNA molecules.

1.3.3 Transfer Messenger RNA (tmRNA) Detection

tmRNA, which is a small molecule encoded by the *ssrA* gene[106] but is different from transfer RNA (tRNA) and ribosomal RNA (rRNA), was discovered in 1978[107] as a new RNA component. This stable RNA piece can be found in many bacteria with a high copy number per cell, *Escherichia coli* being the most common example.[108] In all eubacteria and some eukaryotic organelles, tmRNAs play critical roles in translational surveillance and ribosome rescue to maintain the protein synthesis capacity of a cell.[109] The tmRNAs can be used as biomarkers in order to differentiate between bacterial species and genus, since each bacterial strain is known to contain unique regions of sequence.[110] Additionally, viable bacterial populations can be distinguished from non - viable ones

using these biomarkers.[111]

Thus far, the tmRNA molecules were used as targets in conventional techniques for several detection purposes such as bacterial identification[110] or observing tmRNA localization in bacteria[112] via fluorescence *in situ* hybridization technique and for pathogen detection using techniques based on nucleic acid sequence - based amplification[113], real - time PCR[106], real - time RT - PCR[114] or surface plasmon resonance.165

Using photonic microcavities for tmRNA detection, O. Scheler and co - workers[115] discriminated the tmRNAs for different bacterial species. For this purpose, they fabricated chips having 32 individually addressed microrings integrated with a microfluidic assembly. An aryl aldehyde moiety having probes related to either *Streptococcus pneumoniae* or *Streptococcus agalactiae* bacteria was covalently conjugated to a reactive hydrazine group having microrings via hydrazone bonding. The fragmented tmRNA molecules were specifically detected via hybridization with their probe DNA counterparts. However, in this technique, the detection of the tmRNA molecules required a preprocessing of the tmRNA samples via thermal tmRNA denaturation with / without a 10 - fold excess of chaperones or by chemical tmRNA fragmentation, by which the secondary structures of the tmRNA molecules are disrupted. The LOD obtained for this study was reported as 53 fmol *S. pneumoniae* tmRNA, which corresponds to approximately 3.16 x 10^7 CFU[3] of bacteria. Although the suggested approach provided rapid and specific detections of different tmRNA species, as the authors also adverted to, the results showed a difference in terms of the WGM shift magnitudes, which was possibly observed due to undesired residual secondary structures of the tmRNA targets following the pre - process.

[3]Colony forming units.

1.4 Aptamer Based Protein Detection Using Optical Resonators

The use of aptamers instead of antibodies is a recent approach in optical microresonator - based biosensing. The aptamers specifically recognize molecular patterns with high affinity. The main difference of the aptamers from protein based antibodies is that they consist of nucleotides rather than amino acid chains, and they are synthesized artificially instead of being produced within living organisms.[116] Although they have more simple primary structures, i.e. smaller dimensions in terms of length and molecular weight[117], the aptamers have successfully been demonstrated to have considerable affinity towards their targets, which are mostly proteins. Besides, they are more stable than their protein counterparts in terms of alterations in their environment and shelf life.[118] Their attachment to a Si / SiO_2 surface is practically the same as in the oligonucleotide attachment strategies, which are well known and relatively easier than covalent binding of the antibodies.

All the aforementioned factors make aptamers convenient for probing biological entities. Yet, their use in optical microresonator - based biodetection is not abundant. Although being quite promising, there are only a handful of examples regarding their use in this field. The rare use of the aptamers in optical microresonator - based biosensing is likely due to the possible difficulties encountered during the optical measurements rather than the aptamers themselves.

1.5 Peptide - Nucleic Acid (PNA) Based Protein Detection Using Optical Resonators

The PNAs are artificially synthesized oligomers of peptides which have backbones analogous to the ones that nucleic acids have.[119] The PNAs are more resilient than the DNA probes towards degradation by enzymes, and they can be modified

in order to capture DNA strands with high specificity and affinity.

In a recent work of G. A. Rodriguez and co - workers[118], interaction between the PNAs and the DNAs was exploited using porous Si (PSi) ring resonators in the biosensing applications. The PSi ring resonators enable a larger area of interaction for the target molecules with the sensor surface compared to the surface area limited detection using other types of sensors. The Psi structure was obtained via controlled electrochemical etching of Si and a refractive index alteration was created by partial thermal oxidation.

The whole surface of the PSi ring resonator was modified with APTES molecules and SPDP was used as a crosslinker to conjugate DNA probes for capturing target PNAs. The probe DNA attachment to the SPDP - modified ring resonator surface caused a significant WGM shift due to the high probe concentration used. In addition, target PNAs hybridized with the probe DNAs led to an observable WGM shift of 11.10 nm.

Moreover, the Q - factor of the fabricated PSi ring resonators in the buffer was reported to have an order of magnitude of 10^4 while it was one order of magnitude higher in air. This is partially related to the wavelength of the laser ($\sim$ 1550 nm) used in this work, at which water absorption[28] in aqueous media cannot be neglected. Still, the authors reported that the sensitivity for PNA was 3 nM as calculated by 3σ analysis, while directly measured lower concentration was reported as 42 nM. Overall, the authors suggested that the sensitivity of the PSi microrings could be engineered to be higher than that of the conventional Si microrings.

Chapter 2

Microfabrication Process of the Optical Resonators

The microtoroid production can be divided into 2 main steps. At first step, SiO_2 microdiks standing on Si pillars are fabricated in clean - room using a UV nanoimprint lithography device (EVG 620, EVG, Germany). For this purpose, Si wafers having thermal oxide SiO_2 (University wafers, USA) are used. At second step, the fabricated microdics are reflowed with a CO_2 (Diamond C - 55A, Coherent Inc., USA) laser to form microtoroids.

2.1 Fabrication of Microdisks

In order to fabricate microdisks, double side polished <100> SiO_2 on Si wafers (2 μm thermal oxide SiO_2, University wafers, USA) were used.

The microdisk fabrication process can be summarized in the following steps:

- The main wafer is diced into pieces using an automatic dicing saw.
- The wafer piece is cleaned.

- Then, the wafer is coated with a UV positive photoresist using a spin coater.
- The photolithograhy is applied to form microdisk shapes.
- The SiO_2 layer is chemically etched using a Buffered Oxide Etch (BOE) solution.
- The mikrodisk sets are diced into individual mikrodisk batches.
- Following the dicing, the Si layer is etched via plasma etching method to form Si layers.
- The residual photoresist layer is removed using acetone.

Using the automatic dicing saw (DAD3220, Disco Corporation, Japan), the 2 μm SiO_2 having Si wafer was diced into 20 x 20 mm pieces. Following the dicing, the wafer pieces were cleaned with acetone (semiconductor grade) and isopropyl alcohol (IPA, semiconductor grade) for 10 mins, respectively. Then, the wafer pieces were washed thoroughly with distilled (DI) - H_2O. The washed pieces were dried under a N_2 gun and kept at 120 °C for 1 min, respectively.

Subsequently, the wafer is coated with HMDS to enhance adhesion, using a spin coater (WS650SZ - 6NPP - lite, Laurell Technologies, USA). Following the HMDS coating, the wafer is coated with a UV positive photoresist, AZ 4533 (MicroChemicals GmbH, Germany). The coating process parameters were kept the same for both HMDS and AZ 4533 coating: 4000 rpm speed, 2000 rpm acceleration with a duration of 45 secs. Then, the photoresist coated wafer was baked at 110 °C for 50 secs. The wafer coating steps are shown in Figure 2.1.[1]

The photolithography (200 μm working distance and 85 mJ.cm^{-2} dose rate) was applied to the UV positive photoresist coated wafer using a custom - made mask having Cr microdisk shapes, to form microdisks on the wafer. Following the photolithography, the residual weak photoresist which exposed to the UV light, was removed using a developer, AZ 400K (MicroChemicals GmbH, Germany)

[1]The illustration was done by Ersin Hüseyinoğlu (UNAM - National Nanotechnology Research Center, Bilkent University).

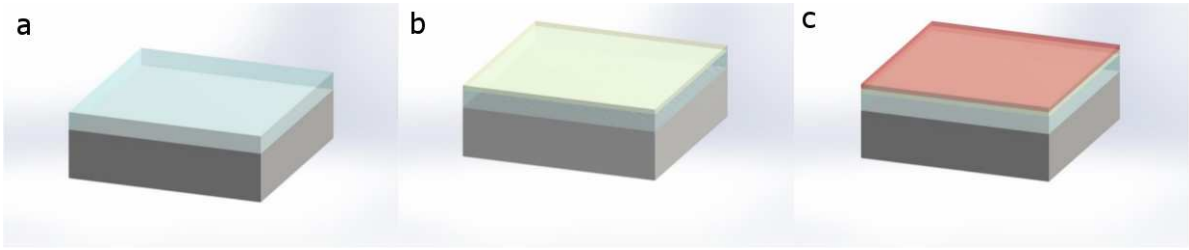

Figure 2.1: Photoresist coating on (a) a thermal oxide (blue layer) having Si wafer (gray layer). Sequential (b) HMDS (yellow layer) and (c) AZ 4533 (red layer) coating of the wafer.

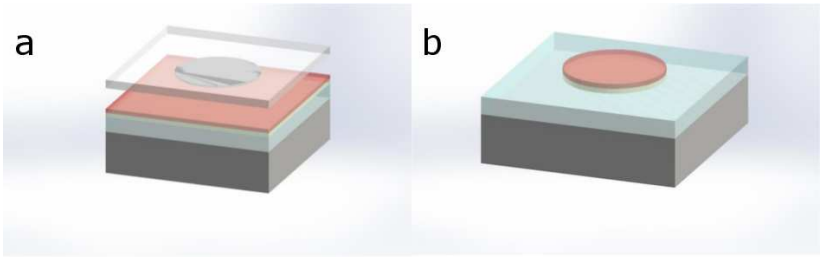

Figure 2.2: (a)A Cr mikrodisk written on the photomask (transparent layer) during the photolithography process and (b) the imprinted mikrodisk shape after the process on the wafer.

solution (25 v/v %[2] AZ 400K in DI - H_2O) for $\sim$ 20 secs. Then, the wafer was washed thoroughly with DI - H_2O and dried under the N_2 gun in succession. At the end of this step, the microdisk imprinted wafer was obtained (schematically given in Figure 2.2[3]). Also, the optical microscope (100 X, Zeiss, Germany) image of the formed microdisks is shown in Figure 2.3.

In order to form SiO_2 microdiks, following the photolithography, the wet etching[4] was done using the BOE solution (MicroChemicals GmbH, Germany)[5]. The SiO_2 layer was chemically etched until reaching the Si layer by the BOE solution for $\sim$ 35 mins. After 35 mins, the wafer was placed into a DI - H_2O having beaker to end the etching process. Then, the wafer was again washed thoroughly with DI - H_2O and dried under the N_2 gun in succession.

[2]volume / volume percent.

[3]The illustration was done by Ersin Hüseyinoğlu (UNAM - National Nanotechnology Research Center, Bilkent University).

[4]During this process, the area under the photoresist is protected to be chemically etched.

[5]Buffered Oxide Etch. 7:1 v/v NH_4F : HF.

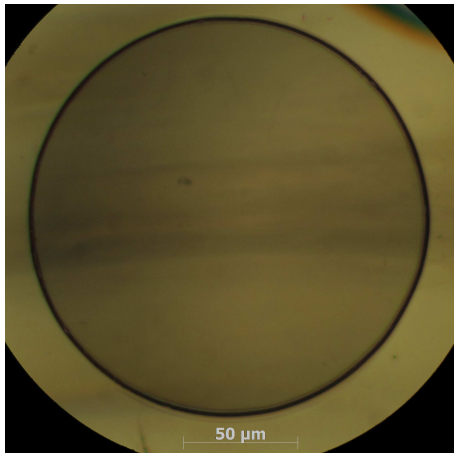

Figure 2.3: An optical microscope image of a fabricated microdisk.

Using the automatic dicing saw, the wafer was cut into strips to obtain batches. Then, the small pieces were washed thoroughly with DI - H_2O and dried under the N_2 gun to remove dust particles.

In order to form Si pillar, the dry etching was done via isotropic SF_6 etching using an inductively coupled plasma device (LPX SR (CI), SPTS Technologies, USA). After forming the Si pillars, the residual photoresist layer was removed using acetone (semiconductor grade) for 15 mins. Then, the batch was washed thoroughly with DI - H_2O and dried under the N_2 gun in succession. The schematic drawing shows the dry etching process forming the Si pillars. Additionally, an Scanning Electron Microscopy (SEM) image of a fabricated microdisk is shown in Figure 2.4.

2.2 Fabrication of Microtoroids

A CO_2 laser (Continuous - wave, Diamond C - 55A, Coherent Inc., USA) which was focused with a ZnSe plano - convex lens (∅ 2.54 cm, f = 25.4 mm) was used to reflow the formed microdisks. For this purpose, the batch was inserted onto a stage and the CO_2 laser ($\sim$ 20 W) was focused onto the microdisk being reflowed, via a optical path. Additionally, a He - Ne (632.8 nm, Thorlabs, USA) laser was

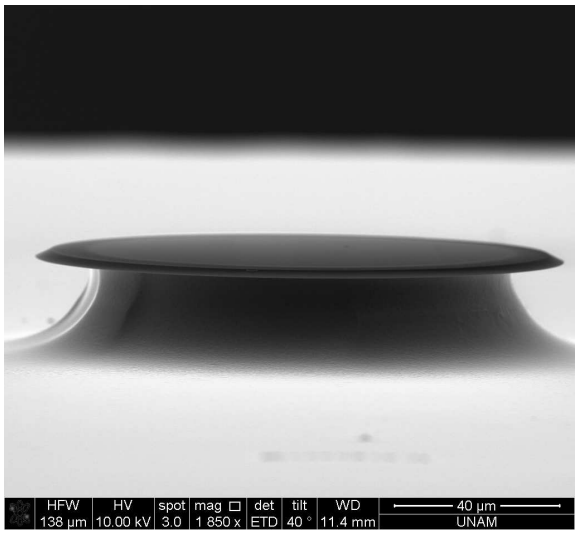

Figure 2.4: An SEM image of a fabricated microdisk.

Figure 2.5: The photograph of the microdisk reflow set - up. (1) Sample holder, (2) Charge - Coupled Device camera, (3) ZnSe lens, (4) Flip mirror, (5) CO_2 laser and (6) He - Ne laser.

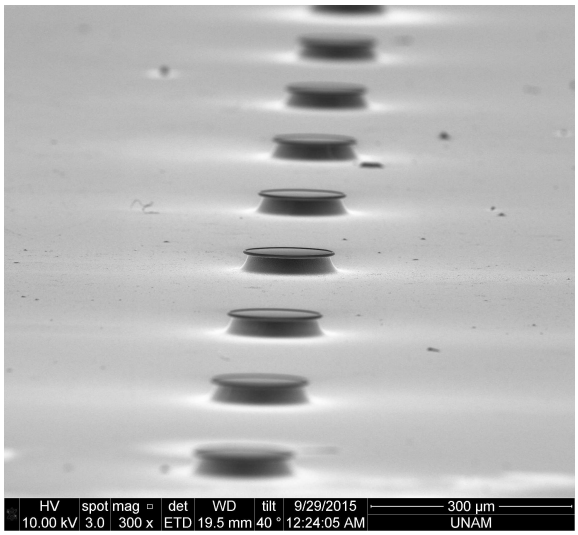

Figure 2.6: An SEM image of fabricated microtoroids in arrays as a single batch.

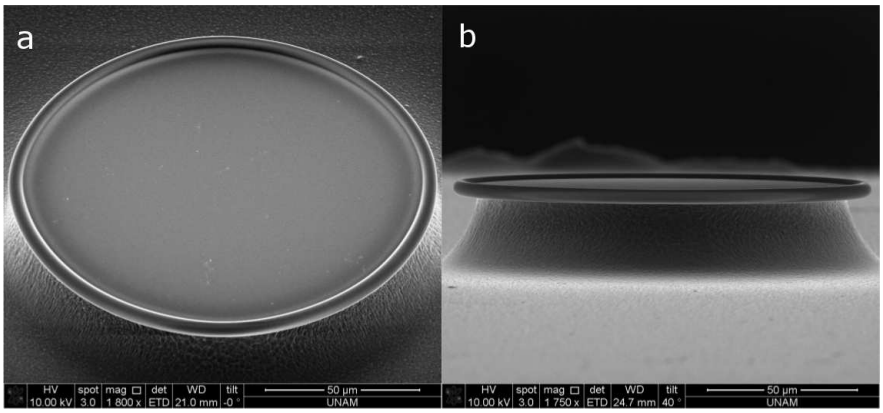

Figure 2.7: The SEM images of a fabricated microtoroid from (a) top and (b) side views.

used to align the optical components.[6] The photograph of the reflow set - up is shown in Figure 2.5.

The optical phonons in SiO_2 are absorbed at a wavelength of $\lambda = 10.6$ μm at which the CO_2 laser emission occurs.[121] While the SiO_2 region reaches to substantially high temperatures under the CO_2 laser beam, the Si pillar serves as a platform where the heat is simultaneously removed. Thus, the SiO_2 region, which is in the vicinity the Si pillars remains unaffected while the edges of the

[6]It is important here to note that the alignment of the CO_2 laser beam directly affects shape of the microtoroids. Thus, the alignment should be done carefully before the reflow process.

microdisk is being reflowed.

After the reflow process, the microtoroids having a diameter of ~ 110 μm were obtained. The SEM image of the fabricated microtoroids, as in arrays on a chip, was shown in Figure 2.6. Also, the SEM images of an individual microtoroid from the array were provided (top view) (Figure 2.7a) and (side view) (Figure 2.7b).

Chapter 3

Biosensing via Whispering - Gallery - Modes (WGMs)

3.1 Understanding The WGMs

The WGMs were first observed as sound waves by Lord Rayleigh in St. Paul's Cathedral, London in 1878.[122] The phenomena was observed over the curved surface by hearing a whisper against the surface while not hearing it at the center of the cathedral. In other terms, a circular structure, which allows sound waves to travel at certain frequencies through the inner circumference. Later on, a similar phenomenon was discovered in micro - optical structures, in which the light waves travel through a circular path due to total internal reflection.[16] An analogous phenomenon in optical systems also occurs when an electromagnetic wave couples to a resonator and travels through a path, covering the periphery of the resonator, due to total internal reflection. Within this context, those are referred as the WGMs of the resonator.

Label - free detection of the biological species is an analytical method providing fast and reliable qualitative and quantitative information regarding the composition of the analyte, and comprehension of interaction among the

biomolecules.[10, 11, 12] Among various label - free biodetection techniques such as surface plasmon resonance (SPR)[123] and quartz crystal microbalance[124], optical microresonators of the WGM type, where light is confined in a circular path inside the periphery of the resonator by means of continuous total internal reflection[17], particularly possess outstanding potentials by virtue of their extreme sensitivity towards the alterations of the refractive index of the media they reside within.[19] Light can be evanescently coupled to these optical microcavities using tapered optical fibers as resonant modes[125], which can be tracked by continuously scanning the wavelength of a tuneable laser around the resonant wavelength and observed as Lorentzian shaped dips in the transmission spectrum of the tapered fibre.[126, 127] The linewidth of the resonant mode is inversely proportional to the Q - factor of the microresonator, representing its ability of storing optical power[128]. Especially surface tension induced microcavities, which surface roughness, one of the main sources of optical losses due to scattering from the surface, is diminished by a thermal treatment causing the melting and reflowing of the material constituting the microresonator[28], such as microspheres[129] and microtoroids[26], have extremely narrow resonance linewidths. This enables detection of even single adsorption events causing shifts in the resonance wavelength[23]. There are several important examples of microresonator optical biosensors based on the WGM shift principle for detection of particular biological species such as DNA[130], viruses[131], and proteins[132].

The WGMs are observed when the resonance condition is satisfied. In such structures, the resonant modes exist only at discrete multiples of wavelengths which are determined by the length of the resonators.[133] When an analyte is adsorbed on the microresonator surface, the path length of the light inside the microresonator is altered, causing a shift in the resonant wavelength, which is tracked for sensing and quantifying biological species.[134] The approximate resonance condition can be expressed by,

$$2\pi r n_{eff} = l\lambda \tag{3.1}$$

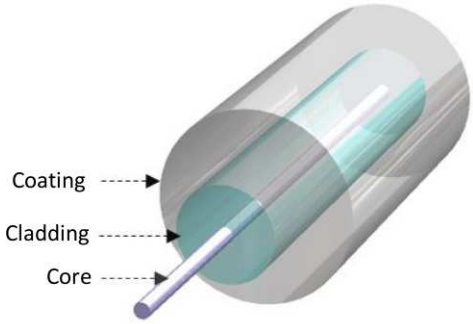

Figure 3.1: The schematic drawing of the SMF - 28® fiber with its core, cladding and coating.

where r, n_{eff}, λ and l are the major radius of the microtoroid, effective refractive index, wavelength of the electromagnetic field in vacuum and an integer, respectively. Any change in the n_{eff} is accompanied by a WGM shift, thanks to which, the microresonators can be used as sensors.

3.2 The Fiber Tapering Process

As the waveguide, a tapered SMF - 28® type optical fiber was used during all studies. As shown in Figure 3.1, there is the SiO_2 fiber core (8 μm in diameter) in a cylindrical sleeve (SiO_2 cladding) having 125 μm in diameter. The cladding is covered by the polymer coating to protect the fiber against external factors. The refractive index difference between the core and the cladding provides the light propagation along the core section. The SMF - 28® is a single mode fiber supporting wave propagation in the C - band (1530 - 1565 nm).

Tapering of a single - mode SiO_2 fiber (1460 - 1620 nm, $\emptyset$ 125 μm cladding) was performed using a hydrogen torch. The adiabatic tapering process at constant pulling speed (0.10 mm / sec), with 2 linear stages moving in opposite directions, was controlled with a custom - made software and monitored simultaneously using a camera. An adiabatically tapered, single - mode SiO_2 fiber with high transmission was obtained via this process (Figure 3.2).

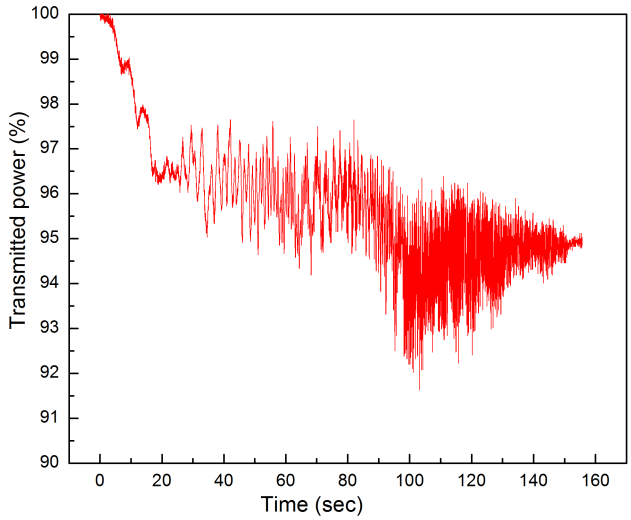

Figure 3.2: Transmitted power (%) versus time (sec) was plotted for a tapered single - mode SiO_2 fiber (1460 - 1620 nm, ∅ 125 μm cladding) using a hydrogen torch during tapering process. The tapered single - mode fiber had a transmission of 95 %. The tapering process was controlled using a custom - built software.

Transmitted power (%) versus time (sec) was plotted for a tapered single - mode SiO_2 fiber (1460 - 1620 nm, ∅ 125 μm cladding) using a hydrogen torch during the tapering process. The single - mode tapered fiber had a transmission of 95 % (Figure 3.2). The adiabatic tapering process was controlled using a custom - built software. During the fiber tapering process, the fluctuations in the transmitted power are observed in the multi - mode regime. Additionally, Figure 3.3a and Figure 3.3b show an SMF - 28® fiber, non - tapered and tapered, respectively. After the tapering process, a sub - μm diameter having fiber can easily be obtained.

3.3 Coupling of the Optical Microresonators

During the all biosensing experiments, the light was coupled from the tapered fiber to the fabricated microtoroid. An evanescent field is generated in the tapered region of the fiber. This evanescent field decays outwards through the tapered region of the fiber, providing the coupling of the propagating light to the

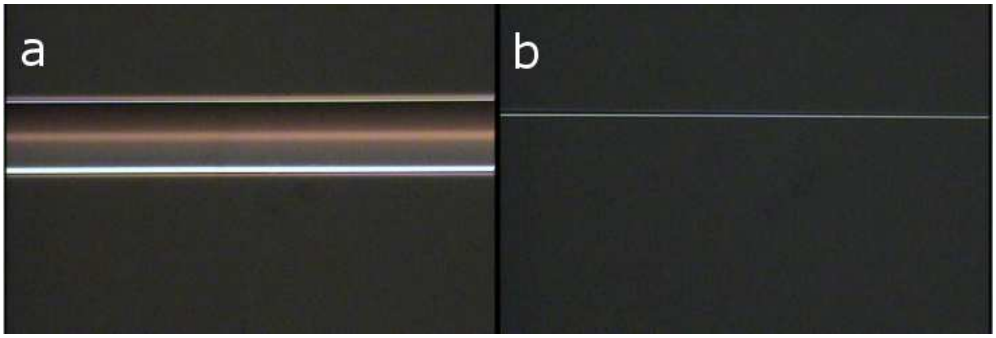

Figure 3.3: The photographs of (a) a non - tapered and (b) a tapered SMF - 28® fiber. The tapered region diameter ranges in between sub - μm to 3 μm.

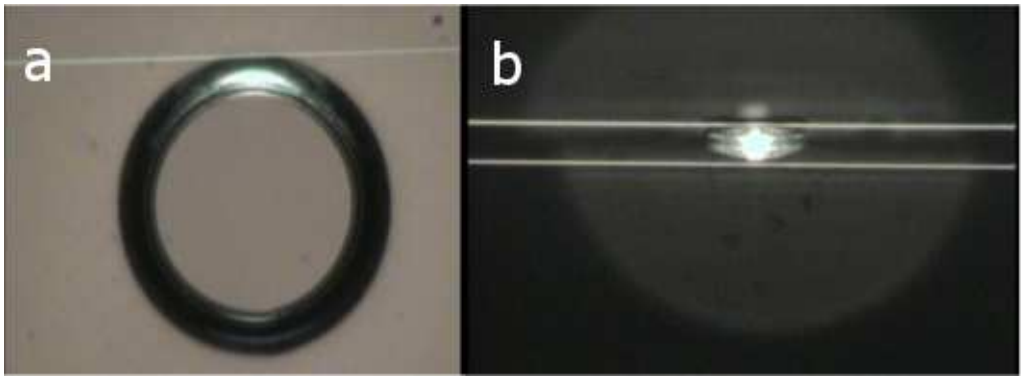

Figure 3.4: A photograph of a microtoroid coupled to a tapered SMF - 28® fiber from (a) top and (b) side views. The photographs were taken using 2 individual cameras providing top and side views of the coupling.

optical microresonator. Figure 3.4a and Figure 3.4b show the photographs of a microtoroid brought into the vicinity of the tapered region of the fiber from top and side views, respectively.

Figure 3.5 schematically illustrates a microtoroid coupled to a tapered fiber inside a micro - aquarium. During the measurements, critically coupling the fiber to the microtoroid plays a vital role since the optical power is totally transferred to the optical resonator at the critical coupling. Further, in an over coupling at which the optical resonator and the tapered fiber is quite close or adjacent, the linewidth of the WGM mode, observed in the critical coupling, widens and thus results in a dramatic decrease in the quality factor (Q - factor)[1].

[1]The Q - factor is described in detail in the Chapter 4.

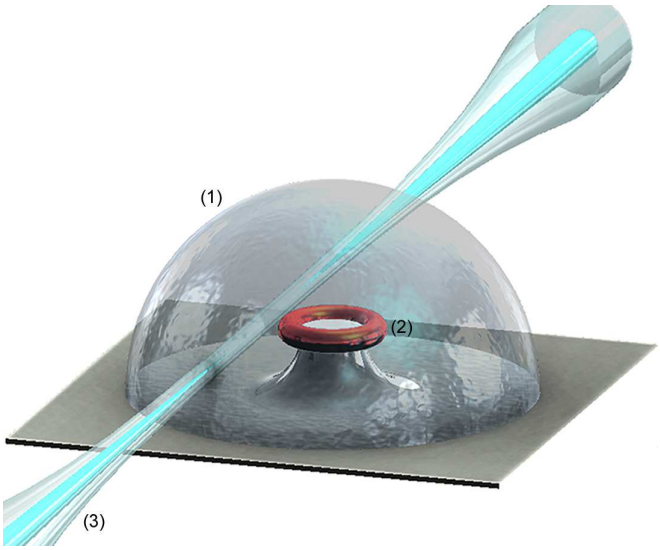

Figure 3.5: A schematic drawing showing in (1) a micro - aquarium, (2) a microtoroidal optical resonator is coupled to (3) a tapered fiber with its core (blue) and cladding (transparent).

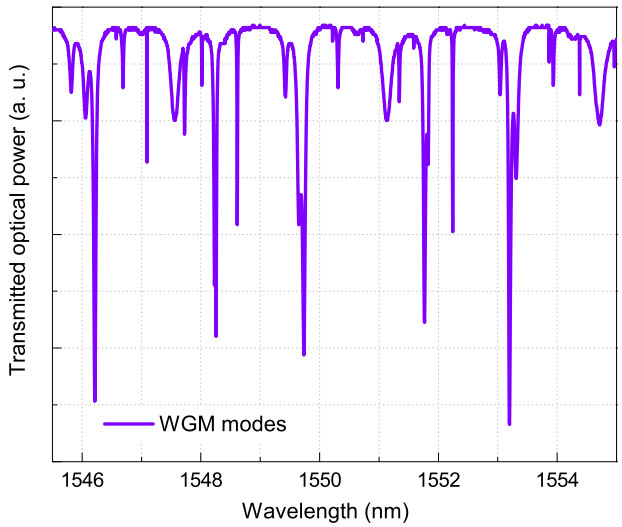

Figure 3.6: Total transmission spectra of the WGM modes under coupling, measured in air during the coupling of a microtoroidal optical resonator to a tapered SiO_2 fiber.

Additionally, phase matching condition[135] should be carefully considered in terms of the sizes of the tapered fiber and the microtoroid for an effective optical coupling. Figure 3.6 shows total transmission spectra of the WGM modes (TE^2 / TM^3) obtained from coupling a microtoroid to a tapered SMF - 28® fiber in air.

[2]Transverse electric.
[3]Transverse magnetic.

Chapter 4

Optical Biosensing Set - up

4.1 Components of the Biosensing Set - up

The biosensing set - up consists of 6 main parts: a tunable laser (TLS - 510, Santec, Japan), a biosensing platform, a piezo controller (APT, Thorlabs, USA), an oscilloscope (TDS - 1012B, Tetronix, USA), a photo - detector (918D - IR - OD3, Newport, USA) and a powermeter (1935C, Newport, USA). A schematic demonstration of the biosensing set - up is shown in Figure 4.1.

The sensing platform, located on a closed - loop piezo - stage (NanoMax - TS, Thorlabs, USA) which provided motion with 5 nm resolution in x - y - z axes. The closed - loop piezo stage was controlled by the piezo controller to prevent any mechanical perturbations during the optical measurements.

As the waveguide and the light source, the tapered SiO_2 fiber (SMF - 28, 1460 - 1620 nm, HES kablo, Turkey) and the tunable laser operating at 1550 nm were used, respectively. TE or TM modes were eliminated using a polarizer. The coupling between the microtoroid and the tapered fiber was viewed using 2 individual cameras (10 X / 0.28, f = 200, Mitutoyo, Japan) providing top and side views of the microtoroid coupled to its waveguide.

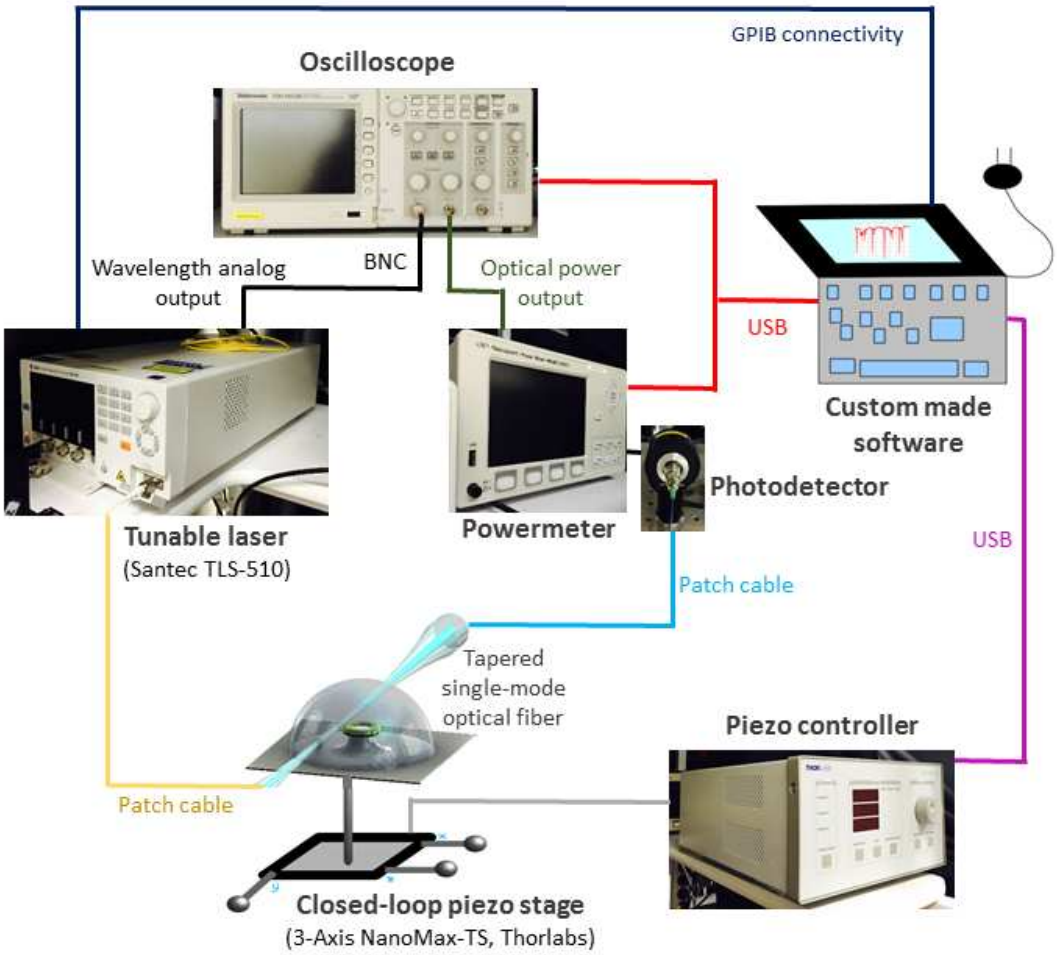

Figure 4.1: The schematic demonstration of the optical biosensing set - up. The wavelength of the light was continuously swept around resonant mode, while being monitored using a powermeter. The output laser wavelength and transmitted power values were monitored using an oscilloscope. All the system was controlled using a custom - built software. The microtoroid was placed on a closed - loop piezo stage controlled by a piezo controller. The infusion and withdrawal of the fluid was performed using 2 syringe pumps simultaneously.

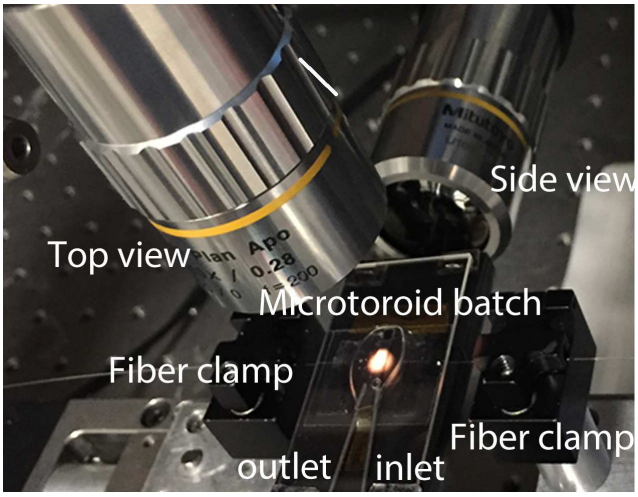

Figure 4.2: The photograph of the biosensing module with the cameras providing top and side views of the bionsensing module. The photograph shows a microtoroid batch coupled to a tapered fiber, trapped inside a micro - aquarium.

The wavelength of the laser was swept continuously around a defined wavelength in the range of 1510 - 1620 nm, with a constant sweep rate, which can be varied from 1 to 100 nm/s. The output intensity of the laser light was simultaneously tracked by the powermeter. The wavelength and the transmitted power values were recorded by the oscilloscope. The laser, oscilloscope, powermeter and piezo controller were all controlled by a custom - made software[1]. In order to reduce hysteresis of the laser, the transmission of the each resonance wavelength was tracked frame - by - frame by the software with a sweep delay (ranging between 100 ms - 2 s).

4.2 Biosensing Measurements

A droplet of buffer, which we call the micro - aquarium, was hand - spotted on the biosensing stage having a microtoroid coupled to its waveguide. Also, the biosensing stage was mounted to the piezo stage. The micro - aquarium was then trapped by covering the top using a microscope slide. To avoid undesired

[1]The sofware was made by Ozan Aktaş (UNAM - National Nanotechnology Research Center, Bilkent University) via C Sharp (programming language).

displacement of the waveguide, the fixation of the tapered fiber from both sides was done before dribbling the buffer with epoxy droplets (Thorlabs, USA), which were cured using a UV spot curing system (ELC - 410, Thorlabs, USA).

Flow and withdrawal to / from the micro - aquarium were performed using 2 individual syringe pumps (New Era Pump Systems, USA) working at a same and constant flow / withdrawal rate to obtain a constant micro - aquarium volume. Sterilized syringe bodies (5 ml, Terumo® Syringe, Belgium), inserted into the syringe pumps, were used during all biosensing studies. Tygon® tubings having 6.35 mm inner diameter were used for fluid flow. The tubings having sterilized needles in one of their end were fixed to the biosensing platform and their other ends were connected to the syringe pumps. During all optical biosensing measurements, the syringe and the micro - aquarium buffers were kept the same to avoid any refractive index change while performing the experiments.

4.3 Mathematical Modeling of Target Mass Diffusion Due To Concentration Gradient

The target (analyte) concentration gradient inside the micro - aquarium was mathematically modeled. To mathematically model the micro - aquarium system, the system volume (V) was assumed as constant and homogeneous.

In order to find a proper approximation (unsteady - state or pseudo steady - state), Fourier mass number ($F_{o,mass}$), a dimensionless number for transient mass transfer by diffusion, was calculated accordingly to the equation given below[136]:

$$F_{o,mass} = \frac{D_{AB}t}{L_{ch}} \tag{4.1}$$

where D_{AB}[2], t and L_{ch} are the mass diffusivity (m^2/s), the characteristic

[2]Mass diffusivity of proteins in buffer solutions.

timescale (s) and the length scale of interest (m), respectively. For our case the $F_{o,mass}$ was obtained as ~ 0.46 indicating an unsteady - state approximation (since, $F_{o,mass} < 1$ [136]).

For the unsteady - state approximation, in a system, a general expression for any quantity conserved, can be written as[136]:

$$\dot{\Psi}_{in} - \dot{\Psi}_{out} \pm \dot{\Psi}_{gen/consp} = \dot{\Psi}_{acc/dep} \tag{4.2}$$

where $\dot{\Psi}_{in}$, $\dot{\Psi}_{out}$, $\dot{\Psi}_{gen/consp}$ and $\dot{\Psi}_{acc/dep}$ stand for rates of input, output, generation / consumption and accumulation / depletion of the quantity conserved, respectively.

Additionally, for our system, the $\dot{\Psi}_{gen/consp}$ term can be neglected (since, $\cong 0$). Thus, the expression can be simplified as:

$$\dot{\Psi}_{in} - \dot{\Psi}_{out} = \dot{\Psi}_{acc/dep} \tag{4.3}$$

Considering the conservation of the total mass, the expression above can be expanded as:

$$C_o\dot{Q}_{in} - C\dot{Q}_{out} = V\frac{dC}{dt} \tag{4.4}$$

where C, C_o, V, $\dot{Q}_{in}$ and $\dot{Q}_{out}$ are concentration of the analyte inside the micro - aquarium (mol/mm^3) at a given time t (min), concentration of the infused analyte solution, the volume of the micro - aquarium (mm^3), constant input and output volumetric flow rates (mm^3/min), respectively. By dividing both sides with V, then the expression becomes:

$$C_o \frac{\dot{Q}_{in}}{V} - C \frac{\dot{Q}_{out}}{V} = \frac{dC}{dt} \tag{4.5}$$

Noting that the volumetric flow rates are equal and constant ($\dot{Q}_{in} = \dot{Q}_{out} = \dot{Q}$), the equation under proper boundary conditions (from $C_{initial}$ to C_{final} and $t_{initial}$ to t_{final}) becomes:

$$\int_{C_{initial}}^{C_{final}} \frac{dC\tau}{C_o - C} = \int_{t_{initial}}^{t_{final}} dt \tag{4.6}$$

where $\tau = V/\dot{Q}$, $C_{final} = C$, $t_{initial} = 0$ and $t_{final} = t$. Thus, the Equation can be solved into:

$$C = C_{initial} e^{-\dot{Q}t/V} + C_o(1 - e^{-\dot{Q}t/V}) \tag{4.7}$$

where $C_{initial}$ is initial analyte concentration inside the micro-aquarium. Since $C_{initial} = 0$, the expression can be finalized into:

$$C = C_o(1 - e^{-\dot{Q}t/V}) \tag{4.8}$$

Using the Equation 4.8, the concentration of the analyte inside a constant volume micro - aquarium can be calculated for a known volumetric flow rate and time.

4.4 Data Analyses

4.4.1 The Resonance Wavelength Shift

In order to analyze the data obtained during optical measurements, a custom - made Matlab code was used. Basically, the raw data was fitted to a 4 - variable Lorentzian function to find wavelength values corresponding to the minima of power measurements. The most general 4 - variable (p_1, p_2, p_3, C) Lorentzian function can be written as:

$$L(x) = \frac{p_1}{(x - p_2)^2 + p_3} + C \tag{4.9}$$

The raw data is fitted using that 4 - variable Lorentzian function after providing proper initial values.

To reduce noise which can be encountered easily during a measurement, and also to keep the original data trend, median filter was applied by calculating the median of each data point within a neighborhood of 15 (7 left / right neighbors). The intervals were different for each measurement as expected and depend on the factors such as, the duration, the sweep delay and other similar variables, which are characteristic for a measurement. Finally, each 3 data points were represented as 1 mean data with $\pm$ its standard deviation. It is important here to note that sudden changes in data, such as increases or decreases, accompanied by large standard deviations. Also, the first wavelength value was subtracted from each data point, to track the shift clearly.

4.4.2 Finding Q - Factor of the Microtoroid

The quality factor of an optical microresonator (Q - factor) can be defined as the ability of the microresonator to trap light or number of the round trips of the light along optical path of the microresonator. The Q - factor of an optical

microcavity depends on several parameters like resonator geometry and surface roughness of the resonator.

Q - factor can be defined as:

$$Q = \frac{f_r}{\Delta f} \tag{4.10}$$

where f_r is the resonant frequency and Δf is the full width at half maximum (FWHM) or simply the resonant width. Therefore, after fitting the raw data to the Lorentzian function, the Q - factor can be calculated directly.

During the biosensing measurements performed with the microresonators, sensitivity of the measurement heavily depends on the Q - factor of the optical microcavity. In biosensing experiments, with the Q - factor 10^6 and above, quite low LOD values starting from nano - molar level to single molecule level, can be obtained.

If a tunable laser working at $\sim$ 1550 nm is used during the biosensing measurements, in the aqueous environment, the Q - factor of the optical microcavity decreases by at least an order of magnitude due to water absorption at 1550 nm. In other terms, broadening in the linewidth of the transmission dip results in a decrease in the Q - factor. In Figure 4.3a and Figure 4.3b, the transmission dips obtained from a microtoroid (blue circles) along with their Lorentzian fits (red curves) were shown in air and in 10 mM Tris - HCl[3] / NaCl[4] (pH 7.0) buffer, respectively. The Q - factor of the microtoroid decreased from 3.1 x 10^7 to 4.6 x 10^4 in the buffer solution at $\sim$ 1550 nm, as the linewidth broadened.

[3]BioPerformance grade, Sigma - Aldrich, USA.
[4]Molecular biology grade.

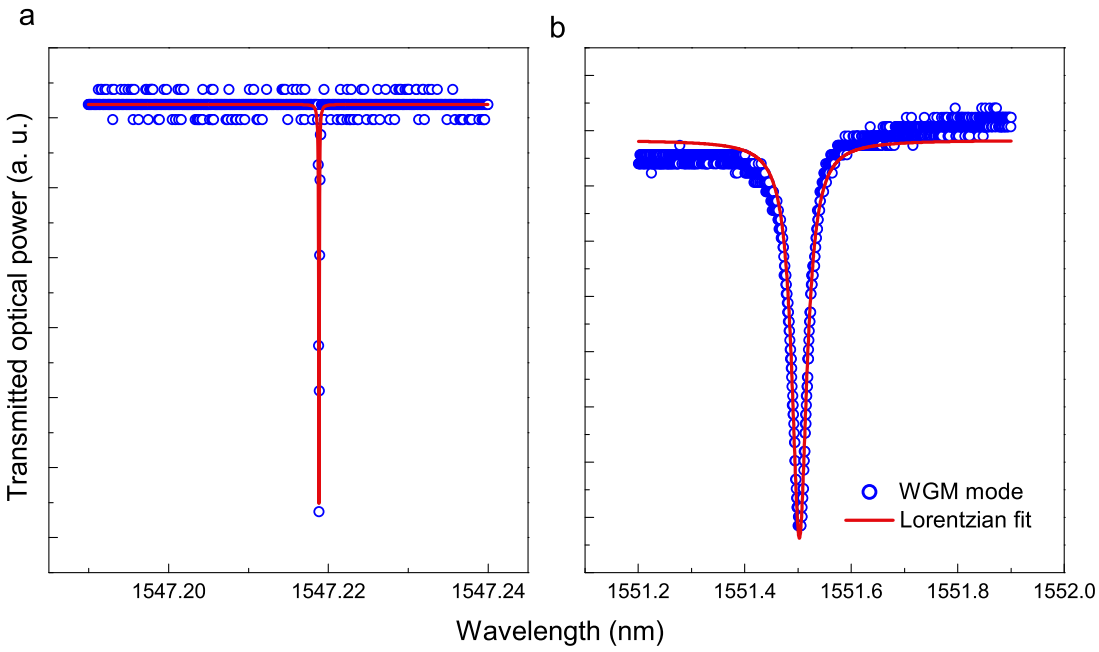

Figure 4.3: The Q - factor decrease in a buffer solution. The Lorentzian fits (red curves) of the WGMs (blue circles) are plotted versus transmitted optical powers (a. u.). The Q - factors were calculated as (a) 3.1 x 10^7 in air and (b) 4.6 x 10^4 in 10 mM Tris - HCl / NaCl (pH 7.0) buffer. The measurements were performed with a microtoroid using a 1550 nm tunable laser.

Chapter 5

Chemical Modification of Microtoroids for a Selective Biodetection

5.1 Surface Activation of the Microtoroids

In order to modify a SiO_2 microresonator surface, surface cleaning should be carefully applied before applying any surface modification strategy. For this purpose chemical cleaning or UV / Ozone cleaning was preferably done. Before any of these surface cleaning approaches, the microtoroid surface was cleaned with mild Hellmanex III (Hellma - Analytics, Germany) solution, ultra pure H_2O, ethanol (analytical reagent grade), acetone (analytical reagent grade) and ultra pure H_2O, each for 5 mins, respectively. Then, the surface was dried under N_2 gas.

Following the surface cleaning, chemical cleaning was applied using Piranha solution[1] (H_2SO_4 : H_2O_2 3 : 1 v/v [2]) at 60 °C for 5 mins, to remove residual organic contaminants on the microcavity surface and induce reactive silanol groups (Si -

[1]Piranha solution is highly aggressive and should be handled with care in a fume hood.
[2]volume / volume ratio

O - H). The silanols are reactive groups which can interact with silane coupling reagents by forming covalent linkages.[137] Additionally, UV / Ozone cleaning was applied individually or following the Piranha cleaning, using a UV / Ozone cleaning system (PSD - UV, Novascan, USA) for 15 or 30 mins in ambient air or in the presence of O_2.

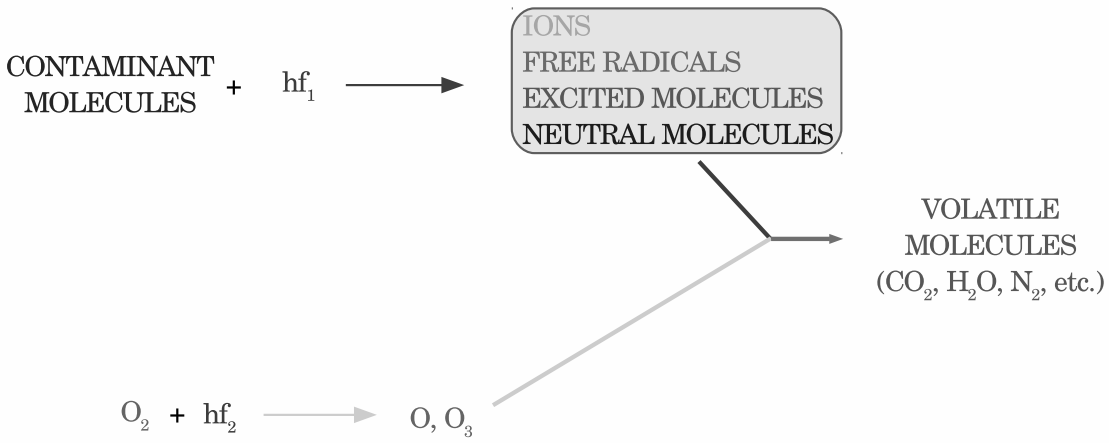

Figure 5.1: The schematic description of the UV / Ozone treatment approach. h and f_1, f_2 are the Planck constant and photon frequencies, respectively.[138]

The UV / Ozone treatment is a photon - induced process in which UV light (at 254 nm) excites and / or dissociates residual organic molecules on the surface. Simultaneously, UV light at 185 nm, produces O_3 and atomic O in the presence of O_2. The O_3 and atomic O are produced when O_2 and O_3 are dissociated by the absorption of the UV light, respectively. [138, 139] The mechanism of the UV / Ozone treatment is schematically described in Figure 5.1.

Figure 5.2a, Figure 5.2b and Figure 5.2c show photographs of water droplets on bare SiO_2 surfaces (1 μm thermal oxide on Si wafers, diced into 0.5 x 0.5 cm) after the surface cleaning, Piranha cleaning and UV / Ozone treatment, respectively. The static contact angle of the cleaned surface was measured as 58.30 $\pm$ 3.56°. Since the surface hydrophilicity incerased due to removing the organic contaminants from the surface, a dramatic decrease in the static contact angles were observed both after the Piranha or UV / Ozone treatments. For the static

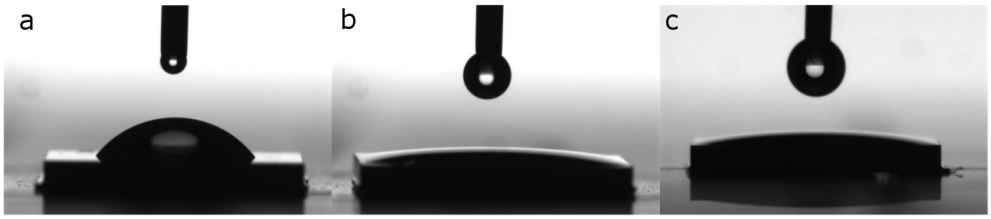

Figure 5.2: The photographs of 0.3 μl water droplets on (a) Cleaned, (b) Piranha cleaned and (c) UV / Ozone treated SiO_2 wafers.

contact angle measurements, a contact angle meter (DataPhysics, Germany) was used, with a 0.3 μl dosing volume and 1 μl / s dosing rate. The static contact angle of the cleaned surface was calculated using SCA20 software.

5.2 Silanization of the Microtoroids via Condensation Reaction

On the surface of a WGM biosensor, various functional groups can be obtained using silane coupling reagents. Each functional group provides a specific characteristic for the biosensing system, while the strategy follows a common pattern based on the silane chemistry[18], as illustrated in Figure 5.3. Following the microtoroid surface activation (Figure 5.3(1)), silanization of the resonator surface is done via a condensation reaction between active surface - OH groups and hydrolyzable groups of a silane coupling reagent (Figure 5.3(2)) allowing covalent probe conjugation (Figure 5.3(3)) and specific biodetection (Figure 5.3(4)).

The general structure of a silane coupling reagent[137] comprises a hydrolyzable group: OR′ (methoxy, ethoxy or acetoxy), an alkyl chain: $(CH_2)_n$ and a functional group: X (alkyl, aryl or organofunctional group), shown in Figure 5.4(2).

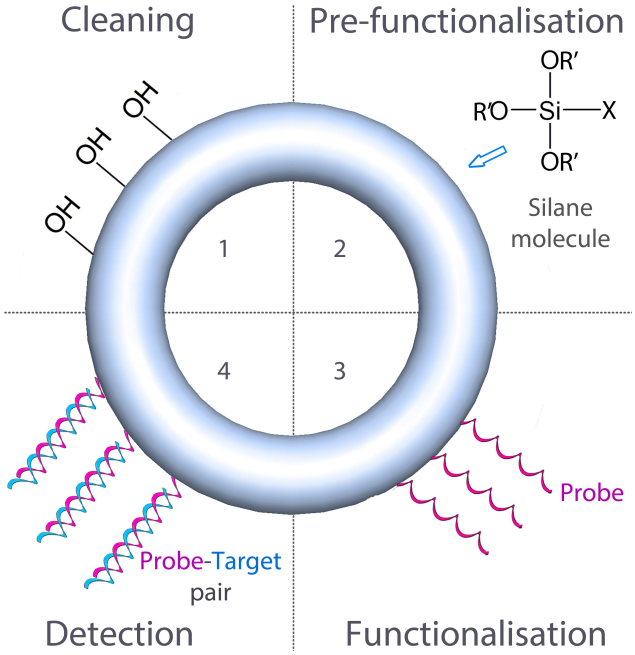

Figure 5.3: Surface modification of an optical resonator for specific target detection. Schematic drawing shows a general approach to the chemical modification of a SiO_2 based optical resonator for specific oligonucleotide based detection. (1) Cleaning of biosensor via UV / Ozone or chemical (Piranha) treatment to induce reactive silanol groups. (2) Pre - functionalization of the biosensor surface with a silane molecule via silane condensation reaction. Where OR′ can be a methoxy, ethoxy or acetoxy and X can be an alkyl, aryl or organofunctional group. (3) Surface functionalization by covalently conjugating an oligonucleotide probe (either modified or non - modified) to the silane coated biosensor. Also, in between a silane molecule and a probe, a linker molecule can be used. (4) Specific target detection using probe - target interactions.

In a silane condensation reaction, basically, hydrolyzed groups of the silane coupling reagent comprising reactive silanols, undergo a hydrogen bond formation with other silanol groups in a solution and on the inorganic biosensor surface. Following the hydrogen bond formation, a condensation reaction[137] occurs via covalent bond formation, to form a silane based coating on the microresonator surface.

5.3 Gaining Simultaneous Anti - Fouling and Bioconjugability Characteristics to a SiO_2 Surface

5.3.1 The Approach

Various alterations in materials characteristcs can be achieved via chemical modification of a surface by using different methods. Among all methods, the most commonly used strategy is "Self - Assembly Approach", which provides mono - or multi - layers on a surface based on moleculer interactions over the surface. During the self - assembly process, the molecule covalently or non - covalently bounds to the surface via a functional head group having high linking affinity.[18, 140, 141]

For a self - assembly strategy, the organosilane molecules are commonly used. The silanes usually form mono - layers on a target surface due to naturally occuring polymerization among the silane molecules, however, this factor highly depends on various parameters[18] like silane concentration, coating/curing temperature, solvent type, solvent pH, coating/curing time and curing pressure.

The surface property of a silane based coating depends on different factors like molecular density[142], type of the surface functional group and moleculer chain length.[143] Obtaining a surface coating, which has dual surface functionalities, is quite difficult when the silane molecules are used. The nature of whole coating can be easily altered by the interactions among the molecules. All in all, the functionalization of the surface using more than 1 silane molecule is possible via simultaneous or sequential coating processes. However, such approaches are not consistent due to the unpredicted nature of the silane molecules.[18]

In order to obtain a novel dual SiO_2 surface, an easy strategy[147] for gaining anti - fouling property along with the bioconjugation ability to the surface, is suggested using 1 type organosilane molecule. For this purpose, using only a single molecule: THPMP (MW 238.12, Sigma - Aldrich, USA), which is a commercially

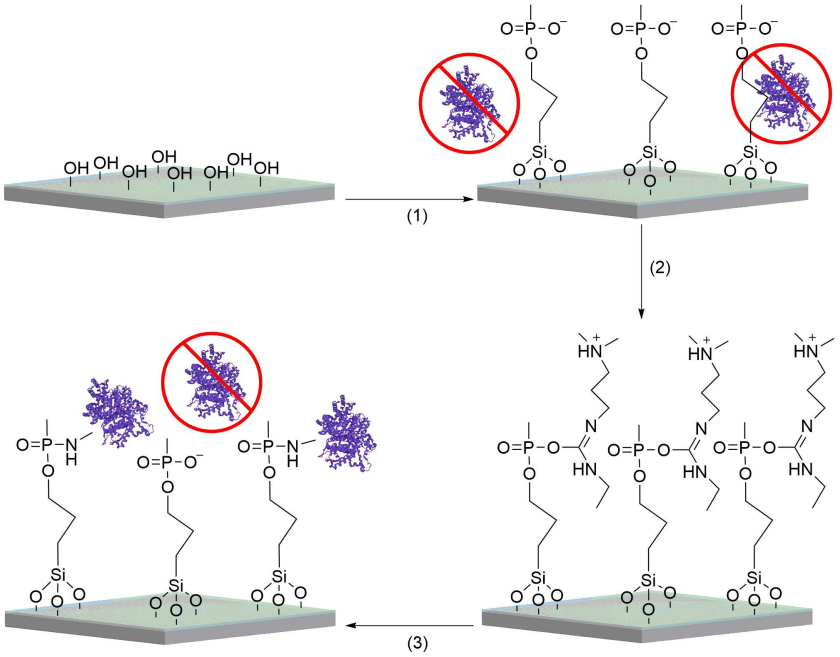

Figure 5.4: The Piranha treated SiO_2 surface is coated with THPMP molecules forming an anti - fouling coating (1). Then, CH_3O_3P groups are activated using EDC molecules, which form *o* - Acylisourea intermediates, which are very unstable over the surface (2). Following covalent conjugation of primary amine containing molecules to the intermediates (3), the THPMP coating gains its anti - fouling property again. The crystal structure of the BSA (purple ribbons) is shown as a primary amine containing molecule.

available CH_3O_3P having organosilane, is utilized to produce a bioconjugable and anti - fouling SiO_2 surface. It has been previously demonstrated by utilizing phosphonates that stabilization of SiO_2 nanoparticles against aggregations[144] and covalent conjugation to primary amine containing molecules[145] can be achieved successfully. It has also been shown that CH_3O_3P can dramatically decrease undesired adsorptions on the surfaces of SiO_2 nanoparticles.[146] In this study, the THPMP film over a SiO_2 surface was characterized in detail. Additionally, the anti - fouling and bioconjugation characteristics of the film were demonstrated. The results verified that the THPMP molecules provide form a suitable film to obtain simultaneous anti - fouling and bioconjugation characteristics over a SiO_2 surface (illustrated in Figure 5.4).

5.3.2 THPMP Coating of the SiO_2 Surfaces

A dicing saw purchased from Disco Corporation (Model DAD3220, Japan) was utilized to dice SiO_2 and quartz surfaces. Ultrasonic cleaning was applied to the diced surfaces in a mild Hellmanex solution (1 v/v % in ultra - pure water) for 15 mins. Afterwards, washing was done with ultra - pure water, ethanol (analytical grade), acetone (analytical grade) and ultra - pure water for 15 mins sequentially in an ultrasonic bath. Then, the surfaces were *in vacuo* dried at 100 °C during 30 mins. The Piranha treatment (at 60 °C for 30 mins) was performed in order to remove undesired organic compounds. The surfaces were activated using the Piranha treatment. Following the surface washing with ultra - pure water, drying was done under N_2 gas.

A solution of 2 v/v % THPMP in ultra - pure water was stirred for 10 mins. The SiO_2 surfaces were then inserted into the THPMP having solution at 60 °C during 1 hr. After the THPMP coating, the ultra - pure water washing was done mildly in order to suspend residual THPMP molecules from the surface. Lastly, for 1 hr, the THPMP coated surfaces were cured *in vacuo* at 100 °C.

5.3.3 Bioconjugation and Recovery for an Anti - Fouling Surface

For a protein bioconjugation, the THPMP coated SiO_2 surface was immersed into a MES buffer[3] having 5 mM EDC. The surfaces were incubated for 2hrs by continuous shaking. The CH_3O_3P groups were activated in the MES buffer instead of commonly used phosphate buffer, especially used to activate carboxylates[148]. Thus, any reaction between the EDC molecules and the phosphates in the solution, which can easily result in a significant decrease in the reaction efficiency, was avoided.[149] The *o* - Acylisourea molecule, which is very unstable in the buffer[137], was obtained via CH_3 terminal of the THPMP molecule. In this

[3]50 mM MES / 0.1 mM NaCl in H_2O (pH 6.0). The pH adjustment was done with NaOH solution.

case, the unstability of the *o* - Acylisourea form was quite beneficial for recovering the surface anti - fouling properties after activating the surface in the presence of the EDC molecules. The unbound EDC molecules were suspended by washing the surfaces with the MES buffer.

In order to conjugate proteins covalently, for 1 hr, the surfaces were immersed into a 1 mg / ml BSA having 1 X PBS solution (pH 7.4) under continuous shaking. Then, washing with the PBS buffer was done in order to remove the residual BSA molecules over the surface. For covalent bioconjugation of the BSA molecules to the CH_3O_3P groups, the EDC molecule was used as an activator. The EDC molecule forms the *o* - Acylisourea intermediates by attacking the terminal O of the CH_3O_3P group, which is negatively charged. This unstable form is later changed by a primary amine, which exists in all proteins.

Furthermore, the anti - fouling surface property was gained again by only washing the surfaces thoroughly with ultra - pure water. Via this simple procedure, the recovery of the SiO_2 surface was achieved.

Additionally, it is also possible to perform the well - known EDC / NHS chemistry via CH_3O_3P group. To demonstrate such an ability, the THPMP coated SiO_2 surface was immersed in a MES buffer having EDC (5 mM) and NHS (2 mM), at room temperature, for 2 hrs. Later, the surface was washed with MES buffer several times to suspend unused products.

5.3.4 Atomic Force Microscopy

The morphology of the coated surfaces were investigated with an Atomic Force Microscope (AFM, XE - 100E, PSIA, Korea) in NC[4] mode with a scan rate of 0.65 Hz. For all samples, 1 x 1 μm area scans were performed from 3 regions. The root - mean - square surface roughness (R_q) was calculated using XEI image processing software. In all AFM measurements, 0.5 x 0.5 cm wafer pieces of SiO_2 (1 μm) on Si, were used.

[4]Non - Contact.

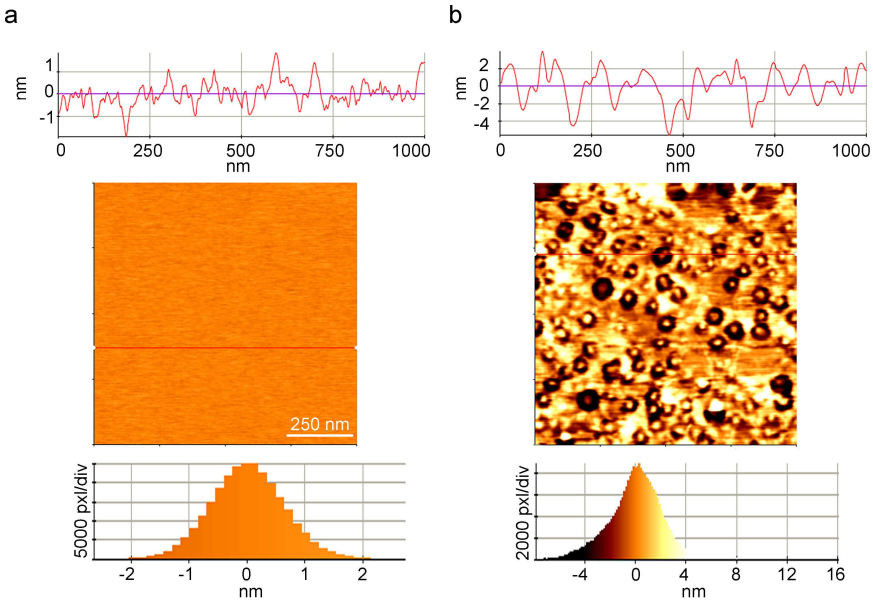

Figure 5.5: The 2D, NC - AFM scans of (a) bare and (b) THPMP having SiO_2 surfaces. For each AFM image, red line profiles (above) and histograms (below) were also provided. The SiO_2 surfaces having dimensions of 1 x 1 μm, were used during this study. The scan rate was kept as 0.65 Hz.

After the THPMP coating, the surface morphology changed significantly (Figure 5.5a and Figure 5.5b). The increase in the R_q value (Figure 5.5b) is commonly encountered after the silanization. The R_q value of the THPMP coated SiO_2 surface was calculated as 2.08 $\pm$ 0.09 nm while the bare SiO_2 surface had a R_q value of 0.59 $\pm$ 0.03 nm. Withal, the R_q value obtained from a covalent BSA conjugated THPMP film was as 3.62 $\pm$ 0.56 nm.

Additionally, the unspecific BSA adsorption onto a Piranha treated SiO_2 surface was shown by an 3D AFM scan (Figure 5.6) with 1 x 1 μ scan area. The R_q value was calculated as 1.23 $\pm$ 0.19 nm from 3 different scans.

5.3.5 The Contact Angle Measurements

In order to perform static contact angle measurements, a contact angle meter (OCA - 30, Dataphysics, Germany) was used. During all studies, a 3 μl water droplet was used. All measurements were performed 3 times by SiO_2 (1 μm) on

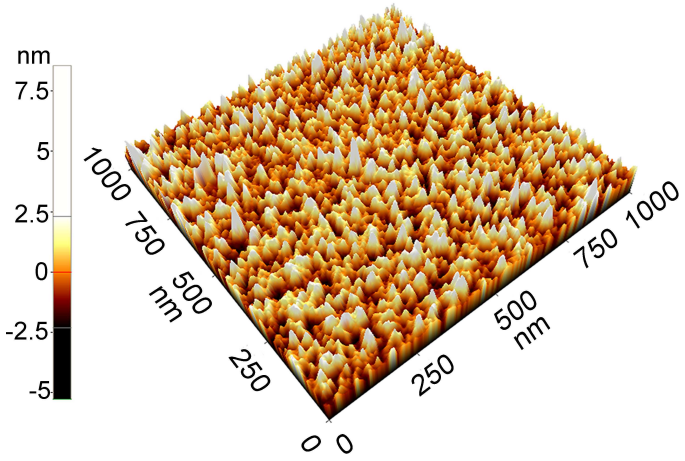

Figure 5.6: The 3D, NC - AFM scan showing the morphology of unspecifically adsorbed BSA molecules onto the Piranha treated SiO_2 surface. The R_q value was calculated as 1.23 $\pm$ 0.19 nm. The SiO_2 surfaces having dimensions of 1 x 1 μm, were used during this study. The scan rate was kept as 0.65 Hz.

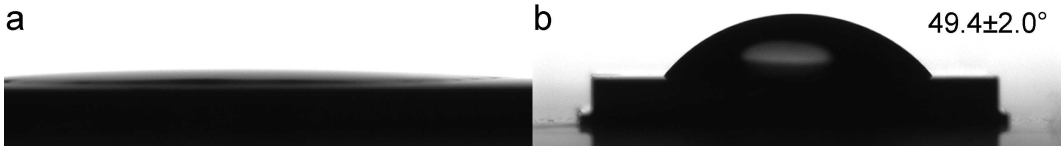

Figure 5.7: The contact angle measurements. The photographs showing the droplets of water (3 μl) on the (a) Piranha treated SiO_2 and (b) THPMP having SiO_2.

Si wafers with sizes of 2 x 2 cm or 0.5 x 0.5 cm. Also, Laplace - Young type fitting was done to calculate the contact angles.

The static contact angle of the Piranha treated surface showed a contact angle of $\sim 3^{\circ}$ since the surface became very hydrophilic (Figure 5.7a). The contact angle of a THPMP coated surface was obtained as $49.4 \pm 2.0^{\circ}$ (Figure 5.7b) by verifying the existence of a thin THPMP film over the SiO_2 surface with slightly hydrophilic CH_3O_3P groups. A closer contact angle value ($\sim 50^{\circ}$) was reported in another study[149] for dense mono - layers of phosphonates with OH- terminates.

5.3.6 The Confocal Microscopy

For the confocal studies, a confocal microscope (Model LSM 510, Zeiss, Germany) using 20 X objectives was used (5 airy units pinhole). For FITC dye, Ar laser (excitation 488 nm, emission 505 nm) was utilized. For Cy5 (Cyanine 5) dye, a He - Ne laser (excitation 633 nm, emission 650 nm) was utilized. For calculating the intensities of each channels, Image J software was used. To obtain background signal, the intensity arising from a Piranha cleaned quartz surface was used. The fluorescence intensities were demonstrated with their $\pm$ standard deviations.

The quartz surfaces (0.5 x 1.5 cm) were immersed in FITC - BSA having 1 X PBS buffers (1 mg / ml at pH 7.4) in a dark room. The THPMP having quartz samples were incubated in a solution containing NH_2- modified ss - DNA labeled with Cy5 fluorophore[5] (100 nM in 1 X PBS) for 2 hrs in a dark room following the EDC activation.

In order to verify anti - fouling property of the THPMP coating, undesired FITC - BSA adsorption was investigated (Figure 5.8). The uncoated and coated quartz samples showed significant differences in terms of undesired FITC - BSA adsorptions (Figure 5.8a and Figure 5.8b). In Figure 5.8c and Figure 5.8d, the difference in between a covalently protein conjugated sample and an ultra - pure

[5]Cy5 labeled ss - DNA molecules were synthesized by Sentegen, Ankara with high purity.

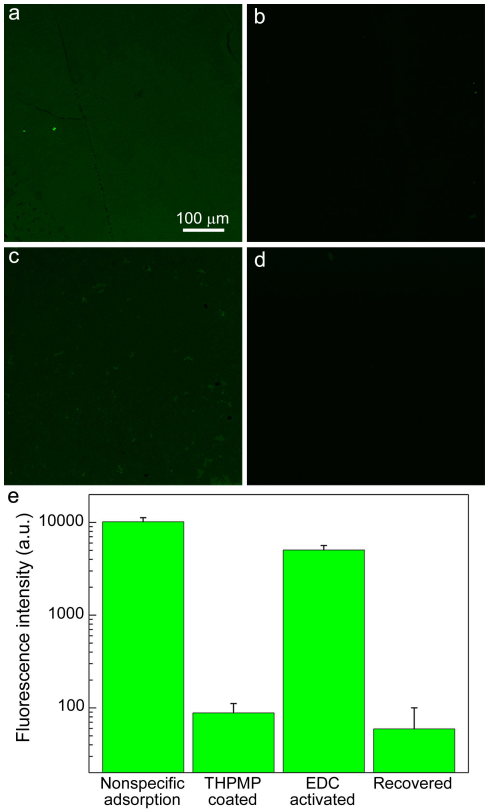

Figure 5.8: Undesired interaction of the FITC - BSA molecules with the Piranha cleaned quartz sample (a) was significantly reduced following the THPMP application (b). The covalent conjugation of the FITC - BSA molecules following the EDC activation (c). Also, an observed significant decrease in the undesired FITC - BSA interaction with the THPMP having surface washed after the EDC activation (d). The calculated fluorescence intensities of the FITC dye arising from the samples, demonstrated with their ± standard deviations (e).

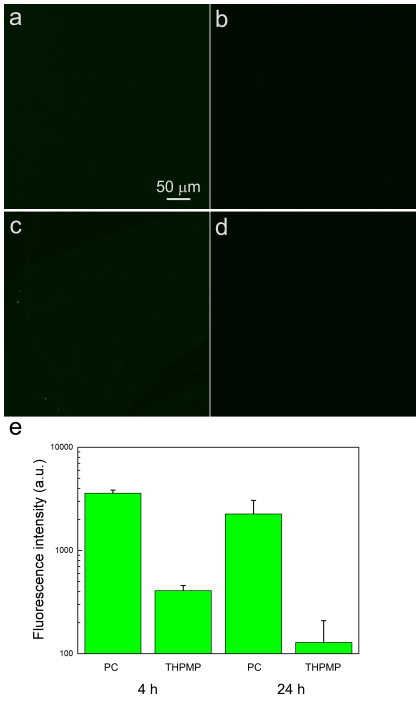

Figure 5.9: Time dependent anti - fouling property of the THPMP coating. The THPMP coated quartz wafers showed a significant anti - fouling towards 4 hrs (b) and 24 hrs (d) in 1 mg / ml FITC - BSA having buffer compared to bare quartz samples for 4 hrs (a) and 24 hrs (c) under same parameters. The calculated fluorescence intensities demonstrated with their ± standard deviations (e).

water washed activated surface was demonstrated, respectively. Figure 5.8d verifies the reversibility of the THPMP coated surface in terms of its anti - fouling property. Also, the anti - fouling property of the film for longer time periods was also shown (Figure 5.9).

Furthermore, the covalent conjugation of the FITC - BSA molecules to the activated THPMP film can be done. In order to verify the bioconjugation capability of the film, the NH_2- modified and Cy5 labeled ss - DNA strands were conjugated covalently (Figure 5.10a). The bioconjugated film was then incubated in the protein solution to prove its anti - fouling property (Figure 5.10b) for 1 hr. As demonstrated in Figure 5.10c, after the incubation, no significant FITC signal was obtained from the film while the signal arising from the ss - DNA strands were in the same range.

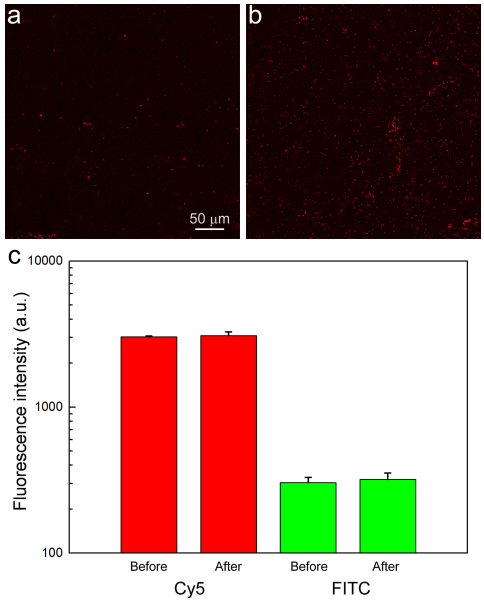

Figure 5.10: The biconjugation of the NH_2- modified and Cy5 labeled ss - DNA strands to the THPMP film on a quartz surface (a). The bioconjugated surface was 1 hr incubated in a FITC - BSA (1 mg / ml) having 1 X PBS buffer (b). The relative fluorescent intensities were shown for both Cy5 and FITC channels with their ± standard deviations (c).

5.3.7 The X - Ray Photoelectron Spectroscopy (XPS) Studies

During the XPS measurements, an XPS device (Thermo Fisher Scientific, UK) having Al K - α monochromatic source (spot size 400 μm, 2.5 mA, 12 kV and 0.1 eV step size) was utilized. All measurements were performed at an angle of 90°. Surrvey spectra were scanned with 50 ms dwell time and 200 eV pass energy. For regions, N1s, O1s, C1s and Si2p, each spectrum was scanned with 50 ms dwell time and 30 eV pass energy.

All P2p regions were scanned with 200 ms dwell time and 30 eV pass energy to enhance the signal by minimizing the environmental noise. The Avantage software was utilized for peak analyses. The charge correction was performed via C1s (neutral) signal located at 284.8 eV[150]. For the measurements, SiO_2 (1 μm) on Si surfaces (0.5 x 0.5 cm) were utilized.

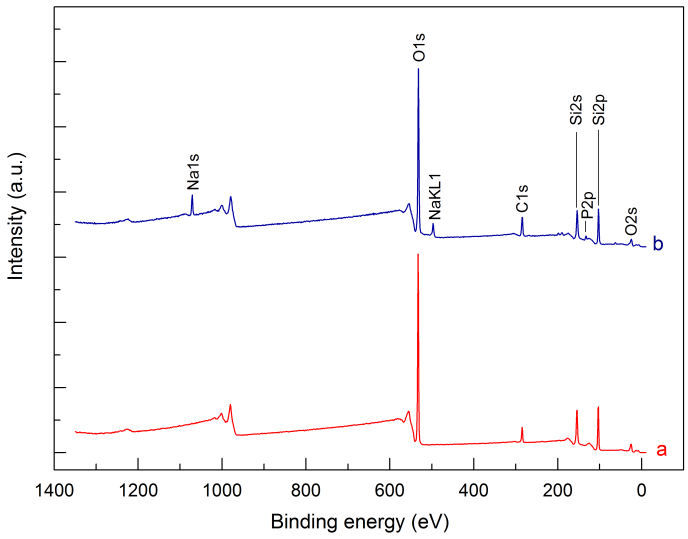

Figure 5.11: The overall survey spectra of the (a) cleaned (red data) and (b) THPMP having (blue data) SiO_2 samples. From the coated sample, a signal in the P2p region was gathered.

As shown in (Figure 5.11), a signal in the P2p region, located at 133.2 eV, was observed following the THPMP coating. The result verified the thin coating on the SiO_2 surface. The obtained P2p signal had significantly low atomic percentage as compared to the other compounds (Table B.1).

Figure 5.12 shows the detailed region scans for the cleaned SiO_2 (left column) and the THPMP having SiO_2 (right column) surfaces. The component peaks were observed after the silane coating[150]. The detailed scan of cleaned SiO_2 surface demonstrated a high intensity peak (103.6 eV) verifying the existence of the thermal oxide layer.[151] The THPMP coated surface showed a new peak (102.1 eV) due to silane bonding.[152]

Furthermore, the O1s region scans of the cleaned SiO_2 and the THPMP having samples showed the same signal (532.9 eV) due to the O environment.[153]. A signal, at 531.1 eV, was observed after the silane coating. In the C1s region scans, both samples showed C - C (284.8 eV) and C - O (286.5 eV) bondings. The increase in the low energy C1s signal was observed due to the silane bonding.

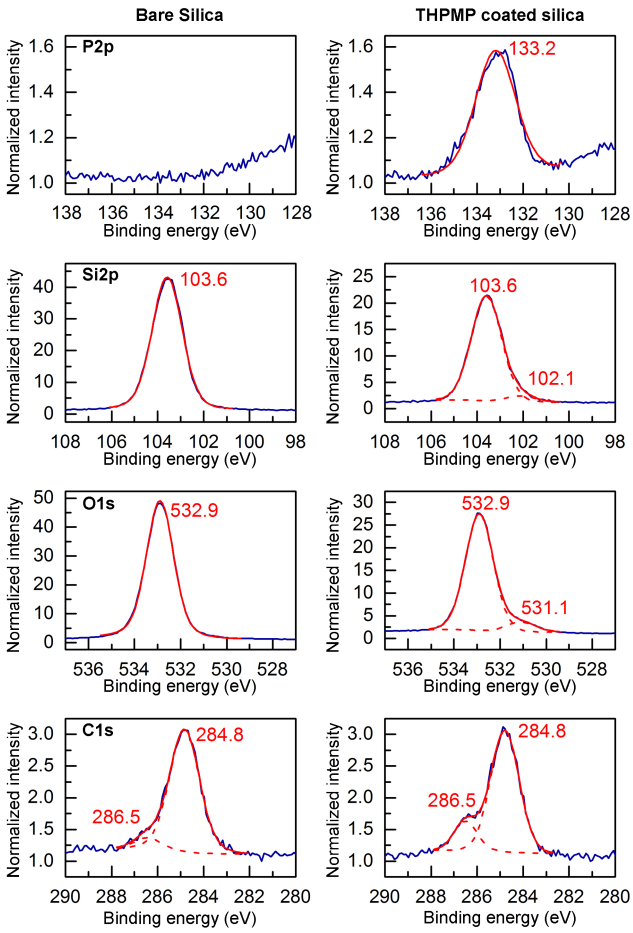

Figure 5.12: The detailed region scans for P2p, Si2p, O1s and C1s from the bare (left column) and THPMP having SiO_2 (right column) samples. The real data and the peak fits were shown in blue solid and red dashed lines, respectively. The peak envelopes were shown with red solid lines.

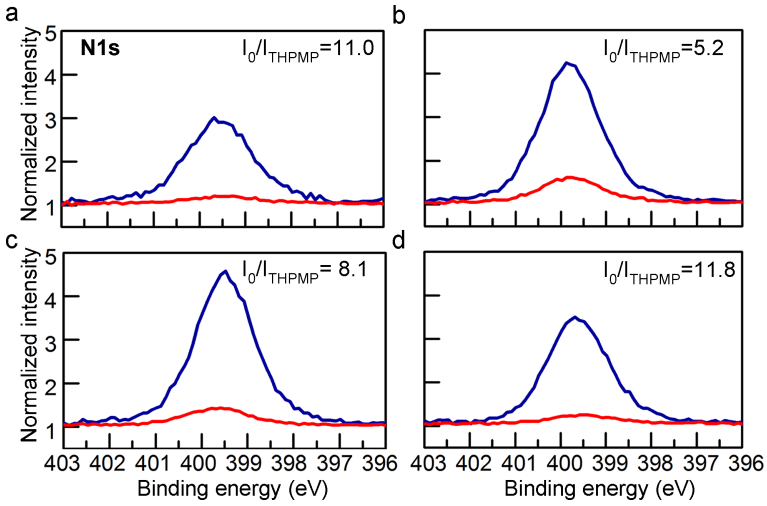

Figure 5.13: The detailed region scans for N1s, from Piranha cleaned and THPMP having SiO_2 samples incubated in (a) BSA, (B) γ - globulin, (c) fibrinogen, and (d) lysozyme having buffers. The coating showed a dramatic anti - fouling property in all measurements. The intensities from the Piranha treated (I_0) and THPMP coated (I_{THPMP}) samples were also obtained.

The anti - fouling property of the THPMP coating was demonstrated using different protein solutions Figure 5.13 with different natures [155]. The N1s region scans from the Piranha treated and THPMP having SiO_2 samples were demonstrated significantly different anti - fouling properties in terms of N1s signals. Instead of atomic percentage analysis[156], correction was done in background for a quantitative comparision.

The region scans (P2p and N1s) for a recovered sample (Figure 5.14a and Figure 5.14b) also appealed that the THPMP film has ability to return its anti - fouling state. No N1s signal was observed after the buffer washing by proving the absence of the *o* - Acylisourea forms on the sample surface.

As a further verification, the well - known EDC / NHS chemistry was applied to the coating. Figure 5.14c shows NHS - ester verification on the sample surface by N - C (400.0 eV) and N - O (402.2 eV) bondings[157]. The results also proved a formed phosphonamidate form[158] on the sample surface.

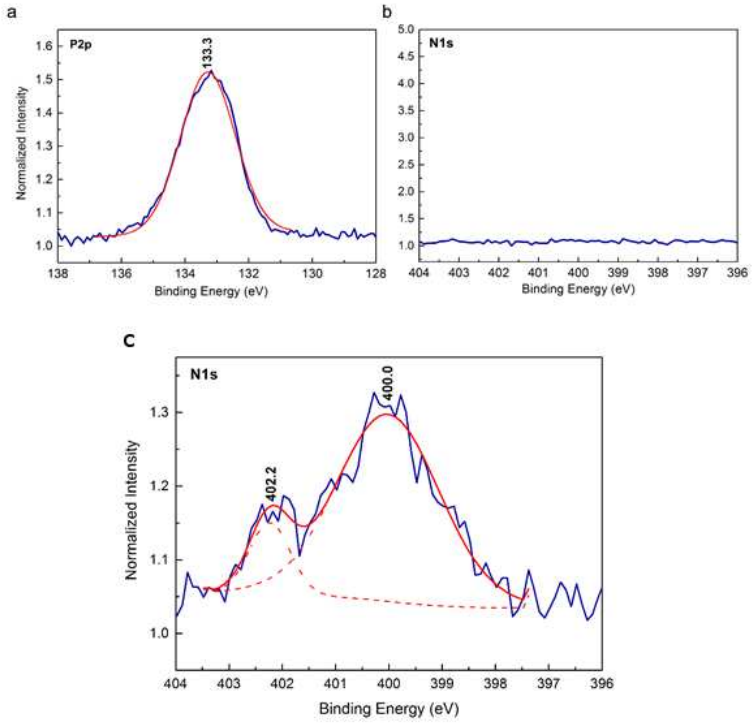

Figure 5.14: The detailed region scans for P2p (a) and N1s (b) from a sequentially EDC activated and washed SiO_2 sample. (c) The N1s region scan from an EDC / NHS chemistry performed SiO_2 sample. The peaks (402.2 and 400.0 eV) verified the existence of NHS - esters on the sample surface. The data were demonstrated in blue, while the fits and the envelopes were demonstrated in red dashed and solid lines, respectively.

5.3.8 The Ellipsometry Analysis

For the ellipsometry analysis, a spectroscopic ellipsometer (V - VASE, J.A. Woollam, USA) was utilized. The operating wavelength was 633 nm as a single wavelenth. However, the incident angle was varied from 30° to 90° by steps of 2°. The optical constants (amplitude component (Ψ) and phase difference (Δ) were measured during the analysis. Then, the film thicknesses were estimated by fitting data with the literately obtained optical constants.[159] During the all ellipsometry studies, SiO_2 (250 nm) on Si wafers (0.5 x 1.5 cm) were utilized.

Furthermore, the ellipsometry analysis was done in order to obtained the undesired adsorption of the BSA amounts (ng / cm^2) over the samples before and after

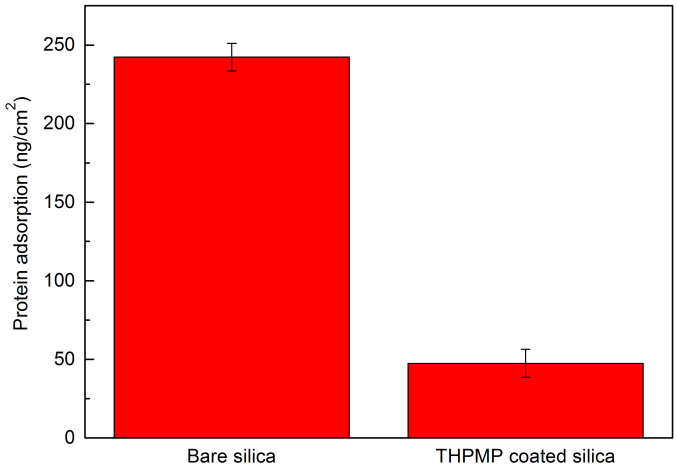

Figure 5.15: The ellipsometry results. The undesired BSA adsorption (ng / cm^2) onto the Piranha cleaned and the THPMP having SiO_2 samples.

the THPMP coating process (Figure 5.15). As can be seen from the Figure 5.15 that the adsorbed BSA amount decreased 5 - fold by the THPMP coating. The film thicknesses were obtained accordingly to a previously published study[160]. This result is comparable to the ellipsometry studies performed previously [161]. The THPMP film thickness was measured as 0.65 $\pm$ 0.02 nm (Table B.2). Since the protein adsorbed sample surface has voids[162], it is difficult to obtain the real film thickness. Nevertheless, the estimated thicknesses for different regions (Table B.2), demonstrated a significant difference between the Piranha cleaned and the THPMP having samples.

Chapter 6

Label - Free Selective Biosensing in Complex Media Using Microtoroids

6.1 The Challenges of Biosensing in a Complex Media

The supreme sensitivity of the WGM type microresonators is initially conceived as an advantage. However, there is a major concern regarding the lack of intrinsic discrimination mechanism among different species inducing refractive index alterations through non - specific interactions between the microresonator and the constituents of its surrounding media, except for the measurements taken in precisely determined experimental conditions, such as in buffer solutions. This represents a conundrum regarding the applicability and reliability of the optical microresonators with high selectivity in real life situations such as specific detection of biomolecule markers in serum samples.

Several works demonstrated the applicability of the WGM microresonators as biosensors for measurements in complex media, where an initial calibration is

performed with using the media in order to subtract the signal caused by non - specific molecular interactions[82, 132]; however, the sensitivity of the biosensors compared to the measurements in the buffer solutions were significantly decreased in each case, probably due to steric effect of the weak yet abundant non - specific interactions caused by irreversible adsorption of constituents, mostly proteins, from the media onto the resonator surface. Using a well - established silane based anti - fouling surface modification[18] could significantly reduce the effect of non - specific interactions in biosensing with the SiO_2 based WGM microresonators, as demonstrated previously[163]; however, functionalization of these biosensors with molecular probes, such as antibodies, without compromising their protein resistant characteristics remains as an essential challenge. The protein resistance of molecular coatings heavily depends on their functional groups[143]; therefore, having a coating with multiple functionalities, such as protein resistance and bioconjugability, is challenging to obtain in terms of efficiency. Besides, unlike the thiol based coatings, where mixing compounds with different characteristics is straightforward[148], due to the complex nature of silane chemistry[18], forming multifunctional coatings with silane based molecules, convenient for optical microresonators, is a meticulous endeavour.

The coating of an organosilane molecule having a CH_3O_3P functional group could be used to form a simultaneously protein resistant and bioconjugable SiO_2 surface[147]. This multifunctional coating could indeed solve the aforementioned problem of the biosensing with the WGM microresonators by enabling recognition of antigens after functionalization of microtoroids with corresponding antibodies with high sensitivity in complex media and also by suppressing non - specific interactions simultaneously. Figure 8.1 schematically describes our approach in this work[24]. The microtoroids were functionalized with the described robust process being done mostly at room temperature, which is applicable to many other types of the SiO_2 based WGM microresonators, are shown to possess a substantial protein resistance, while this does not deteriorate their biosensing capabilities. The outcomes of this research could considerably facilitate the utilization of the WGM microresonators as optical biosensors with extreme sensitivities in much challenging tasks including point of care diagnostics, food safety and public health, and

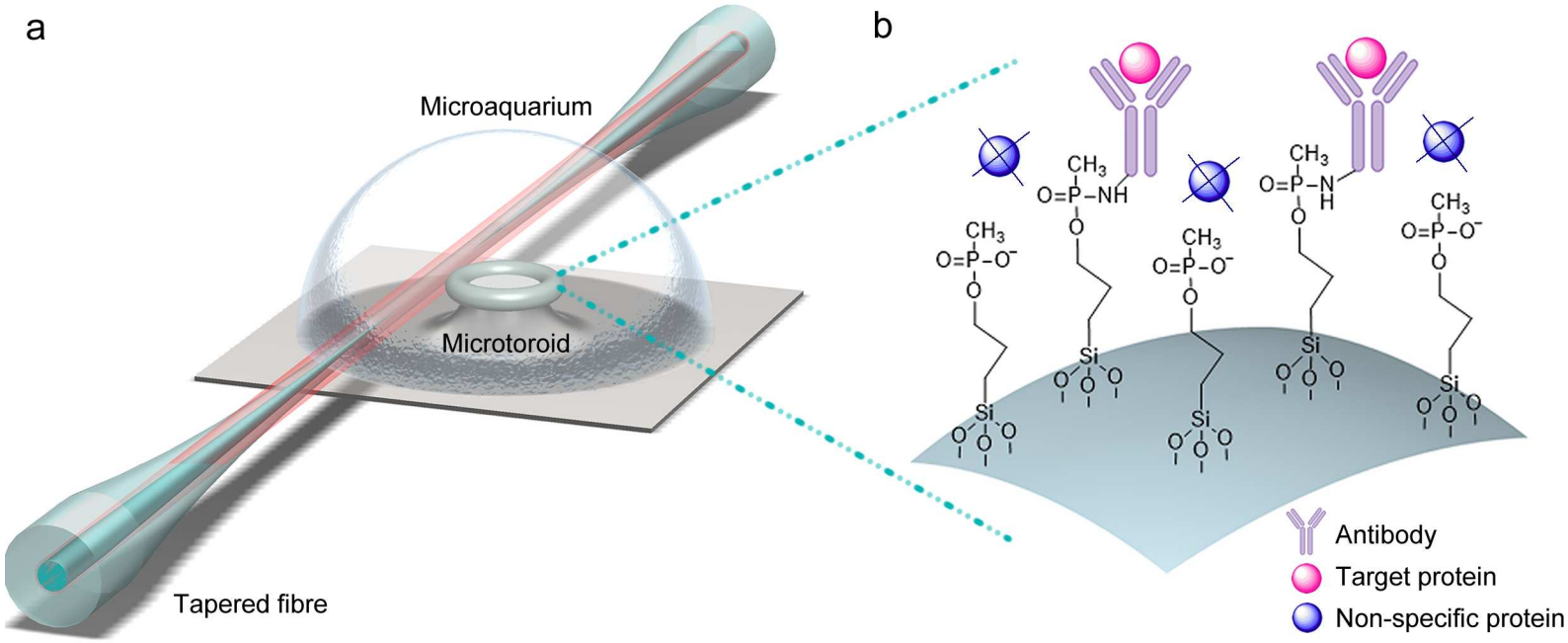

Figure 6.1: Selective biodetection using microtoroids. Microtoroidal optical resonator modified with silane molecules was used to attain a label - free biosensor with high selectivity. (a) Biosensing experiments were performed in liquid media using a microtoroidal optical resonator. Light is evanescently coupled to the microtoroid using a tapered optical fiber. (b) The surface chemistry used throughout this study depends on attaching covalently THPMP molecules onto the microtoroid surface. The THPMP forms a protein resistant thin film, as well as convenient sites for bioconjugation of molecular probes such as antibodies via activation of the THPMP coating with the EDC molecules. This method enables selective detection of biological species in complex media.

civil defence against bio - terrorism or biological weapons.

6.2 Selective and Label - Free IL - 2 Antigen Sensing Using Surface Modified Microtoroids

6.2.1 Chemical Modification of The Microtoroid Surface for a Selective IL - 2 Detection

The microtoroid surface was cleaned with mild Hellmanex solution (1 % v/v), ethanol (analytical grade), acetone (analytical grade) and DI - H_2O, respectively. Then, the Piranha solution (H_2SO_4 : H_2O_2 3 : 1 v/v) at 60 °C was used for microtoroid surface activation. Then, the activated microtoroids were coated with 2.5 v/v % THPMP in methanol solution[1] for 1 hr at room temperature. After gently washing with the methanol solution, the THPMP coated microtoroids were then cured at 100 °C in vacuum for 1 hr. The anti IL - 2 antibodies[2] were covalently conjugated to the THPMP coated microtoroid surfaces after incubation in 5 mM EDC in the MES buffer for 2 hrs at room temperature. To remove the residual EDC molecules, the surfaces were washed with the MES buffer and 1 X PBS sequentially, and then soaked into a 2.5 μg / ml anti IL - 2 containing 1 X PBS solution at 4 °C for 2 hrs on a lab shaker. Finally, the anti IL - 2 conjugated microtoroids were washed with 1 X PBS to remove unbound anti IL - 2 molecules and stored in 1 X PBS at 4 °C.

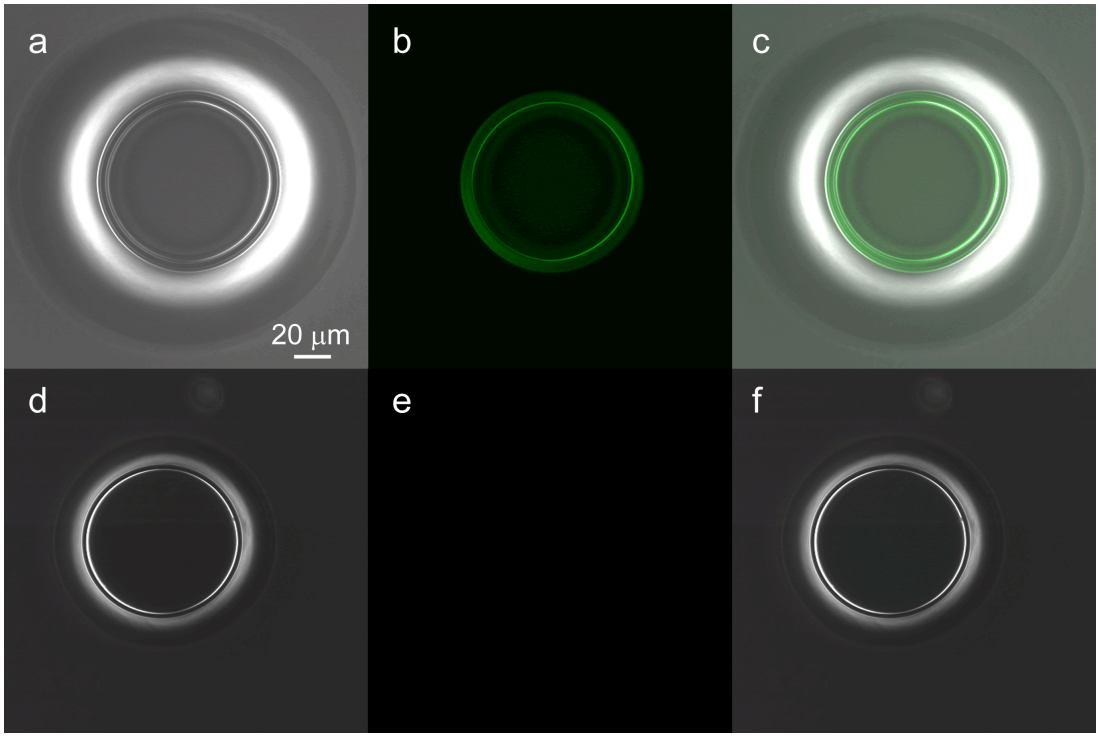

Figure 6.2: Demonstration of the protein resistant characteristics of the THPMP coated microtoroids. The confocal microscopy was used to demonstrate the protein resistance of the coating. The Piranha cleaned and the THPMP coated microtoroids were incubated in the 1 mg / ml FITC - BSA in 1 X PBS buffer for 1 hr prior to confocal imaging. (a - c) Differential Interference Contrast (DIC), fluorescence and merged images of the Piranha treated microtoroids incubated in the FITC - BSA having 1 X PBS solution. (d - f) DIC, fluorescence and merged images of THPMP coated microtoroids incubated in in the FITC - BSA having 1 X PBS solution. All measurements were performed using the same configurations. No fluorescence signals were obtained from the THPMP coated microtoroids.

6.2.2 The Confocal Microscopy Studies

The protein resistance of the THPMP coated microtoroids were shown using the confocal microscopy. The confocal imaging was done using a confocal microscope (Model LSM 510, Zeiss, Germany) with 20 X objectives. The samples were incubated in FITC - BSA (1 mg / ml, Sigma - Aldrich, USA) having 1 X PBS solution for 1 hr prior to measurement. An argon laser at 488 nm was used for excitation and emission over 505 nm was collected using photomultiplier tubes. The settings for gain and offset were kept constant throughout all measurements. The pinhole was set to 3 airy units, and the images were formed by averaging each scan line 16 times.

The Piranha cleaned and the THPMP coated microtoroids were compared regarding non - specific adsorption of the FITC - BSA molecules using the confocal microscopy. As can be seen from Figure 6.2, there was a considerable non - specific protein adsorption over the Piranha cleaned microtoroid, while the THPMP coated microtoroid exhibited a significant protein resistant property.

6.2.3 The Optical Measurements

The analyte infusion and withdrawal were performed using 2 syringe pumps operating at infusion / withdrawal rates of 5 μl / min or 10 μl / min, depending on the experiment. IL - 2 antigen[3] was diluted to a final concentration of 250 ng / ml in 1 X PBS, or 1 X PBS containing 0.1 X FBS solutions. After the optical coupling condition was satisfied, initial solution was dropped over the microtoroids by the help of a micropipette, and the solution was covered with a microscope slide forming a 200 μl micro - aquarium around the microtoroid. The resonance wavelengths were investigated in under - coupled regime in order to minimize the linewidth of the coupled mode. Baseline was measured for 5 min before the

[1]The methanol solution contains 5 v/v % DI - H_2O in methanol (analytical grade) at pH 4.6, adjusted with acetic acid.

[2]Polyclonal human antibodies, produced in chicken, Sigma - Aldrich, USA.

[3]Human antigen, MW 15.5 kDa, recombinant, expressed in *Escherichia coli*, Sigma - Aldrich, USA.

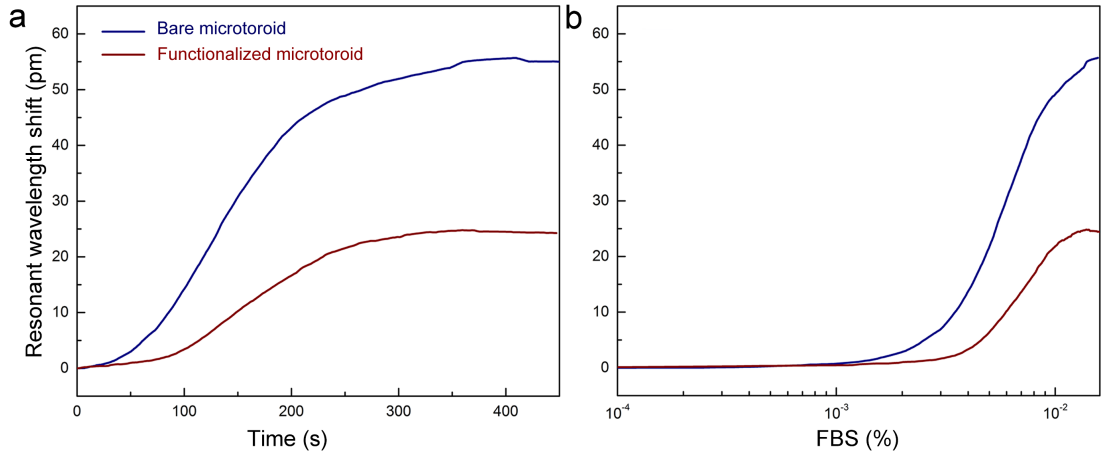

Figure 6.3: Comparison of responses of functionalized and bare microtoroids towards complex media. After the microtoroids were functionalized with THPMP and antibodies, their responses in terms of the WGM resonant shift were compared with bare microtoroids towards complex media. (a) Temporal increase of the WGM resonant wavelength after infusion of 10 v/v % FBS with an infusion rate of 5 μl / s beginning at t = 0. The infusion continued for 300 secs, and the bare microtoroid (blue) showed a higher sensitivity compared to functionalized microtoroid (red). (b) The WGM resonance shift with respect to the increasing FBS concentration. The cumulative data were smoothed by adjacent averaging, considering an averaging time of 1 min.

simultaneous initiation of infusion and withdrawal. After 10 mins of the liquid flow, the data were captured for 5 more mins to observe the effect of stopping the infusion / withdrawal. As a control measurement, mouse IL - 12 antigen[4] was used. Additionally, only for this study, the LOD of the measurements were calculated by considering standard deviation (StDev) before infusing the analyte into the system. the LOD value was considered as 3 x StDev by determining after calculation of the StDev within a time frame of 1 min before the infusion.

6.2.4 Anti - Fouling Property in The Buffer and Complex Media

The bare and the THPMP functionalized microtoroids were exposed to the complex media. To reduce the effect of viscosity, as buffer solution and complex media, 1 X PBS and 10 v/v % FBS in 1 X PBS were used, respectively. As can be seen from Figure 8.3a considerable reduction in the WGM resonance shift was observed from the functionalized microtoroid as compared to the bare one.

The WGM shift with respect to the increasing FBS concentration within the micro - aquarium, was also calculated according to the Equation 4.8, and shown in Figure 8.3b. Especially, at lower FBS concentrations, a significant reduction in the WGM shift against the FBS was observed. After 1 % FBS concentration, the resonance shift tended to be saturated in the cases of both bare and functionalized microtoroids. The WGM shift caused by the FBS infusion occured cumulatively by the refractive index change (bulk effect) and non - specific protein adsorptions (surface effect). Although the change in the refractive index within the surrounding environment affected both the bare and functionalized microtoroids, the adsorption of proteins on the microtoroid surface appeared to be eliminated significantly after the THPMP functionalization.

6.2.5 Real - Time and Selective Biodetection of The IL - 2 Antigen

In order to investigate the biosensing capabilities of functionalized microtoroid, the sensitivity in 1 X PBS buffer was measured. The human IL - 2 antigen was used as an analyte, with a concentration of 16 nM, in 1 X PBS buffer. Figure 6.4 and Figure 6.5 represent the temporal response of the resonance wavelength after IL - 2 infusion in 1 X PBS, and also the information related to the effect of IL-2 concentration on the WGM shift, respectively. The concentration values were calculated according to the Equation 4.8. The LOD of the functionalized

[4]Recombinant mouse protein, MW 70 kDa, R & D Systems, USA.

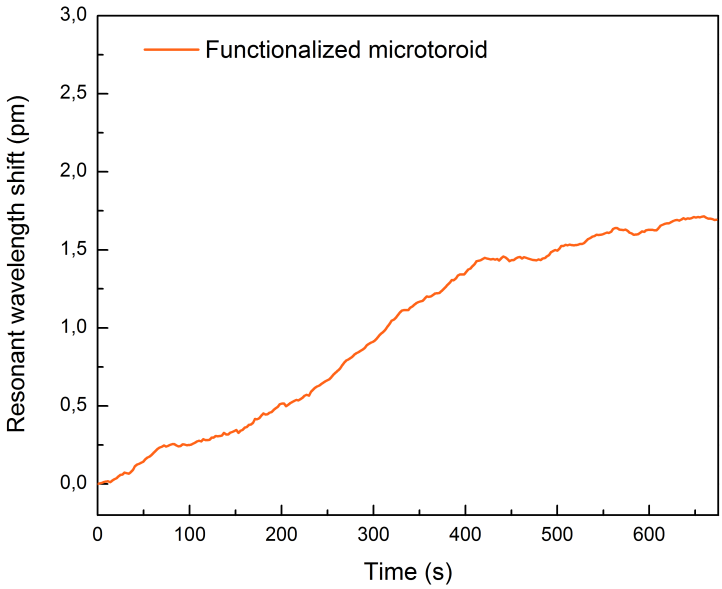

Figure 6.4: The WGM shift with respect to time due to the IL - 2 infusion (orange line). The human IL - 2 protein in 1 X PBS buffer was infused to the IL - 2 antibody conjugated microtoroid. The infusion was started at t = 0 and continued for 600 secs with an infusion rate of 5 μl / s. The cumulative data were smoothed by adjacent averaging, considering an averaging time of 1 min.

microtoroid in 1 X PBS buffer was calculated as 0.10 nM.

The applicability of biosensing within the complex media was also demonstrated by performing IL - 2 detection measurements in 10 v/v % FBS in 1 X PBS (Figure 8.6). The experiments in complex media were initiated in 10 v/v % FBS rather than 1 X PBS, to prevent a WGM shift would have been caused due to ambient refractive index change, and to only observe the effect of IL - 2 infusion on the resonance wavelength shift. The IL - 2 antigen was also diluted in 10 v/v % FBS. The mouse IL - 12 antigen, which does not have an affinity towards the IL - 2 antibody, was used as a control. Comparing responses of the functionalized microtoroids towards IL - 2 and IL - 12 infusions in 10 v/v % FBS solution, a significant WGM shift was observed from the IL - 2 infusion (Figure 8.6, purple line), while no significant response was observed towards the IL - 12 infusion (Figure 8.6, teal line), as expected. The LOD of the functionalized microtoroid in 10 v/v % FBS was calculated as 0.11 nM, suggesting that the microtoroidal biosensor substantially preserved its sensitivity in the complex media.

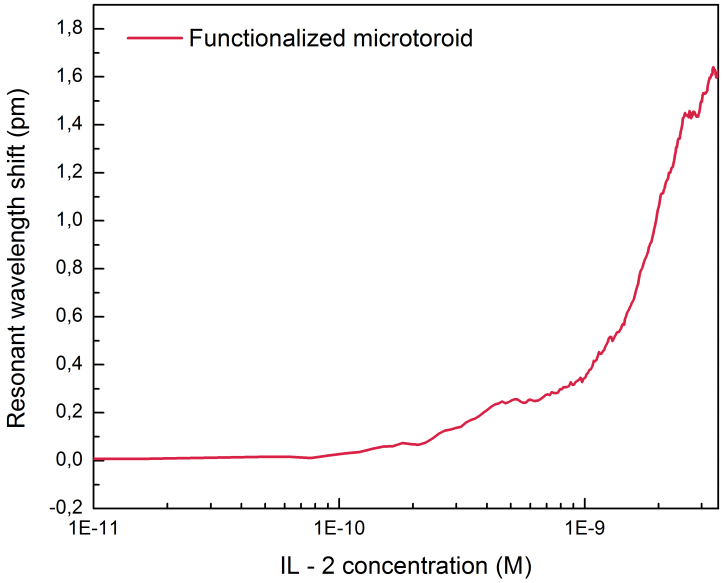

Figure 6.5: The WGM shift with respect to concentration due to the IL - 2 infusion (red line). The human IL - 2 antigen in 1 X PBS buffer was infused to the IL - 2 antibody conjugated microtoroid. The infusion was started at t = 0 and continued for 600 secs with an infusion rate of 5 μl / s. The cumulative data were smoothed by adjacent averaging, considering an averaging time of 1 min.

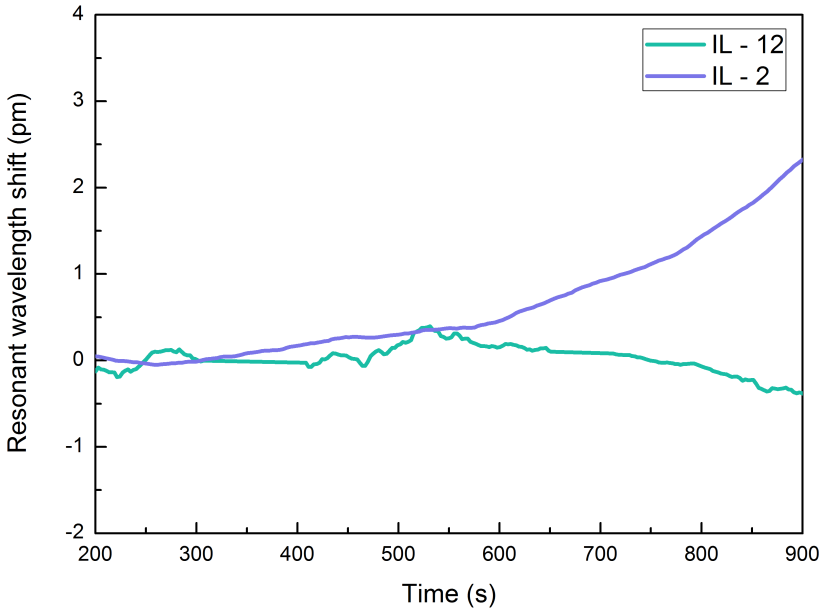

Figure 6.6: The human IL - 2 antigen was detected in 10 v/v % FBS having 1 X PBS buffer. As a control, mouse IL - 12 antigens were infused in complex media. The infusions were both started at t = 0 with an infusion rate of 10 μl / s, and continued for 600 secs. The functionalized microtoroids showed a significant WGM resonance shift during IL - 2 infusion in complex media (purple line), while no significant WGM shift was observed due to the IL - 12 infusion (teal line). The cumulative data were smoothed by adjacent averaging, considering an averaging time of 1 min.

Chapter 7

DNA Hybridization and Point Mismatch Discrimination Using Microtoroids

7.1 DNA Hybridization Using Optical Microresonators

Since the identification of the structure of DNA[164] in 1953, at an increasing pace we are learning more about it. DNA molecules perform 2 important tasks: they replicate themselves by making copies of themselves from the beginning of life and they indirectly supervise the protein expression.[165] Thus, unsurprisingly, there is a tight relationship between various disease states and DNA alterations.[166] Understanding and detecting disease - related variations in DNA molecules are essential in early detection, which increases our chance of living.

There has been a tremendous effort to develop sensitive and sequence - specific DNA sensing platforms until now. Throughout the years, several DNA biosensing approaches have been developed, such as PCR[167], DNA arrays[168], nanomechanical DNA sensors[169], electrochemical DNA sensors[170] and DNA

biosensors based on graphene[172], surface plasmon resonance[172], nano - fiber-ref173 and nanowire[174]. In this subsection, the DNA sensing approaches using optical microresonators are introduced.

It would be beneficial to advert a former work of Vollmer F. and co - workers[130] in which multiplexed quantification of DNA was done using 2 SiO_2 microspheres. In order to hybridize with their fully complementary targets, individually, 27 - mer oligonucleotides of interest were conjugated to dual microspheres via streptavidin - biotin interactions. By evanescently coupling light from a tuneable laser source to dual microspheres in a liquid sample cell, the resonances from each microsphere were identified separately in the transmission spectra as the individual Lorentzian dips. In order to demonstrate the ability of the suggested biosensing platform in terms of distinguishing single mismatch alterations, hybridization between match and mismatch of an 11 - mer oligonucleotide was shown. Also, the mismatch detection ability of the biosensor platform was demonstrated at an optimized specific temperature ($\sim$ 23 °C) and an optimized salt concentration (20 mM tris, 30 mM sodium chloride at pH 7.8). The sensitivity of the suggested technique was reported as 6 pg.mm^{-2} mass loading.

A work of Wu Y. and co - workers[175] can be given as an example of the high specificity and sensitivity of DNA detection as an alternative approach besides its reusability and versatility. DNA loading and unloading from a microsphere was provided via a DNA catalytic network scheme with a LOD of 22 - mer DNA oligonucleotide of $\sim$ 80 pM (32 fmol). Since the suggested idea was based on analyte unloading from the microresonator, a reusable DNA biosensor was obtained using this technology.

Moreover, microrings as another branch of optical resonators are also opportune tools for DNA biosensing[176] and identifying the point mismatches[34, 175, 177] providing high - throughput and real - time analyses with on - chip integrations as in arrays. In a work of A. J. Qavi and co - workers[176] an isothermal approach to discriminate single nucleotide polymorphisms was demonstrated. 32 Si microrings (30 μm in diameter) consisting of reference microrings for thermal drifts on a sensor array were assembled into a flow channel. S - 4FB modified

ss - DNA strands were covalently conjugated to S - HyNic functionalized microrings. Multiplexed DNA detection was provided by hand - spotting 4 different ss - DNA probes having solutions complementary to 4 different target ss - DNAs on a sensor array. Detection of the single base alterations was done by monitoring the desorption rates of the target ss - DNAs leaving the formed DNA duplexes on the biosensor surface.

As one of the prominent examples of the optical microresonator - based DNA detection scheme, a work of M. D. Baaske and co - workers[21] can be given, in which they presented single nucleic acid detections using plasmonic nanorods adsorbed on SiO_2 microspheres. The microspheres as optical resonators are promising and sensitive tools for observing DNA - DNA interactions due to their high Q - factors. However, lowering their detection limits down to single nucleic acids requires integration of the optical microresonators with plasmonic nanoparticles, which enhances the optical field strength at the microresonator surface.[21, 178] Once the intensity of the surface plasmon resonance absorption increases, enhancement of the electric field is obtained. Gold and silver have a mean free path of $\sim$ 50 nm, hence when their sizes are smaller than $\sim$ 50 nm, only interactions with the surface are allowed since bulk interactions are not possible. The surface plasmon resonance condition is satisfied when the wavelength of light is much larger than the size of the nanoparticle and it depends on the size, shape and dielectric constants of the metal and surrounding material.[179] It was reported in the above mentioned study23 that gold nanorod ($\sim$ 12 nm x 12 nm x 42 nm) was chosen as the plasmonic nanoparticle since it provides strong field enhancements.

An alternative approach for detecting formed DNA duplexes with microresonators was demonstrated in the work of R. M. Hawk and co - workers[166]. In this study, a microtoroid was functionalized with GPTMS and then amino - modified 20 - mer ss - DNA probes were covalently conjugated to the microtoroid surface. The hybridization between the probes and their Cy5 - labeled counterparts was detected by a spectrograph. The study proposed a fluorescence - based DNA hybridization technique in real - time with detection of the target ss - DNAs down to 1 nM.

Another approach for the DNA sensing is through the use of OFRRs or liquid core optical ring resonators (LCORRs), which are suitable platforms for a sensitive DNA detection and quantification.[180] The OFRRs offer ring resonator - based biosensing combined with microfluidics technology. A shift in the WGM mode can be observed with a refractive index change at near surface as the target ss - DNAs hybridizing with their probe counterparts attached on the inner surface of the OFRR during sample flow.

Lastly, J. D. Suter and co - workers[181] used an OFRR or LCORR coupled to a tapered fiber (1550 nm) to show the DNA hybridization with targets having different target lengths (25 - 100 bases) and the biosensor was able to distinguish base pair mismatches (from 1 to 5). The inner surface of the OFRR was modified with the 3 - APS molecules and, using a homobifunctional linker DNA, amino modified ss - DNA probes were covalently conjugated to the modified inner surface. The LOD of 25 - mer DNA samples was given as 2.7 x $10^1$0 molecules per cm^2. The mass loading limit of detection was reported in the order of 4 pg.mm^-2, which was closer to the value obtained in the above mentioned study.

7.2 Reducing Steric Hindrance to Increase DNA Hybridization Efficiency

7.2.1 The Approach

Genetic information is the most essential characteristic of life and possibly the mere reason for our existence.[165] As we develop a profound understanding of the genomic material, we increase our chance of apprehending, and moreover treating the physiological and pathological phenomena related to DNA and DNA alterations (i.e., mutations). Biosensor platforms, built to investigate DNA, and particularly DNA mutations have a significant role within this context. Therefore, a tremendous effort has been spent to develop biosensing systems, especially label-free sensors, for DNA studies.[57, 131, 182] Because label - free sensing systems

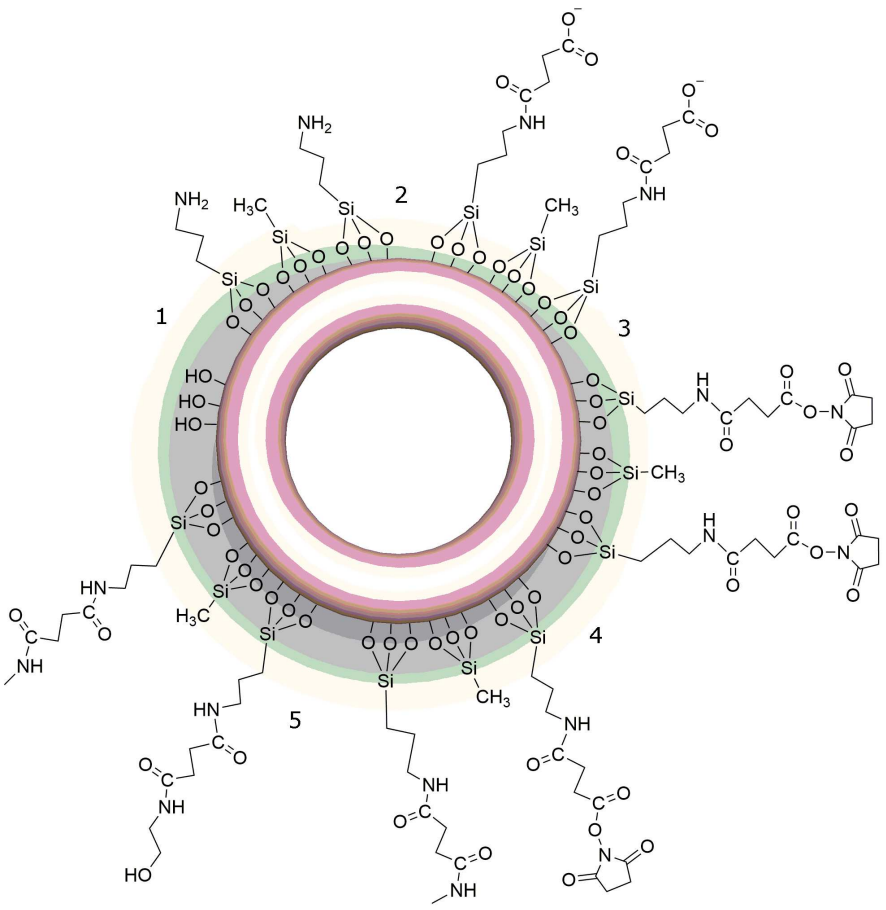

Figure 7.1: Chemical modification of the microtoroid surfaces. (1) APTES / TMMS coating of UV / Ozone pretreated surfaces, (2) Succinic anhydride incubation in DMF for 4 hrs, (3) EDC / NHS incubation in DMF for 2 hr, (4) Covalent NH_2- modified probe ss - DNA conjugation in 1 M KH_2PO_4 at 37 °C overnight, and (5) ethanolamine capping to remove residual NHS - esters.

using optical resonators have significant advantages such as high sensitivity[21], on - chip sensing[82] and real - time monitoring down to a single molecule[132], they still offer the most promising solutions for the biosensing applications.

There are several noteworthy examples[21, 130] regarding detection and characterization of single DNA strands with high sensitivity, accuracy, and efficiency. Target ss - DNA detection via an optical biosensor possessing a selective surface is crucial. Surface density of the probe[183], surface diverseness[184], non - specific interactions[184], probe / target length[185] and ionic strength of the hybridization buffer[186] can affect the yield of hybridization on the surface and

kinetics of target capture. Likewise, tethered ss - DNA conformation[187] and configuration[185] plays a vital role in the hybridization process. Providing configurational freedom to the surface - bound probes by reducing steric hindrance can enhance the efficiency of duplex formation on the surface.[185] Spacer molecules can reduce steric effects by locating the ss - DNA probes away from each other.[184, 188] Thus far, spacer molecules in several studies[189, 190, 191] have been used to increase the hybridization yield.

The approach in this work[208] is the real - time detection of single base pair variation in target ss - DNA using an analogous selective microtoroid surface. To increase selectivity by reducing non - specific interactions, first, the microtoroid surface was coated with mixed silane molecules. As shown in Figure 8.1, TMMS[1] molecules served as spacers[192], and covalent conjugation of the ss - DNA probes was achieved by applying EDC / NHS chemistry to the surface bound APTES[2] molecules.

7.2.2 Silanization of the Microtoroid Surface

The microtoroid surface was cleaned with mild Hellmanex III solution, ultrapure H_2O, ethanol, acetone and H_2O, each for 5 mins, respectively. To induce silanol groups, the cleaned microtoroids were treated with the UV / Ozone cleaning system for 30 mins at room temperature.

Silanization of the microtoroid surface was done by mixing APTES (14 mM) and TMMS (46 mM) organosilanes in ethanol solution[3] was stirred on a lab shaker for 15 mins at room temperature. The UV / Ozone treated microtoroids were immediately inserted into a beaker containing the organosilane solution. The deposition was allowed for 1 hr at room temperature. To remove residual nondeposited organosilanes, the microtoroids were washed several times with the ethanol solution and cured in vacuum for 1 hr at 110 °C.

[1] GC grade, Sigma - Aldrich, USA.
[2] 99 %, Sigma - Aldrich, USA.
[3] 5 v/v % Ultrapure H_2O at pH 4.67 adjusted with acetic acid.

7.2.3 Forming Reactive NHS - Esters on the Microtoroid Surface

A previously described method[137] was utilized for carboxylate group formation on the microtoroid surfaces. To induce carboxylate groups, the coated microtoroids were incubated in nearly saturated succinic anhydride[4] in DMF[5] (containing 1 mg/ml triethylamine[6]) for 4 hrs at room temperature. The microtoroids were then washed with DMF and left in DCC[7] / NHS solution (1:1 M in DMF) for 2 hrs on a lab shaker at room temperature. Then, the microtoroids were washed with DMF and 1 M KH_2PO_4[8] in nuclease - free H_2O (pH 4.5), respectively.

7.2.4 Covalent ss - DNA Conjugation to the Microtoroid Surface

The microtoroids were incubated in 200 nM amino - modified ss - DNA[9] in the 1 M KH_2PO_4 solution (pH 4.5) at 37 °C, overnight, then, washed thoroughly with the KH_2PO_4 solution to remove unbound ss - DNA molecules. To cap any residual NHS - esters, the microtoroids were incubated in 1 M KH_2PO_4 solution containing 1 v/v % ethanolamine[10] for 2 hrs and washed several times with the KH_2PO_4 solution.

[4]GC grade.
[5]Analytical reagent grade.
[6]BioUltra grade.
[7]99 %.
[8]Molecular biology grade.
[9]Single stranded DNA. All amino - modified, Cy5 / Cy3 - labeled, and label free ss - DNA sequences were synthesized with high purity by Sentegen, Turkey.
[10]ACS grade.

7.2.5 Quality Assessment of the Microtoroid Surface Modification

Confocal microscopy studies were conducted to show DNA hybridization using fluorophore-labeled ss - DNA molecules. Confocal microscope (Model LSM 510, Zeiss, Germany) with 20 X objectives was used during the confocal studies. Cy5 and Cy3 dyes were excited using He - Ne lasers at 633 nm and 543 nm, respectively. During all measurements, gain and offset settings were kept constant. Each scan line was averaged 16 times while forming the images. ImageJ program was used to analyze the images. From 3 different points for each image, the backgrounds signals were subtracted from microtoroidal region signals and the relative fluorescence intensities were calculated.

For the confocal microscopy studies Figure 7.2, 3 different microtoroid samples were prepared to verify the suggested surface chemistry: probe ss - DNA (5′ - NH_2 TTGGAACATTC Cy5 3′) conjugated (Figure 7.2a - d), control ss - DNA (5′ - NH_2 TCAAGTCGGCCAA 3′) conjugated / capped (Figure 7.2e - h), and control ss - DNA conjugated / uncapped (Figure 7.2i - l). All microtoroids were incubated in the hybridization buffer containing 200 nM target ss - DNA (5′ Cy3 GAATGTTCCAA 3′) at room temperature for 3 hrs. Following incubation, the microtoroid surfaces were washed once with the buffer to remove unbound ss - DNA molecules. Also, control ss -DNA conjugated / capped microtoroid surface (Figure 7.2m - p) was imaged individually to observe the background fluorescence. Figure 7.2a shows a homogeneous distribution of covalently attached probe ss - DNA, mostly located on the microtoroidal region. Similarly, a homogeneous distribution with signal of the same order was obtained from captured ss - DNA (Figure 7.2b) verifying the hybridization (Figure 7.2d). To our knowledge, this level of homogeneity in microtoroid biofunctionalization, enabling effective target detection from overall surface, was not demonstrated previously. As it can also be clearly seen from Figure 7.2f that the capped microtoroid surface showed a significant reduction in non - specific ss - DNA adsorption while the uncapped surface showed three times higher Cy3 signal arising from heterogeneously adsorbed target ss - DNA (Figure 7.2j). The obtained Cy3 signal from the capped

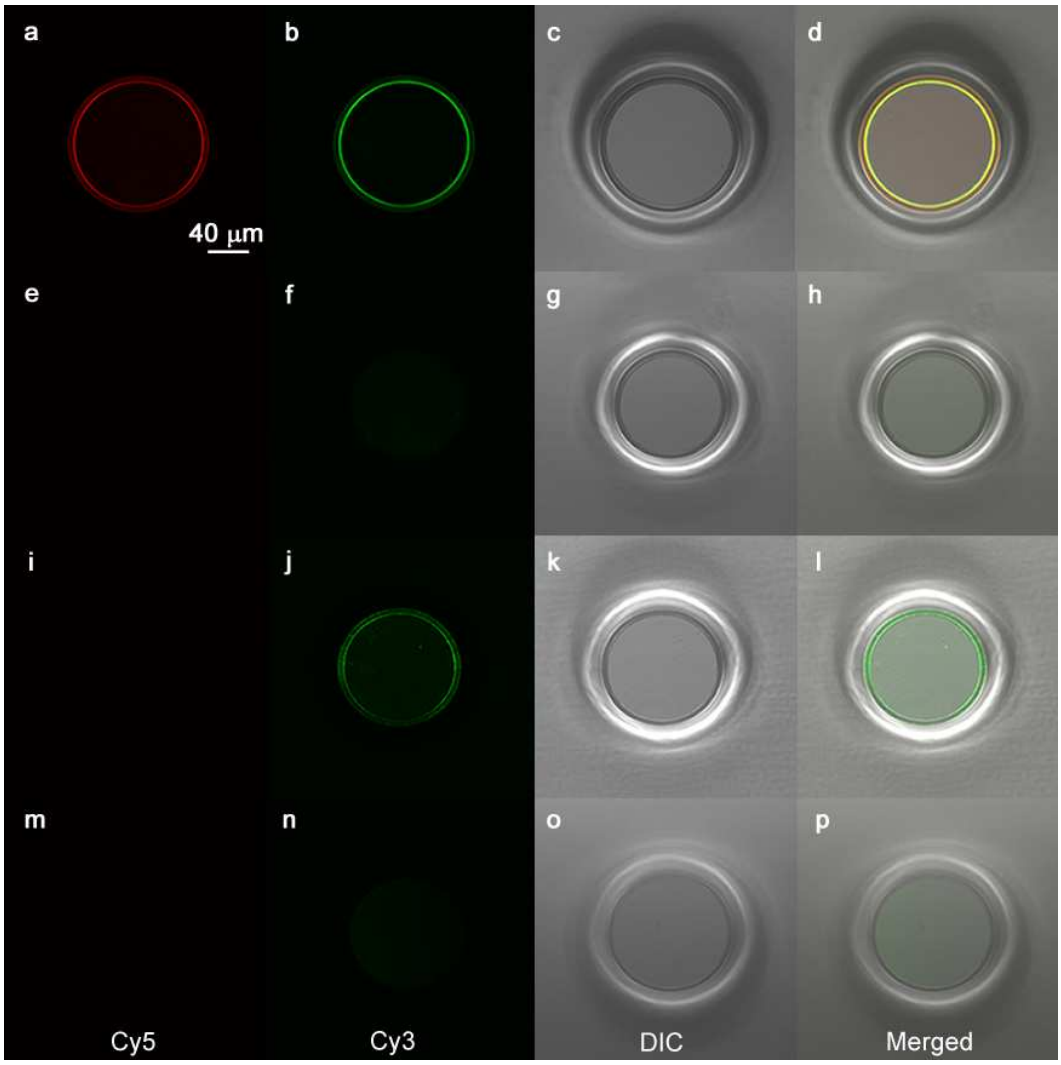

Figure 7.2: Confocal and DIC microscopy images of the (a - d) probe ss - DNA (Cy5 labeled) conjugated, (e - h) control ss - DNA conjugated / capped, (i - l) control ss - DNA conjugated / uncapped microtoroids incubated in 10 mM Tris - HCl / NaCl (pH 7.0) buffer containing 200 nM target ss - DNA (Cy3 labeled) at room temperature for 3 hrs. (m - p) Control ss - DNA conjugated / capped microtoroid was imaged in terms of obtaining background fluorescence. Cy5, Cy3, DIC and merged channels were given, respectively (from left to right for each row). For Cy5, Cy3, DIC, and merged channels, the images were collected separately.

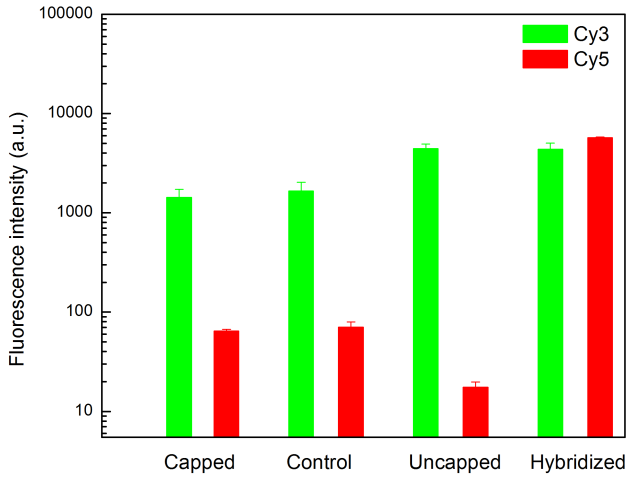

Figure 7.3: Relative fluorescence intensities of the confocal images. Cy3 and Cy5 channels for each image are shown in green and red columns, respectively.

surface (Figure 7.2f) was of the same order with the background signal obtained from the control sample (Figure 7.2n). Relative fluorescence intensities for each channel were given in Figure 7.3.

7.3 The Surface Characterization of the Microtoroids

7.3.1 The Atomic Force Microscopy Studies

Surface morphology of the microtoroids were shown using the AFM in NC mode with a scan rate of 0.75 Hz. From 3 different microtoroidal regions, 1 x 1 m areas were scanned for each microtoroid. The R_q values were calculated using the XEI image processing program.

R_q of a bare microtoroid surface was calculated as 1.25 $\pm$ 0.08 nm (Figure 8.4). R_q values for APTES / TMMS coated (Figure 8.5) and 13 - mer ss - DNA conjugated (Figure 8.6) microtoroid surfaces were calculated as 3.92 $\pm$ 0.21 nm and 3.11 $\pm$ 0.72 nm, respectively. The NC - AFM scans showed a change in the

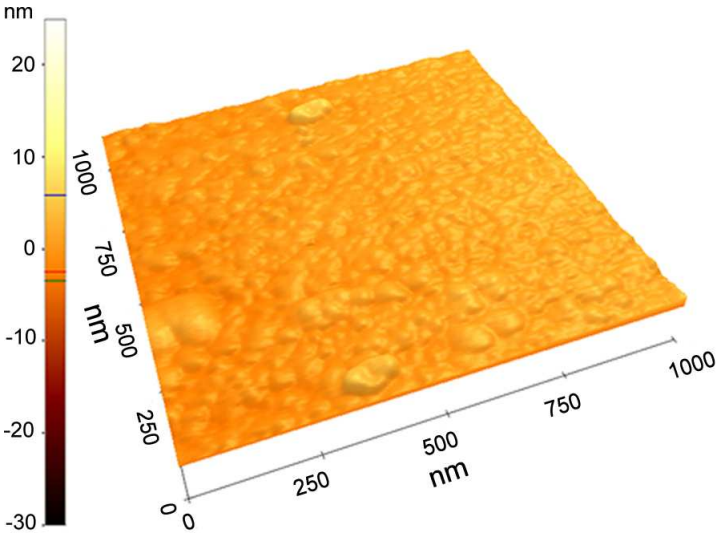

Figure 7.4: 3D, NC - AFM image of a reflowed microtoroid surface. R_q value was calculated as 1.25 ± 0.08 nm. Scan rate was 0.75 Hz.

microtoroid surface morphology at the end of each step.

7.3.2 The X - Ray Photoelectron Spectroscopy Studies

The XPS measurements were performed with the XPS spectrometer (Thermo Fisher Scientific, UK) having Al K - α X - Ray monochromator (0.1 eV step size, 12 kV, 2.5 mA, spot size 100 m). The electron takeoff angle was 90 °C. All high resolution Si2p, O1s, C1s and N1s region scans were conducted 10 times (50 ms dwell time, 30 eV pass energy). For peak calibrations and fittings, Avantage software package was used. "Smart" background type was chosen with "Gaussian - Lorentzian mix" function type. Charge calibration of the binding energy scales were performed accordingly to the neutral C1s peak at 284.8 eV[150].

The detailed Si2p XPS scan of a UV / Ozone - treated microtoroid showed 2 characteristic peaks[193] located at 102.8 and 98.8 eV arising from SiO_2 and Si environments, respectively (Figure 7.7). Similarly, the O1s region scan showed one main peak at 532.3 eV arising from Si - O - H bonding[194]. Additionally, no C1s signal was detected due to the removal of organic contaminants after the

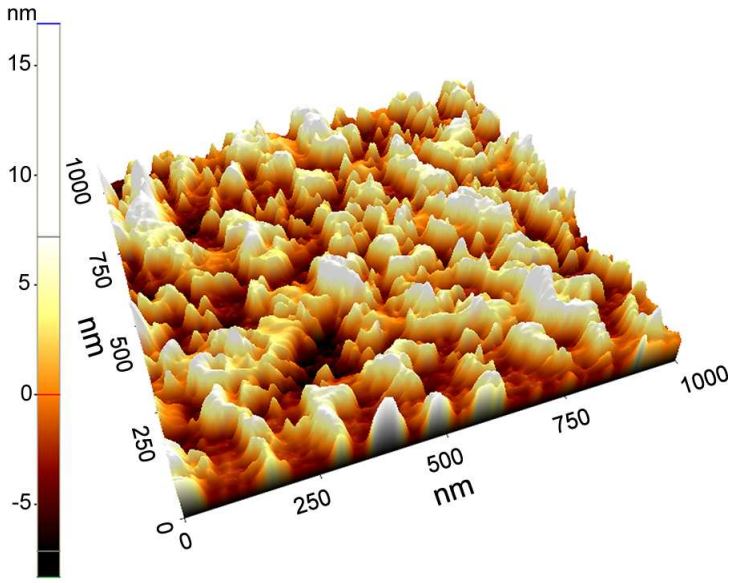

Figure 7.5: 3D, NC - AFM image of APTES / TMMS coated microtoroid surface. R_q value was calculated as 3.92 ± 0.21 nm. Scan rate was 0.75 Hz.

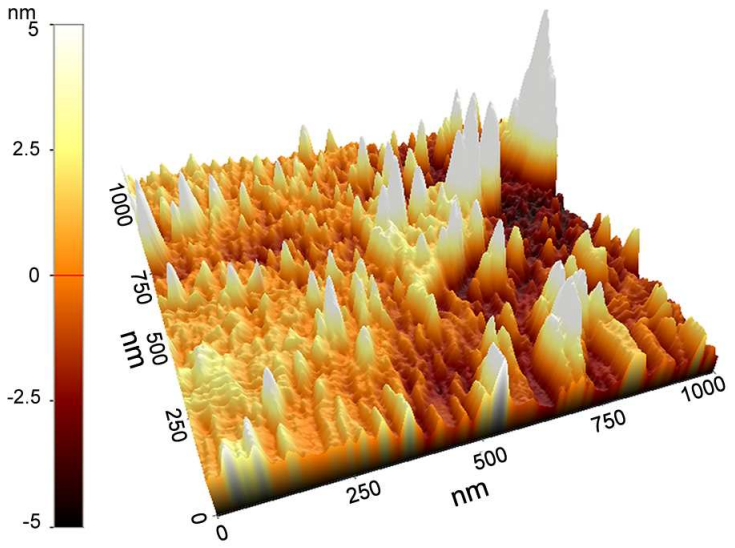

Figure 7.6: 3D, NC - AFM image of 13 - mer ss - DNA conjugated microtoroid surface. R_q value was calculated as 3.11 ± 0.72 nm. Scan rate was 0.75 Hz.

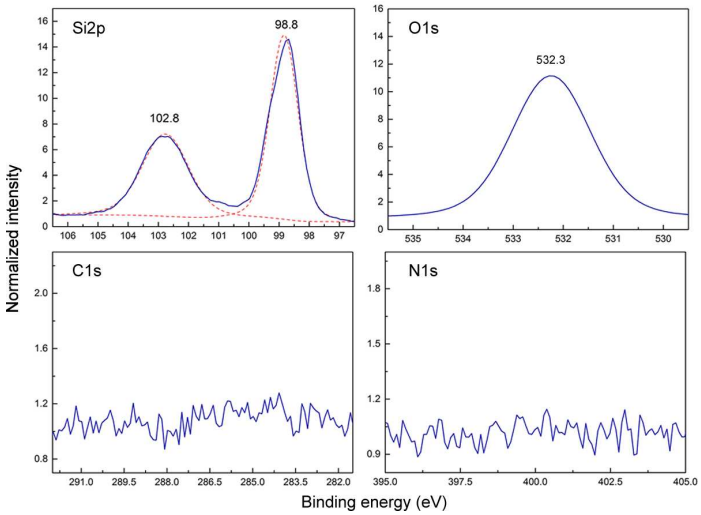

Figure 7.7: High resolution XPS scans of Si2p, O1s, C1s and N1s regions of a 30 mins UV / Ozone treated microtoroid surface.

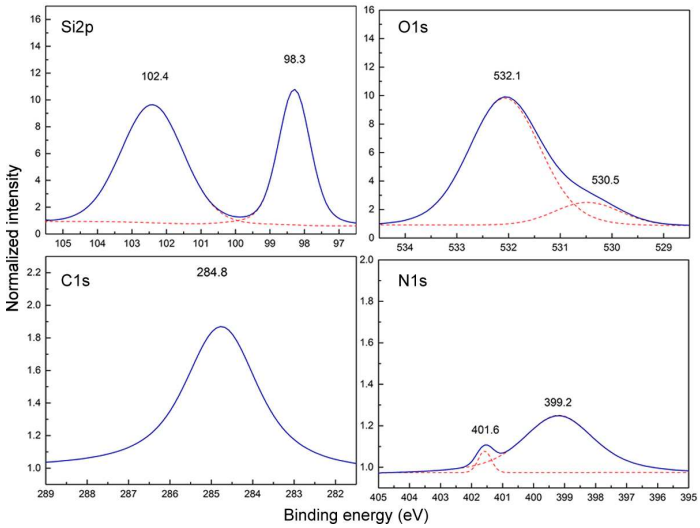

Figure 7.8: The detailed XPS scans of Si2p, O1s, C1s and N1s regions of a APTES / TMMS coated microtoroid surface.

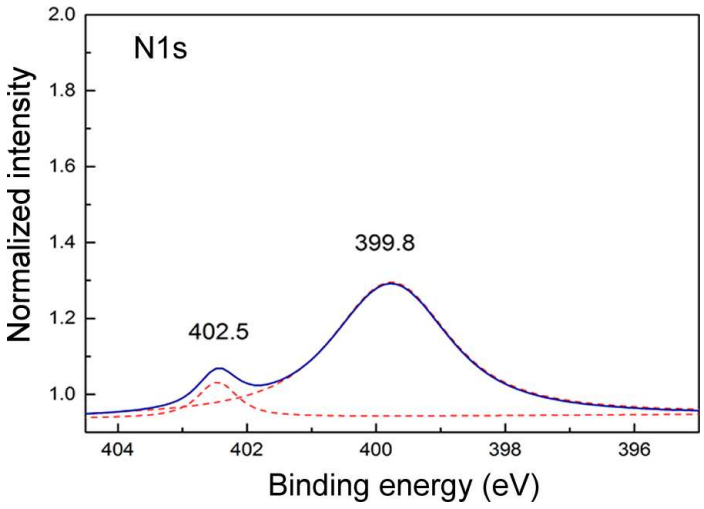

Figure 7.9: The detailed XPS scan of N1s region of a NHS - ester containing microtoroid surface.

UV / Ozone treatment. The C1s scan of an APTES / TMMS coated microtoroid showed 3 peaks located at 286, 285 and 284 eV verifying C - N[195], C - C[196] and C - H[196], and C - Si[197] bondings, respectively, due to covalent bonding of the APTES / TMMS molecules (Figure 7.8). Also, the O1s peak located at 530.5 eV[147] and the increase in intensity of the higher energy Si2p peak after coating, verifies the Si - O bonding[150]. N1s scan showed 2 peaks at 401.6 and 399.2 eV arising from protonated amine (- $NH_3{}^+$) and free amine (- NH_2) groups[196, 198], due to covalent conjugation of APTES molecules, respectively. After applying EDC / NHS chemistry, the N1s region peaks shifted to 402.5 and 399.8 eV verifying the N - O and N - C bondings[147, 157], respectively, due to NHS - ester termination (Figure 7.9).

7.3.3 Surface Bound Probe and Target Densities

To estimate the probe and captured target densities, a previously reported[199] fluorescence based method was used. For both Cy5 and Cy3 dyes, standard calibration curves (Figure 7.10 and Figure 7.11) were obtained accordingly to the method. To obtain fluorescence intensities, labeled ss - DNA containing solutions at varying concentrations were measured using a fluorescence spectrophotometer

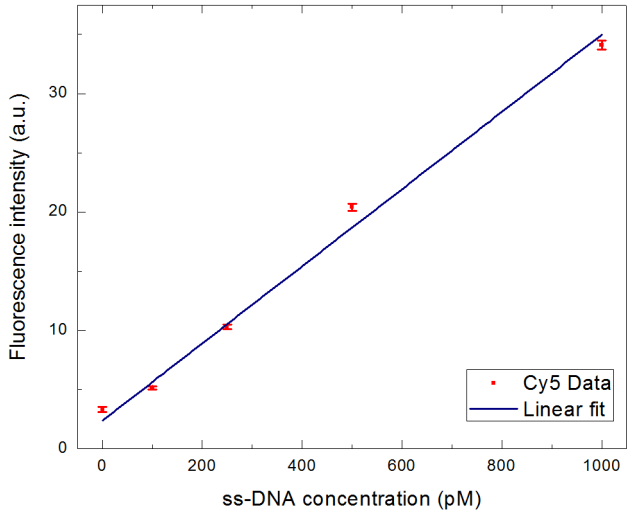

Figure 7.10: Standard linear calibration curve of the probe ss - DNA (5′ - NH_2 TTGGAACATTC Cy5 3′) containing solutions at 0, 100, 250, 500 and 1000 pM.

(Cary Eclipse, Aligent, USA). To estimate probe and captured target densities, a quartz surface having 1.5 cm^2 total area was used.

EDC / NHS chemistry applied following APTES / TMMS coated quartz surface was incubated in 200 pM probe ss - DNA (5′ - NH_2 TTGGAACATTC Cy5 3′) containing 1 M KH_2PO_4 solution (pH 4.5) at 37 °C overnight. After removing the surface, the fluorescence intensity of the solution was measured and the relative concentration was calculated using the equation obtained from the linear fit of the Cy5 data. Then, relative probe number on the quartz surface was calculated by determining the concentration difference before and after the incubation. Afterwards, the surface was capped with ethanolamine and incubated in 200 pM target ss - DNA containing (5′ Cy3 GAATGTTCCAA 3′) 10 mM Tris - HCl / NaCl solution (pH 7.0) at room temperature overnight. The same method was used to determine number of captured targets on the surface. Finally, the relative probe and captured target densities of the quartz surface were estimated. Each measurement was performed three times and given with ± its standard deviation. All parameters were kept the same during measurements. Excitation and emission slits were chosen as 10 nm.

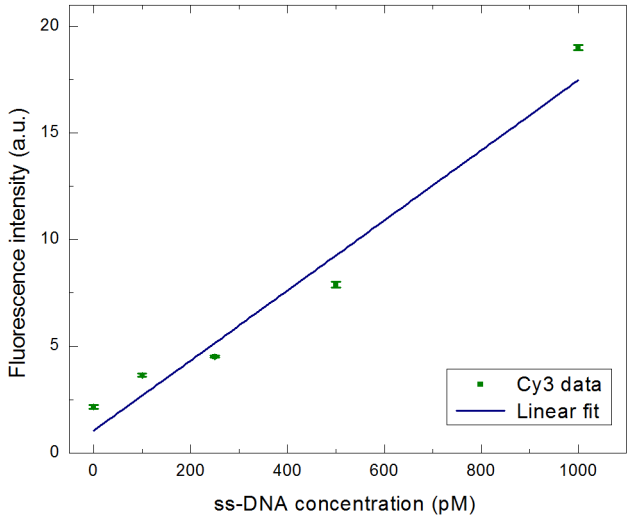

Figure 7.11: Standard linear calibration curve of the target ss - DNA (5′ Cy3 GAATGTTCCAA 3′) containing solutions at 0, 100, 250, 500 and 1000 pM.

After overnight incubations, the surface densities of bound - probe and captured target DNA strands were estimated as 5.5 x 10^{10} probe molecules / cm^2 and 4.6 x 10^{10} target molecules / cm^2, respectively. The results showed a 0.84 surface coverage ratio of captured targets to the attached probes.

7.4 The Optical Measurements

7.4.1 The DNA Hybridization Studies

The biosensing measurements were performed in a 200 μl hybridization buffer as micro - aquarium at room temperature. With a constant flow rate (100 μl / min), infusion and withdrawal of target ss - DNA were simultaneously done using two individual syringe pumps (New Era Pump Systems Inc., USA). Each infused analyte ss - DNA concentration was 200 nM. To avoid any WGM shift due to refractive index change, micro - aquarium and infusion solutions were prepared using the same buffer. After coupling the tapered fiber to the microtoroid, the fiber was fixed to the biosensing stage from both sides using epoxy droplets cured by UV - light. Therefore, undesired displacement of the tapered fiber during

the optical measurements was avoided. Each experiment was repeated at least 3 times and each microtoroid was used only once.

7.4.2 The Effect of DNA Strand Length on the DNA Hybridization

To interpret the WGM shift dynamics with respect to various probe / target lengths, 3 different probe - target pairs were used: 11 - mer (5′ - NH_2 TTGGAGCATTC 3′ and 5′ GAATGCTCCAA 3′), 13 - mer (5′ - NH_2 TCAAGTCGGCCAA 3′ and 5′ TTGGCCGACTTGA 3′), and 15 - mer (5′ - NH_2 TGCCGCTGCACATGG 3′ and 5′ CCATGTGCAGCGGCA 3′) strands. Subsequent to infusion of the complementary strands for each probe individually, we observed the WGM shift responses for 11 - mer (purple), 13 - mer (yellow), and 15 - mer (teal) strands as around 30, 19, and 6 pm, respectively (Figure). The hybridization buffer baseline (gray) is also shown. The standard deviations tended to increase drastically in the regions where a sudden increase or decrease of the WGM shift was observed. This was expected, because the difference between neighboring data in those regions change very rapidly, which is naturally accompanied by the large standard deviations shown in Figure 7.12.

According to our results, the WGM shift tends to increase with decreasing probe / target length, as shown in Figure 7.12. As described formerly, target binding kinetics to the surface attached probes depends on many factors such as DNA strand sequence[200], probe / target length[201], the rate of target diffusion from bulk[202], surface coverage of the attached probes[203], reachability of nucleation sites, and even complementary segment location (complementary to upper or nucleation site - near portion of the probe)[184].

Hinckley and co - workers[200] reported theoretically that short (< 30 - mer), heteregenous DNA sequences did not show consistent trends in terms of hybridization binding rate constants, and the rate constant slightly decreased as the base number increased from 10 - mer to 15 - mer. Also, it had been observed in

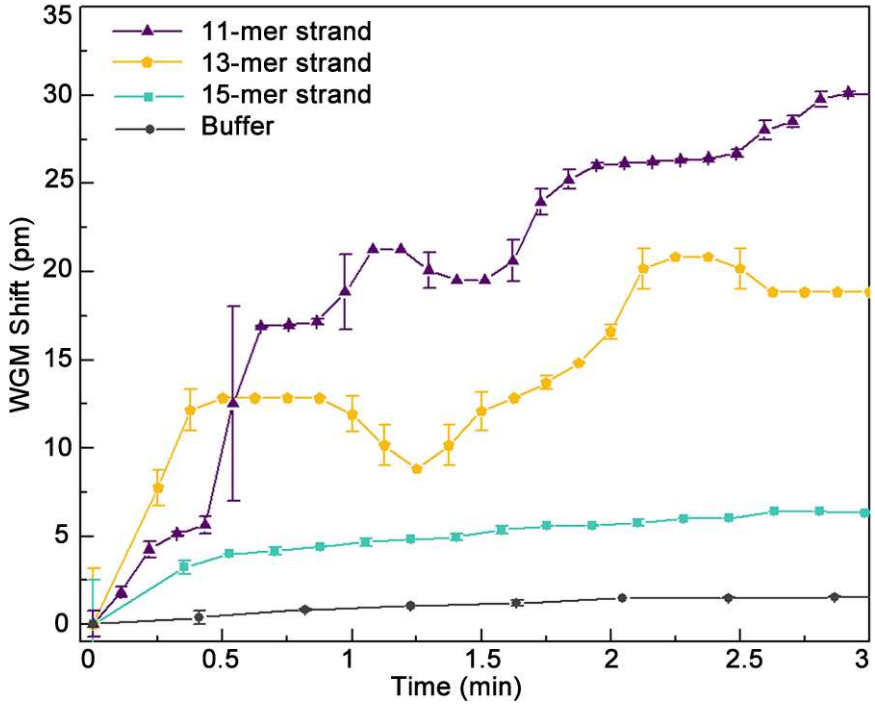

Figure 7.12: WGM shift (pm) of different probe - target pairs: 11 - mer (purple), 13 - mer (yellow), and 15 - mer (teal) strands as well as the hybridization buffer (10 mM Tris-HCl / NaCl, pH 7.0) baseline (gray) versus time (min). Infusions were started at t = 0.

another study43 that increased length decreased the hybridization rate. The observed relationship between the length and the WGM shift for the DNA pairs varying from 11 - mer to 15 - mer, suggests an unpredicted behavior and agrees with the aforementioned study[200].

Although the fact that it is challenging to interpret the data when all the factors considered together, we believe that, the increased pair length can lead to slow target binding kinetics on the biosensor surface by allowing relatively slower target penetration[201] and decrease the number of stable DNA duplexes, thus causing smaller WGM shifts. Another possible effect that can reduce the overall target - probe binding ratio, which is already smaller than unity (0.84) for 11 - mer DNA pair, is the repulsive forces between the negatively charged surface and the target ss - DNA. The longer the strand, the larger this repulsive electrostatic force becomes, because the total negative charge of the DNA increase accordingly, which might contribute to the observed effect.

7.4.3 Real - Time and Selective Detection of Single Nucleotide Mutations in the DNA Strands

To investigate the biosensor response to its complementary, noncomplementary, and point mismatch strands, ss - DNA probes (5′ NH_2 TCAAGTTGGCCAA3′) were conjugated to the microtoroid surfaces. These ss - DNA probes contain a point mutation occurring at early stage mutagenesis of *Pseudomonas aeruginosa* in Cystic Fibrosis (CF) environment. Figure 7.13 shows temporal response of the probe conjugated microtoroid surface to its complementary (5′ TTGGCCAACTTGA 3′), noncomplementary (5′ AGCCAGCCCGGTC 3′), and point mismatch strands (5′ TTGGCCGACTTGA 3′, complementary strand of the wild type sequence).

The inset of the Figure 7.13 shows the biosensor response in terms of ss - DNA concentration (M). It can be seen from Figure 7.13 that due to the DNA hybridization on the microtoroid surface, a significant WGM shift ($\sim$ 22 pm) was

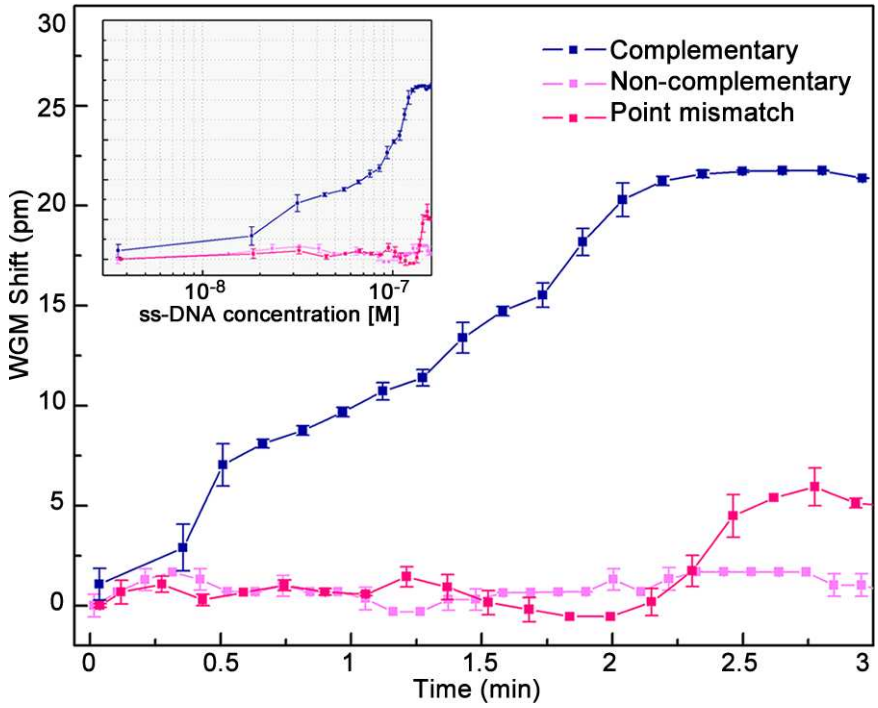

Figure 7.13: The WGM shift (pm) of complementary (navy blue), noncomplementary (light pink), and point mismatch (magenta) strands versus time (min). Inset: the biosensor response in terms of ss - DNA concentration (M) within the microaquarium. Infusions were started at t = 0.

observed (Figure 7.13, navy blue), whereas the biosensor showed no response to the noncomplementary strand (Figure 7.13, light pink). The amount of the shift ($\sim$ 22 pm) is comparable to the shift of its wild - type counterpart which has same strand length (Figure 7.12, yellow). The WGM shift occurring during the DNA hybridization made a plateau at around 133 nM due to the saturation of biosensor surface with the target strands (Figure 7.13, navy blue).

Additionally, a considerably low WGM shift ($\sim$ 5 pm) was observed as a result of the point mismatch strand infusion (Figure 7.13, magenta); yet, the same strand caused a WGM shift of $\sim$ 19 pm with its complementary strand (Figure 7.12, yellow). This demonstrates the feasibility of our microtoroid - based biosensor in specific detection of point mutations. The dramatic difference between the WGM shift magnitudes for the biosensor responses to the complementary and point mismatch strands is most probably caused by 2 main reasons: electrostatic surface repulsion and altered DNA hybridization kinetics. The repulsive interactions occurring on the surface[204, 205] are exerted by the ss - DNA probes and are further enhanced by negatively charged spacer molecules. It is also necessary here to mention that the presence of a base pair mismatch affects the DNA hybridization kinetics by altering thermodynamic stability of the formed DNA duplexes[209] on the microtoroid surface, which yields a significant contribution to a substantially late and low response in terms of the WGM shift.

The LOD[210] for the complementary ss - DNA concentration was calculated as 2.32 nM (Figure 7.13, inset). This value is comparable to a previous report regarding DNA sensing using optical microresonators[130]. It is important to note that, in our experimental setup, the limiting factor of our sensitivity is the wavelength of our tunable laser. If a visible laser operating at around 670 nm was used instead, the sensitivity could be expected to increase a few orders of magnitude, because the absorption in water would be considerably lower at that wavelength.[28]

The most significant result obtained in this experiment is the selective detection of the point mutations thanks to the engineered microtoroid surface. The TMMS molecules were previously shown to form a negatively charged surface

on SiO_2 nanoparticles[206], which is also expected to occur for the SiO_2 microtoroid surface in a similar fashion. It is important to note here that although APTES has a positive charge, after ethanolamine capping following EDC / NHS chemistry, its charge is expected to be negative as well. Considering the fact that DNA has a negative charge overall, the repulsive electrostatic forces (due to bound TMMS molecules on the microtoroid surface and OH- groups formed after ethanolamine capping) seem to be the main reason for the selectivity, whereas fully complementary strands can probably overcome this effect. Although selectivity could be attained using 2 optical microcavities simultaneously[130], it is more convenient to utilize a single microtoroid in terms of reducing experimental complexity, which was demonstrated in this study.

The surface approach that we suggest could also have potential to be utilized in measurements within complex media, such as serum and sputum, because negatively charged surfaces are well - known to possess a substantial protein resistance.[11]

[11]Explained in the following Chapter in detail.

Chapter 8

Label - free Biodetection of Pathogen Virulence Factors in Diluted Artificial Sputum Using Microtoroids

8.1 The Approach

Biodetection in a complex media is a difficult task to perform and several efforts have been done to overcome this challenge. Undesired interaction of the biosensor surface with its surrounding medium can easily lead to a signal and result in a misleading data. For a selective biosensing, calibration is a method used to eliminate signals arising from non - specific interactions, especially in between surface tethered probes like antibodies and non - target components in a complex media; i.e., (non)concentrated solutions of serum and artificial sputum.

However, to effectively eliminate the undesired interactions, surface modification should be carefully applied to the biosensor surface, in a manner that can lead majorly the specific interactions occurring between the targets and their

capture probes. To perform optical measurements in complex media, Y. Shin and co - workers[177] prepared probe conjugated microring arrays to detect DNA biomarkers in human urine. However, lower spectral shifts than the ones obtained from probe - target interactions were reported due to non - specific interactions occuring on the sensor surface. One strategy to eliminate such lower spectral shifts is creating bio - interfaces which supress only the non - specific interactions, while not interfering the biodetection ability. As a step forward in achieving this task, we previously demonstrated a surface modification approach, using THPMP molecules[147], for selective human IL - 2 antigen sensing in a diluted fetal bovine serum[24].

In this study, using the surface modification approach[1], we performed the optical biodetection of *P. aeruginosa* Exotoxin A in a diluted artificial sputum medium, prepared by mimicking the respiratory environment of the CF patients.

8.2 The Role of Pathogen *P. aeruginosa* in CF Disease

The CF disease arises from an occurred mutation in a single gene, which encodes CF transmembrane conductance regulator (CFTR), a chloride ion channel and such a mutation causes a malfunction in the corresponding membrane protein, CFTR, which is commonly found in epithelial cells.[207] The CF disease causes mucus accumulation in the respiratory system, which provides a suitable environment for mucoid bacterial growth and thus causes bacterial infection and inflammation.

The *P. aeruginosa* is the commonly found pathogen in lungs of the CF patients, which causes morbidity and mortality worldwide by pulmonary colonisation. The *P. aeruginosa* shows an extreme resistance to multiple antibiotics by having gradual mutations in its genomic material during the early stage of the

[1]The approach is described in detail in Chapter 5.

CF disease, thus causing chronic infections. Therefore, the detection of the *P. aeruginosa* pathogen is quite critical for early diagnosis and tretment of bacterial infections of the CF patients, which otherwise causes severe morbidity. For the early detection of *P. aeruginosa* related markers, we suggested a microresonator based biosensing approach[2][208] for discriminating early stage point DNA mutations occurring in the pathogen *P. aeruginosa* within the CF environment.

8.3 Conventional Pathogen Related Biomarker Detection Techniques

The *P. aeruginosa* secretes several toxins and virulence factors like exoenzyme S, pyocyanin, elastase, alkaline protease and phenazine pigments, which all mediate toxic effects and thus causes long - term infections. Exotoxin A is a toxin similar to the Exoenzyme S in function[211, 212, 213], which are both secreted by the *P. aeruginosa* pathogen and they have the ability to covalently modify specific proteins in mammalian cells. The Exotoxin A can inhibit protein synthesis like diphtheria toxin since it catalyzes adenosine diphosphate ribosylation of elongation factor 2 protein.[211, 212, 214]

Previously, several approaches were suggested for detecting the *P. aeruginosa* and its species, such as, amplification of the Exotoxin A gene by polymerase chain reaction[211], immunofluorescent - antibody test for *P. aeruginosa* detection in blood culture[215] and *P. aeruginosa* identification by using a disk consisting of phenanthroline and 9 - chloro - 9 - [4 - (diethylamino)phenyl] - 9, 10 - dihydro - 10 - phenylacridine hydrochloride[216]. However, the aforementioned techniques can be considered as labor - intensive, effortful and time - consuming. As an alternative approach, recently, a technique using a lateral flow biosensor[217] has been suggested for visual detection of *P. aeruginosa* genes, which requires amplification and labelling. In this study[218], in order to directly detect *P. aeruginosa* Exotoxin A without any label presence and in a complex medium

[2]The approach is described in detail in the previous Chapter.

like sputum, a highly sensitive technique, which provides high throughput, by exploiting anti - Exotoxin A (α - Exotoxin A) conjugated microtoroidal optical resonators, was suggested. The bio - interface demonstrated here can be widely used in terms of palliating the symptoms of the CF disease by enabling early diagnosis and treatment of bacterial infections.

8.4 Detecting Exotoxin A in Complex Media Using Surface Modified Microtoroids

8.4.1 Preparation of the Artificial Sputum

The artificial sputum medium, which mimics respiratory environment of the CF, was prepared accordingly a previously published protocol[219]. Simply, all essential L - amino acids (250 mg for each, analytical standard grade), except L - Tryptophan, were added to a buffer solution having mucin (from pig stomach mucosa, type III), salmon sperm DNA (MB grade), DTPA (MW 393.35), NaCl (MW 58.44, MB grade), KCl (MW 74.60, MB grade) and Tris base (MW 121.14) under continuous stirring, as described in the protocol[219]. Then, the solution pH was stabilized to 7.0 using Tris base and the total volume was raised to 1000 ml by adding MB[3] grade H_2O. Under sterile conditions, L - Tryptophan and egg yolk emulsion (microbiology grade) were added respectively, following sterilization of the medium at 110 °C for 15 mins in an autoclave (Tuttnauer, Germany). Before any use, the aliquoted sputum samples were kept in a cold-room at 4 °C. The photograph of the prepared artificial sputum medium is shown in Figure 8.1.

[3]Molecular biology.

Figure 8.1: The photograph of the prepared artificial sputum.

8.4.2 Covalent anti - Exotoxin A Conjugation for a Selective Biodetection

The surface cleaning of the fabricated microtoroids was done using mild Hellmanex III solution, ultrapure H_2O, ethanol (HPLC grade), acetone (HPLC grade) and ultrapure H_2O, respectively. In order to activate the microtoroid surface, 5 mins Piranha cleaning was applied at 60 °C after the UV / Ozone treatment for 15 mins in ambient air.

Following the surface activation, the microtoroids were immediately incubated in a methanol solution[4] containing 2 v/v % THPMP molecules for 1 hr at room temperature to form a thin THPMP film, as also described previously [35, 36]. Following the incubation, the microtoroid surface was washed gently with the methanol solution and cured at 100 °C under vacuum for 1 hr using a vacuum oven (Thermo Scientific, USA). The THPMP coated microtoroid surface was activated using 5 mM EDC in the MES buffer for 2 hrs at room temperature. Then, anti - Exotoxin A (α - Exotoxin A)[5] (at 1 : 50 dilution in 1 X PBS) was covalently conjugated to the activated surface. The α - Exotoxin A conjugation to the microtoroid surface was performed at 4 °C for 2 hrs. Residual, unbound antibodies were removed from the microtoroid surface by washing thoroughly

[4] 5 v/v % ultrapure H_2O containing methanol (analytical reagent grade), at pH $\sim$ 4.6 adjusted by acetic acid (ACS reagent grade).

[5] Antibody from *P. aeruginosa*, whole antiserum, produced in rabbit, Sigma - Aldrich, USA.

with the 1 X PBS buffer. Before any use, the 1 X PBS buffer was filtered with a sterile syringe filter (Gema Medical S. L., Spain) having 0.20 μm pore size.

8.4.3 The Surface Characterization

For surface morphology studies, an AFM (PSIA, Korea) was used in NC mode with a scan rate of 0.66 Hz and a 1000 x 1000 nm^2 scan area. The R_q values were calculated using the XEI image processing software. For the static contact angle measurements, the contact angle meter (DataPhysics, Germany) was used. With a 4 μl dosing volume and 1 μl / s dosing rate, each measurement was performed 3 times with different samples. The static contact angles of bare surfaces were calculated using GIMP 2.8 software while the contact angles of the functionalized surfaces were calculated using SCA20 software. During all surface characterisation studies, 1 m thermal oxide SiO_2 having Si wafers (diced into 0.5 x 0.5 cm) were used.

In order to demonstrate the fabricated microtoroids besides verifying the surface coating, AFM studies and contact angle measurements were conducted. As expected, the surface morphologies, gathered by the NC - AFM scannings, showed a smooth, bare SiO_2 surface after the UV / Ozone cleaning (Figure 8.2a,b) and a rough surface (Figure 8.2c,d) was observed after functionalizing the surface with the α - Exotoxin A molecules. The R_q value for the bare SiO_2 surface was obtained as 0.45 nm, agrees with our other study[147]. The corresponding line profile of the 2D image, shown with a blue line, was given in Figure 8.2b, demonstrating a smooth SiO_2 surface. As can be seen in the 3D AFM image of the α - Exotoxin A functionalized surface (Figure 8.2c) and in the corresponding line profile (Figure 8.2d), the surface roughness was increased apparently and the Rq value was calculated as 1.24 nm. The α - Exotoxin A molecules were uniformly bound to the SiO_2 surface, as also observed in the previously published protein immobilization studies[220, 221].

The contact angle measurements were also verified the surface functionalization. As can be seen from the photographs (Figure 8.3a and Figure 8.3b), a

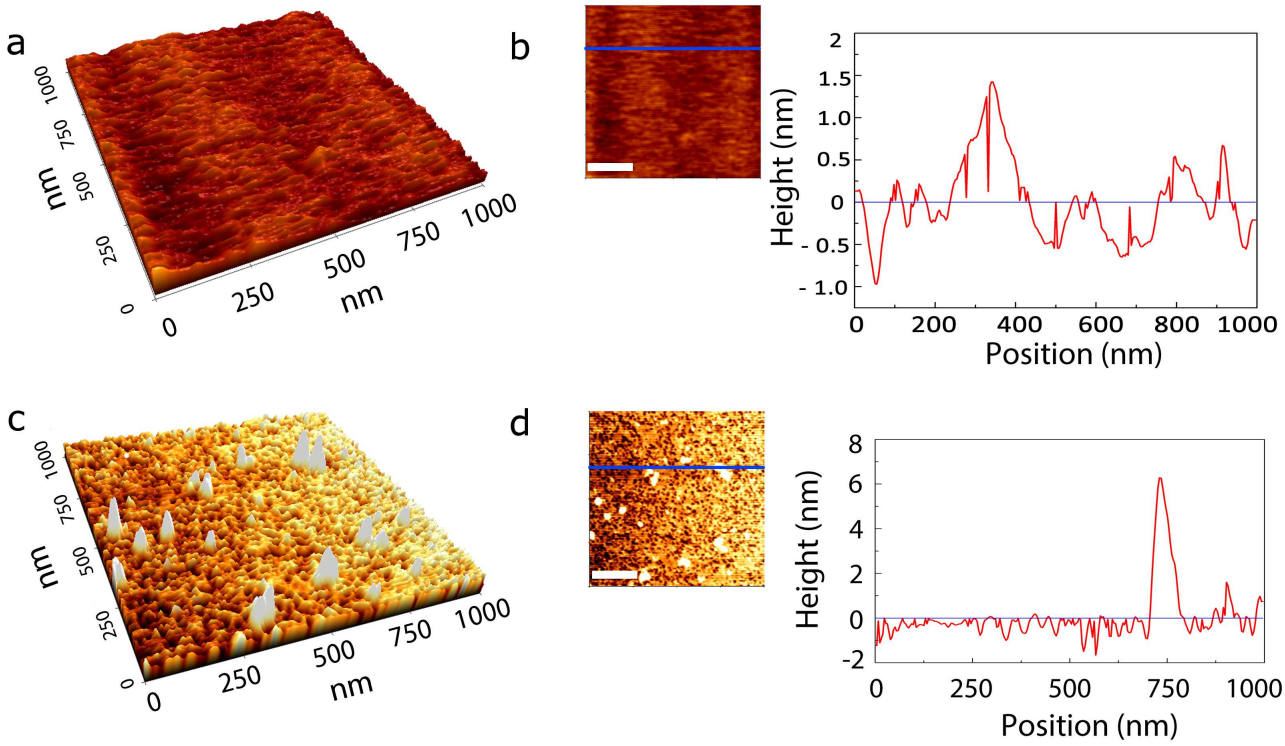

Figure 8.2: NC, 3D AFM scans show (1000 nm) a (a) bare and (c) α - Exotoxin A functionalized SiO_2 surfaces with their 2D views and line profiles, (b) and (d), respectively. Scale bar is 250 nm.

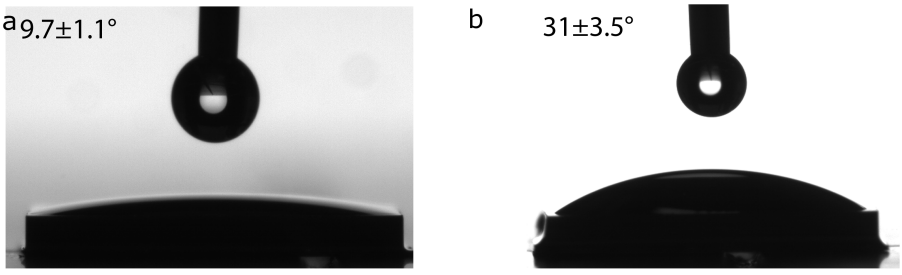

Figure 8.3: The photographs of water droplets (4 μl) on the (a) bare and (b) α - Exotoxin A functionalized SiO_2 surfaces.

dramatic increase in the contact angle was observed. The contact angles of the bare and the α - Exotoxin A conjugated surfaces were calculated as 9.7 $\pm$ 1.1 $^{\circ}$ and 31 $\pm$ 3.5 $^{\circ}$, respectively.

8.4.4 The Confocal Studies

For confocal studies, the anti - GFP[6] conjugation (20 μg / ml in filtered 1 X PBS), to the THPMP modified microtoroid surface, was done at 4 °C for 4 hrs in a dark environment. To remove unbound anti - GFP molecules, the microtoroid was washed thoroughly with the filtered 1 X PBS solution. Then, the microtoroid was incubated in GFP[7] (8 μg / ml) having filtered 1 X PBS solution at 4 °C for 4 hrs in a dark environment. Finally, washing with the filtered 1 X PBS solution was done to remove non - interacted GFP molecules. The confocal measurements were performed using a confocal microscope (Zeiss, Germany) with 20 X objectives. The excitation of the anti - GFP and GFP molecules were done at 633 nm using He - Ne laser and 477 nm using Argon laser, respectively. While gathering the images, each scan line was averaged 16 times. To analyze the images, fluorescence intensity of each image was calculated using GIMP 2.8 software, for both red (anti - GFP) and green (GFP) channels and the intensities are given with $\pm$ its standard deviation.

In order to demonstrate the bioconjugability of the microtoroid surfaces, the anti - GFP molecules were covalently attached to a THPMP modified microtoroid surface. Then, the anti - GFP functionalized microtoroid was incubated in the GFP having filtered 1 X PBS solution to verify antibody - antigen interactions on the surface engineered microtoroid. As a positive control, the confocal images of a bare microtoroid were gathered and the corresponding fluorescence intensities were compared with intensities obtained from confocal images of an anti - GFP functionalized microtoroid. In DIC, anti - GFP and GFP channels, Figure 8.4a - c and 8.4d - f show the images of the bare and the anti - GFP functionalized

[6]Monoclonal GFP antibody with CF^{TM}633 dye conjugate, produced in mouse, Sigma - Aldrich, USA.

[7]MW 39 kDa, produced in *Escherichia coli*, Abcam, UK.

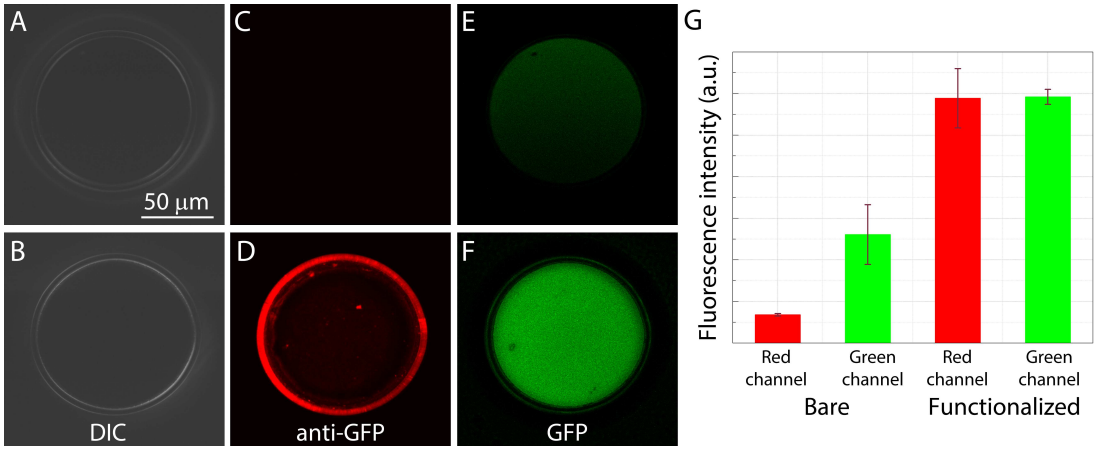

Figure 8.4: The anti - GFP conjugation to demonstrate bio - functionalization of the THPMP modified microtoroidal resonators. (a - b) DIC, (c - d) anti - GFP and (e - f) GFP channels for a bare (top row) and an anti - GFP conjugated (bottom row) microtoroids. The anti - GFP conjugated microtoroid was incubated in GFP solution for 2 hrs. (g) Related fluorescence intensities (a.u.) of the bare and functionalized microtoroids in red (anti - GFP) and green (GFP) channels.

microtoroids, respectively.

The calculated intensities of each channel were given in Figure 8.4g. For the red (anti - GFP) channel, the intensity of the functionalized microtoroid was $\sim$ 11 - fold higher than the background signal obtained from the bare microtoroid surface, due to the signal arising from the anti - GFP molecules attached covalently to the microtoroid surface. Additionally, $\sim$ 5 - fold higher signal than of the bare microtoroid showed, was obtained from the GFP molecules bound to their antibodies. As a result, the confocal studies showed the antibody - antigen binding capacity of the suggested microtoroid surface modification approach.

8.4.5 Stationary Baselines in the Diluted Artificial Sputum

Due to undesired adsorption of the ingredients in the diluted artificial sputum, significant WGM shifts from the bare microtoroids were obtained (Figure 8.5a). After 3 mins, the resulted WGM shift obtained from the 3 experiments was 8.49

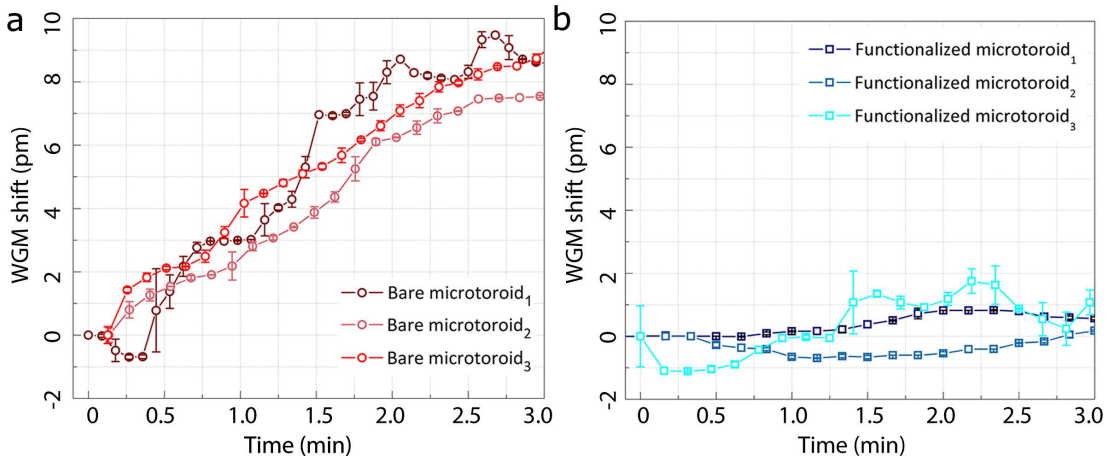

Figure 8.5: Resistance of the THPMP coated microtoroid surface to the artificial sputum medium. The responses of (a) bare (red circles) and (b) α - Exotoxin A functionalized (blue squares) microtoroids in 200 μl, 10 v/v % artificial sputum having 1 X PBS at room temperature. Both experiments were repeated 3 times with different microtoroid batchs using a 1550 nm tunable laser. Also, each data was recorded with 100 ms sweep delay and each 3 data was represented as 1 mean data with $\pm$ its standard deviation.

$\pm$ 0.83 pm. On the other hand, during 3 mins, no significant responses were obtained from the α - Exotoxin A functionalized microtoroids in the diluted artificial sputum (Figure 8.5b). It is worthy here to note that, sudden changes in data, such as increases or decreases, result in large standard deviations. According to the results, for the bare microtoroids, the WGM shifts tended to increase dramatically while the functionalized ones showing a significant resistance in the diluted artificial sputum medium. This considerable reduction in the WGM shift occuring due to resistance behaviour of the THPMP coating, as providing a suitable platform for selective Exotoxin A detection in complex media.

Inlet Exotoxin A flow and outlet bulk flow (at 25 μl / min constant flow rate) were supplied to the system using the individual syringe pumps. The syringe concentration of the Exotoxin A was 500 ng / ml in diluted sputum medium (10 v/v % in 1 X PBS).

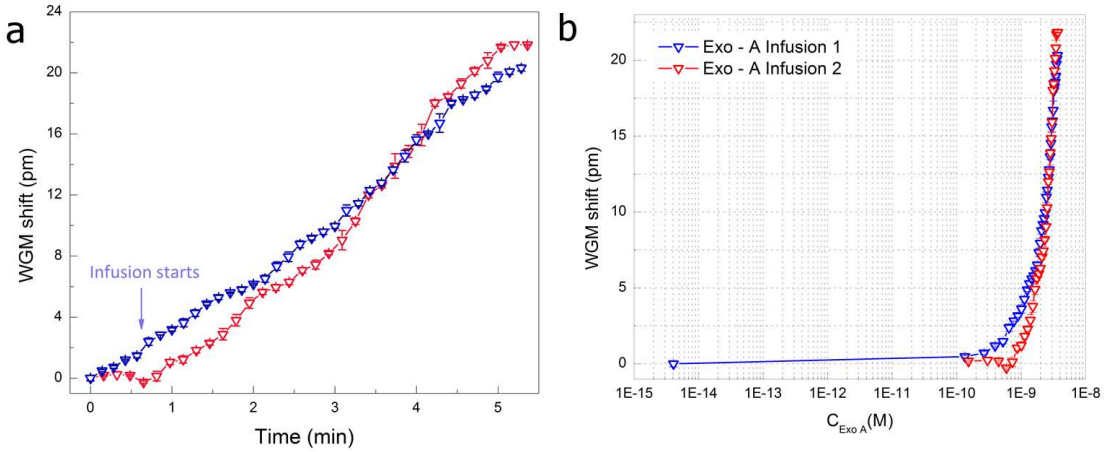

Figure 8.6: Selective Exotoxin A detection in the complex media. Responses of 2 different α - Exotoxin A conjugated microtoroid batchs to Exotoxin A infusions with respect to (a) time (min) and (b) concentration, C_{ExoA} (M). Each experiment was taken in 200 μl diluted artificial sputum with 25 μl / min infusion / withdrawal flow rate, at room temperature. Each data was shown with triangles (as a mean data) in different colors (blue and red), with their error bars. The syringe concentration of Exotoxin A was 500 ng / ml in 10 v/v % artificial sputum in 1 X PBS. Both infusions were started at $\sim$ 0.65 mins. Also, each data frame was recorded with 100 ms sweep delay.

8.4.6 Selective Biodetection of Exotoxin A in the Diluted Artificial Sputum

To demonstrate the potential of α - Exotoxin A conjugated microtoroids in selective Exotoxin A[8] detection, the functionalized microtoroid was immersed into the diluted artificial sputum medium and introduced Exotoxin A molecules, in a controlled manner. To avoid any refractive index change during the optical measurements, 10 v/v % artificial sputum in 1 X PBS was used as the micro - aquarium and the syringe buffer.

As given in Figure 8.6a and Figure 8.6b interacting α - Exotoxin A and Exotoxin A molecules caused significant WGM shifts of $\sim$ 21.79 pm (red data), $\sim$ 20.04 pm (blue data). The time, at which the Exotoxin A infusion was started ($\sim$ 0.65 mins), was indicated by an arrow. The WGM shifts reached to a plateu at

[8]Exotoxin A from *P. aeruginosa*, MW 66 KDa, Sigma - Aldrich, USA.

$\sim$ 5 mins. From the concentration calculations accordingly to the described formula within the text, the LOD value[210] was obtained as 2.45 nM (Figure 8.6b). As can be concluded from the Figure 8.6, the α - Exotoxin A conjugated microtoroid surfaces showed resistance to any non - specific interactions in the diluted artificial sputum while providing selective and sensitive Exotoxin A detections.

Chapter 9

Conclusion

As a brief overview of the main outcomes of this thesis, the novel surface modification for a dual surface having microtoroid, described in detail, provided ability in higly selective and highly sensitive biodetections of various antigens in the complex media such as diluted FBS or artificial sputum. Additionally, it was also demonstrated that the microtoroids as optical resonators could provide excellent platforms for discriminating DNA strands in terms of single base pair alterations by applying a novel surface chemistry. The aforementioned surface approach has a great ability to increase DNA hyridization efficiency and reduce undesired ss - DNA interactions on the resonator surface, simultaneously.

This last section is also devoted to providing the general strategies that can be applied in order to enhance the applicability of the WGM type biosensors, anticipating their large - scale applications. Material constraint is a critical point in the biosensor technology. Although Si and SiO_2 are relatively cheap materials, and chip scale production techniques are quite successful, plastics still constitute a considerably cheaper alternative, which is more suitable for mass production. A microfabricated optical microresonator can be utilized to form a mold, which then can be used to mass produce optical microresonators from plastics.[222] This means considering a new surface chemistry for bioconjugation as well, but there already exist versatile methods for chemically modifying plastics.[223]

There are also various other geometries of microresonators that have not been used for oligonucleotide - based biodetection. Microgoblets[224] and microbubbles[225] are 2 notable microresonator types that can be exploited for this purpose. Microgoblets are formed as polymer structures standing on Si pillars, similar to microtoroids. They can be batch produced, and they can be used as microlasers by incorporating fluorescent molecules in their polymer. Laser is pumped by free space coupling, which is comparably easier than evanescent coupling, and the shift in the lasing wavelength could be monitored for biosensing.[224]

Microbubbles, on the other hand, are structures similar to the OFFR resonators, but light is coupled to a bubble formed by arc discharge on the glass capillary. This enhances the Q - factor by forming a trap for the travelling light. They could be functionalised in a manner similar to that of the OFFRs.[225] The optical coupling of the WGM - type biosensors remain one of the greatest challenges. On - chip coupling of microtoroids[27] has been previously demonstrated in various studies. More robust methods for on - chip coupling of particularly the STIMs are quite critical regarding this aspect. This would enable an easy microfluidic integration, greatly enhancing the applicability of these biosensors.

One serious problem related to optical biosensing using the WGM microresonators is the expensive machinery behind it. Especially, tunable lasers are costly research tools, and the whole system requires to be elaborately engineered during construction, operation, and maintenance. While current technology enables observation of extremely sharp resonances, tracking them for ultimate sensitivity also requires sensitive, thus expensive devices.

Therefore, a compromise should definitely be made. Point - of - care applications, for instance, do not necessarily require single molecule sensitivity; yet, increasing the shifts from the order of picometers towards nanometers could enable the tunable lasers to be replaced with generic laser diodes. The miniaturization of the system can go further if new laser sources can be developed by microresonators themselves. This could be attained by sensitivity enhancement techniques such as post recognition binding of bulky moieties[105] or catalytic mass unloading[175].

Plasmonic enhancement could be exploited as well to increase the sensitivity of the microresonator towards perturbations in the medium.[21, 226] In this way, detection could be performed by intensity interrogation, in a similar fashion to the SPR measurements by tracking the intensity at a fixed wavelength around the resonant wavelength[227] instead of the spectral shift, providing high - throughput analyses.

On the other hand, single molecule detection experiments can help scientists to decipher many mysteries of life currently inaccessible with contemporary techniques. Single molecule binding events can be observed by using the WGM - type optical microresonators. The WGM biosensors are among the few tools that enable such a difficult task. For a reliable and re - producreproducible experimental set - up to be devised, the coupling problem should be seriously solved to a larger extent, enabling multiplexed detection.

Moreover, the WGM resonators can provide various information about molecular orientations[228] and conformational changes[229], since they support 2 orthogonal polarizations: the TE and TM modes. An electromagnetic wave at a certain polarization can cause a shift both in the TE and in the TM modes since optical anisotropy in the refractive index occurs due to the preferred direction of self - assembled molecules adsorbed on the microresonator surface.[16] The aforementioned idea can be utilized to understand orientations and conformational changes of oligonucleotide molecules, self - assembled on a WGM resonator surface in a label - free manner.

Furthermore, surface engineering of the optical microresonators should seriously consider specificity as well as sensitivity. This applies whether an application is for a point - of - care detection or a single molecule measurement. There are recent examples of highly specific detections of oligonucleotides[208] as well as antigens[24]. Research in this field is promising when these results are considered.

To conclude, the optics possesses important possibilities regarding increasing the quality of our lives and extending our knowledge about the nano world. Referring to accurate questions would probably lead the scientific knowledge towards

unprecedented answers, expanding our horizon.

Bibliography

[1] M. Baaske and F. Vollmer, "Optical resonator biosensors: molecular diagnostic and nanoparticle detection on an integrated platform" *ChemPhysChem*, vol. 13, no. 2, pp. 427 – 436, 2012.

[2] X. Guo, "Surface plasmon resonance based biosensor technique: a review" *J. Biophotonics*, vol. 5, no. 7, pp. 483 – 501, 2012.

[3] G. J. Zhang and Y. Ning, "Silicon nanowire biosensor and its applications in disease diagnostics: a review" *Anal. Chim. Acta*, vol. 749, pp. 1 – 15, 2012.

[4] J. Tamayo, P. M. Kosaka, J. J. Ruz, Á. S. Paulo and M. Calleja, "Biosensors based on nanomechanical systems" *Chem. Soc. Rev.*, vol. 42, pp. 1287 – 1311, 2013.

[5] S. U. Senveli, Z. Ao, S. Rawal, R. H. Datar, R. J. Cote and O. Tigli, "A surface acoustic wave biosensor for interrogation of single tumour cells in microcavities" *Lab Chip*, vol. 16, pp. 163 – 171, 2016.

[6] T. Goda, K. Masuno, J. Nishida, N. Kosaka, T. Ochiya, A. Matsumoto and Y. Miyahara, "A label-free electrical detection of exosomal microRNAs using microelectrode array" *Chem. Commun.*, vol. 48, pp. 11942 – 11944, 2012.

[7] O. Avci, N. L. Ünlü, A. Y. Özkumur and M. S. Ünlü, "Interferometric reflectance imaging sensor (IRIS) a platform technology for multiplexed diagnostics and digital detection" *Chem. Commun.*, vol. 15, pp. 17649 – 17665, 2015.

[8] J. Haus, "Optical sensors: basics and applications" *Wiley-VCH*, Darmstadt, Germany, 2010.

[9] F. S. Ligler and C. R. Taitt, "Optical biosensors: today and tomorrow" *Elsevier*, Hungary, 2008.

[10] B. E. Rapp, F. J. Gruhl and K. Länge, "Biosensors with label-free detection designed for diagnostic applications" *Anal. Bioanal. Chem.*, vol. 398, no. 6, pp. 2403 – 2412, 2010.

[11] H. K. Hunt and A. M. Armani, "Label-free biological and chemical sensors" *Nanoscale*, vol. 2, no. 9, pp. 1544 – 15592, 2010.

[12] S. Mehrabani, A. J. Maker and A. M. Armani, "Hybrid Integrated Label-Free Chemical and Biological Sensors" *Sensors*, vol. 14, no. 4, pp. 5890 – 5928, 2014.

[13] D. W. Kimmel, G. LeBlanc, M. E. Meschievitz and D. E. Cliffel, "Electrochemical sensors and biosensors" *Anal. Chem.*, vol. 84, no. 2, pp. 685 – 707, 2012.

[14] J. R. Crowther, "ELISA: theory and practice" *Humana Press Inc*, New Jersey, USA, 1995.

[15] C. Chen, Q. Xie, D. Yang, H. Xiao, Y. Fu, Y. Tan and S. Yao, "Electrochemical sensors and biosensors" *RSC Adv.*, vol. 3, no. 14, pp. 4473 – 4491, 2013.

[16] F. Vollmer and S. Arnold, "Whispering-gallery-mode biosensing: label-free detection down to single molecules" *Nat. Methods.*, vol. 5, pp. 591 – 596, 2008.

[17] K. J. Vahala, "Optical microcavities" *Nature*, vol. 424, pp. 839 – 846, 2003.

[18] M. J. Banuls, R. Puchades and A. Maquieira, "Chemical surface modifications for the development of silicon-based label-free integrated optical (IO) biosensors: a review" *Anal. Chim. Acta*, vol. 777, pp. 1 – 16, 2013.

[19] M. S. Luchansky and R. C. Bailey, "High-Q optical sensors for chemical and biological analysis" *Anal. Chem.*, vol. 84, no. 2, pp. 793 – 821, 2012.

[20] I. Ament, J. Prasad, A. Henkel, S. Schmachtel and C. Sonnichsen, "Single unlabeled protein detection on individual plasmonic nanoparticles" *Nano Lett*, vol. 12, no. 2, pp. 1092 – 1095, 2012.

[21] M. D. Baaske, M. R. Foreman and F. Vollmer, "Single-molecule nucleic acid interactions monitored on a label-free microcavity biosensor platform" *Nat. Nanotechnol.*, vol. 9, pp. 933 – 939, 2014.

[22] T. J. Kippenberg, S. M. Spillane, B. Min and K. J. Vahala, "Theoretical and experimental study of stimulated and cascaded Raman scattering in ultrahigh-Q optical microcavities" *IEEE J. Sel. Top. Quantum Electron.*, vol. 10, no. 5, pp. 1219 – 1228, 2004.

[23] S. Arnold, M. Khoshsima, I. Teraoka, S. Holler and F. Vollmer, "Shift of whispering-gallery modes in microspheres by protein adsorption" *Opt. Lett.*, vol. 28, no. 4, pp. 272 – 274, 2003.

[24] E. Ozgur, P. Toren, O. Aktas, E. Huseyinoglu and M. Bayindir, "Label-free biosensing with high selectivity in complex media using microtoroidal optical resonators" *Sci. Rep.*, vol. 5, 13173, 2015.

[25] P. Toren, E. Ozgur and M. Bayindir, "Oligonucleotide-based label-free detection with optical microresonators: strategies and challenges" *Lab Chip*, vol. 16, no. 14, pp. 2572 – 2595, 2016.

[26] D. K. Armani, T. J. Kippenberg, S. M. Spillane and K. J. Vahala, "Ultra-high-Q toroid microcavity on a chip" *Nature*, vol. 421, pp. 925 – 928, 2003.

[27] X. Zhang and A. M. Armani, "Silica microtoroid resonator sensor with monolithically integrated waveguides" *Opt. Express*, vol. 21, no. 20, pp. 23592 – 23603, 2013.

[28] D. W. Vernooy, V. S. Ilchenko, H. Mabuchi, E. W. Streed and H. J. Kimble, "High-Q measurements of fused-silica microspheres in the near infrared" *Opt. Lett.*, vol. 23, no. 4, pp. 247 – 249, 1998.

[29] F. Monifi, J. Friedlein, Ş. K. Özdemir and L. Yang, "A robust and tunable adddrop filter using whispering gallery mode microtoroid resonator" *J. Lightwave Technol.*, vol. 30, no. 21, pp. 3306 – 3315, 2012.

[30] K. B. Mullis, "The Polymerase Chain Reaction (Nobel Lecture)" *Angew. Chem*, vol. 33, no. 12, pp. 1209 – 1213, 1994.

[31] O. Piepenburg, C. H. Williams, D. L. Stemple and N. A. Armes, "DNA detection using recombination proteins" *PLoS Biol.*, vol. 4, no. 7, pp. 1115 – 1121, 2006.

[32] S. Lutz, P. Weber, M. Focke, B. Faltin, J. Hoffmann, C. Muller, D. Mark, G. Roth, P. Munday, N. Armes, O. Piepenburg, R. Zengerle and F. von Stetten, "Microfluidic lab-on-a-foil for nucleic acid analysis based on isothermal recombinase polymerase amplification (RPA)" *Lab Chip*, vol. 10, no. 7, pp. 887 – 893, 2010.

[33] P. Singleton, "Dictionary of DNA and denome technology" *John Wiley & Sons*, West Sussex, England, 2012.

[34] Y. Shin, A. P. Perera, K. W. Kim and M. K. Park, "Real-time, label-free isothermal solid-phase amplification/detection (ISAD) device for rapid detection of genetic alteration in cancers" *Lab Chip*, vol. 13, no. 11, pp. 2106 – 2114, 2013.

[35] J. S. del Rio, T. Steylaerts, O. Y. F. Henry, P. Bienstman, T. Stakenborg, W. V. Roy and C. K. O′Sullivan, "Real-time and label-free ring-resonator monitoring of solid-phase recombinase polymerase amplification" *Biosens. Bioelectron.*, vol. 73, pp. 130 – 137, 2015.

[36] H. Yan, R. Bonasio, D. F. Simola, J. Liebig, S. L. Berger, D. Reinberg and M. Berenbaum, "DNA methylation in social insects: how epigenetics can control behavior and longevity" *Annu. Rev. Entomol.*, vol. 60, pp. 435 – 452, 2015.

[37] J. Du, L. M. Johnson, S. E. Jacobsen and D. J. Patel, "DNA methylation pathways and their crosstalk with histone methylation" *Nat. Rev. Mol. Cell Biol.*, vol. 16, no. 9, pp. 519 – 532, 2015.

[38] K. D. Robertson, "DNA methylation and human disease" *Nat. Rev. Genet.*, vol. 6, pp. 597 – 610, 2005.

[39] P. A. Jones and D. Takai, "The role of DNA methylation in mammalian epigenetics" *Science*, vol. 293, no. 5532, pp. 1068 – 1070, 2001.

[40] P. A. Jones, "Functions of DNA methylation: islands, start sites, gene bodies and beyond" *Nat. Rev. Genet.*, vol. 13, pp. 484 – 492, 2012.

[41] J. A. Law and S. E. Jacobsen, "Establishing, maintaining and modifying DNA methylation patterns in plants and animals" *Nat. Rev. Genet.*, vol. 11, pp. 204 – 220, 2010.

[42] L. Tan and Y. G. Shi, "Tet family proteins and 5-hydroxymethylcytosine in development and disease" *Development*, vol. 139, pp. 1895 – 1902, 2012.

[43] S. Gopalakrishnan, B. O. Van Emburgh and K. D. Robertson, "DNA methylation in development and human disease" *Mutat. Res., Fundam. Mol. Mech. Mutagen.*, vol. 647, no. 1-2, pp. 30 – 38, 2008.

[44] M. Tahiliani, K. P. Koh, Y. Shen, W. A. Pastor, H. Bandukwala, Y. Brudno, S. Agarwal, L. M. Iyer, D. R. Liu, L. Aravind and A. Rao, "Conversion of 5-methylcytosine to 5-hydroxymethylcytosine in mammalian DNA by MLL partner TET1" *Science*, vol. 324, no. 5929, pp. 930 – 935, 2009.

[45] N. W. Penn, R. Suwalski, C. O′Riley, K. Bojanowski and R. Yura, "The presence of 5-hydroxymethylcytosine in animal deoxyribonucleic acid" *Biochem. J.*, vol. 126, no. 4, pp. 781 – 790, 1972.

[46] M. R. Branco, G. Ficz and W. Reik, "Uncovering the role of 5-hydroxymethylcytosine in the epigenome" *Nat. Rev. Genet.*, vol. 13, pp. 7 – 13, 2012.

[47] T. Y. Lee, Y. Shin and M. K. Park, "Miniaturisation for chemistry, physics, biology, materials science and bioengineering" *Lab Chip*, vol. 14, no. 21, pp. 4220 – 4229, 2014.

[48] C. Bock, S. Reither, T. Mikeska, M. Paulsen, J. Walter and T. Lengauer, "BiQ analyzer: visualization and quality control for DNA methylation data from bisulfite sequencing" *Bioinformatics*, vol. 21, no. 21, pp. 4067 – 4068, 2005.

[49] J. C. Susan, J. Harrison, C. L. Paul and M. Frommer, "High sensitivity mapping of methylated cytosines" *Nucleic Acids Res.*, vol. 22, no. 15, pp. 2990 – 2997, 1994.

[50] J. G. Herman, J. R. Graff, S. Myohanen, B. D. Nelkin and S. B. Baylin, "High sensitivity mapping of methylated cytosines" *Proc. Natl. Acad. Sci. U.S.A.*, vol. 93, no. 18, pp. 9821 – 9826, 1996.

[51] J. Yoon, M. K. Park, T. Y. Lee, Y. J. Yoon and Y. Shin, "LoMA-B: a simple and versatile lab-on-a-chip system based on single-channel bisulfite conversion for DNA methylation analysis" *Lab Chip*, vol. 15, no. 17, pp. 3530 – 3539, 2015.

[52] Y. Shin, A. P. Perera, J. S. Kee, J. Song, Q. Fang, G. Q. Lo and M. K. Park, "Label-free methylation specific sensor based on silicon microring resonators for detection and quantification of DNA methylation biomarkers in bladder cancer" *Sens. Actuators B,*, vol. 177, pp. 404 – 411, 2013.

[53] M. W. Y. Chan, L. W. Chan, N. L. S. Tang, J. H. M. Tong, K. W. Lo, T. L. Lee, H. Y. Cheung, W. S. Wong, P. S. F. Chan, F. M. M. Lai and K. F. To, "Hypermethylation of multiple genes in tumor tissues and voided urine in urinary bladder cancer patients" *Clin. Cancer Res.*, vol. 8, no. 2, pp. 464 – 470, 2002.

[54] M. Widschwendter, J. Berger, M. Hermann, H. M. Mller, A. Amberger, M. Zeschnigk, A. Widschwendter, B. Abendstein, A. G. Zeimet, G. Daxenbichler and C. Marth, "Methylation and ailencing of the retinoic acid receptor-β2 gene in breast cancer" *J. Natl. Cancer Inst.*, vol. 92, no. 10, pp. 826 – 832, 2000.

[55] S. Zöchbauer-Müller, K. M. Fong, A. K. Virmani, J. Geradts, A. F. Gazdar and J. D. Minna, "Aberrant promoter methylation of multiple genes in non-small cell lung cancers" *Cancer Res.*, vol. 61, no. 1, pp. 249 – 255, 2001.

[56] C. H. Wang, H. C. Lai, T. M. Liou, K. F. Hsu, C. Y. Chou and G. B. Lee, "A DNA methylation assay for detection of ovarian cancer cells using a HpaII/MspI digestion-based PCR assay in an integrated microfluidic system" *Microfluid. Nanofluid.*, vol. 15, no. 5, pp. 575 – 585, 2013.

[57] R. M. Hawk and A. M. Armani, "Label free detection of 5′hydroxymethylcytosine within CpG islands using optical sensors" *Biosens. Bioelectron.*, vol. 65, pp. 198 – 203, 2015.

[58] J. D. Suter, D. J. Howard, H. Shi, C. W. Caldwell and X. Fan, "Label-free DNA methylation analysis using opto-fluidic ring resonators" *Biosens. Bioelectron.*, vol. 26, no. 3, pp. 1016 – 1020, 2010.

[59] A. J. Qavi and R. C. Bailey, "Label-free DNA methylation analysis using opto-fluidic ring resonators" *Angew. Chem. Int. Ed.*, vol. 49, no. 27, pp. 4608 – 4611, 2010.

[60] M. I. Almeida, R. M. Reis and G. A. Calin, "MicroRNA history: discovery, recent applications, and next frontiers" *Mutat. Res. Fundam. Mol. Mech. Mutagen.*, vol. 717, no. 1-2, pp. 1 – 8, 2011.

[61] R. C. Lee, R. L. Feinbaum and V. Ambros, "The C. elegans heterochronic gene $lin-4$ encodes small RNAs with antisense complementarity to $lin-14$" *Cell*, vol. 75, no. 5, pp. 843 – 854, 1993.

[62] B. J. Reinhart, F. J. Slack, M. Basson, A. E. Pasquinelli, J. C. Bettinger, A. E. Rougvie, H. R. Horvitz and G. Ruvkun, "The 21-nucleotide $let-7$ RNA regulates developmental timing in *Caenorhabditis elegans*" *Nature*, vol. 403, pp. 901 – 906, 2000.

[63] N. C. Lau, L. P. Lim, E. G. Weinstein and D. P. Bartel, "An abundant class of tiny RNAs with probable regulatory roles in *Caenorhabditis elegans*" *Science*, vol. 403, pp. 858 – 862, 2001.

[64] K. Okamura, M. D. Phillips, D. M. Tyler, H. Duan, Y. T. Chou and E. C. Lai, "The regulatory activity of microRNA* species has substantial influence on microRNA and 3′ UTR evolution" *Nat. Struct. Mol. Biol.*, vol. 15, pp. 354 – 363, 2008.

[65] L. Vian, M. Di Carlo, E. Pelosi, F. Fazi, S. Santoro, A. M. Cerio, A. Boe, V. Rotilio, M. Billi, S. Racanicchi, U. Testa, F. Grignani and C. Nervi, "Transcriptional fine-tuning of microRNA-223 levels directs lineage choice of human hematopoietic progenitors" *Cell Death Differ.*, vol. 21, pp. 290 – 301, 2014.

[66] A. Shenoy and R. H. Blelloch, "Regulation of microRNA function in somatic stem cell proliferation and differentiation" *Nat. Rev. Mol. Cell Biol.*, vol. 15, no. 9, pp. 565 – 576, 2014.

[67] Y. Zhang, W. Qin, L. Zhang, X. Wu, N. Du, Y. Hu, X. Li, N. Shen, D. Xiao, H. Zhang, Z. Li, Y. Zhang, H. Yang, F. Gao, Z. Du, C. Xu and B. Yang, "MicroRNA-26a prevents endothelial cell apoptosis by directly targeting TRPC6 in the setting of atherosclerosis" *Sci. Rep.*, vol. 5, 09401, 2015.

[68] X. Yan, Y. Huang, J. X. Zhao, C. J. Rogers, M. J. Zhu, S. P. Ford, P. W. Nathanielsz and M. Du, "Maternal obesity downregulates microRNA $let-7g$ expression, a possible mechanism for enhanced adipogenesis during ovine fetal skeletal muscle development" *Int. J. Obes.*, vol. 37, pp. 568 – 575, 2013.

[69] C. Guay and R. Regazzi, "Circulating microRNAs as novel biomarkers for diabetes mellitus" *Nat. Rev. Endocrinol.*, vol. 9, pp. 513 – 521, 2013.

[70] E. van Rooij and E. N. Olson, "MicroRNA therapeutics for cardiovascular disease: opportunities and obstacles" *Nat. Rev. Drug Discovery.*, vol. 11, pp. 860 – 872, 2012.

[71] B. C. Richardson and D. R. Patel, "Epigenetics in 2013: DNA methylation and miRNAkey roles in systemic autoimmunity" *Nat. Rev. Rheumatol.*, vol. 10, pp. 72 – 74, 2014.

[72] L. Welberg, "A social role for microRNA" *Nat. Rev. Neurosci.*, vol. 16, pp. 2 – 3, 2015.

[73] V. A. Erdmann, S. Jurga and J. Barcizewski, "RNA and DNA diagnostics" *Springer*, Switzerland, 2015.

[74] P. Landgraf et al., "A Mammalian microRNA expression atlas based on small RNA library sequencing" *Cell*, vol. 129, no. 7, pp. 1401 – 1414, 2007.

[75] E. Várallyay, J. Burgyn and Z. Havelda, "MicroRNA detection by northern blotting using locked nucleic acid probes" *Nat. Protoc.*, vol. 3, pp. 190 – 196, 2008.

[76] E. Curry, S. E. Ellis and S. L. Pratt, "Detection of porcine sperm microRNAs using a heterologous microRNA microarray and reverse transcriptase polymerase chain reaction" *Mol. Reprod. Dev*, vol. 76, no. 3, pp. 218 – 219, 2009.

[77] S. Roy, J. H. Soh and Z. Gao, "A microfluidic-assisted microarray for ultrasensitive detection of miRNA under an optical microscope" *Lab Chip*, vol. 11, no. 11, pp. 1886 – 1894, 2011.

[78] A. J. Qavi, J. T. Kindt, M. A. Gleeson and R. C. Bailey, "Anti-DNA:RNA antibodies and silicon photonic microring resonators: increased sensitivity for multiplexed microRNA detection" *Anal. Chem.*, vol. 83, no. 15, pp. 5949 – 5956, 2011.

[79] F. Porichis, M. G. Hart, M. Griesbeck, H. L. Everett, M. Hassan, A. E. Baxter, M. Lindqvist, S. M. Miller, D. Z. Soghoian, D. G. Kavanagh, S. Reynolds, B. Norris, S. K. Mordecai, Q. Nguyen, C. Lai and D. E. Kaufmann, "High-throughput detection of miRNAs and gene-specific mRNA at the single-cell level by flow cytometry" *Nat. Commun.*, vol. 5, pp. 5641, 2014.

[80] B. N. Johnson and R. Mutharasan, "Biosensor-based microRNA detection: techniques, design, performance, and challenges" *Analyst (Cambridge, U.K.)*, vol. 139, pp. 1576 – 1588, 2014.

[81] A. J. Qavi, J. T. Kindt and R. C. Bailey, "Sizing up the future of microRNA analysis" *Anal. Bioanal. Chem.*, vol. 398, no. 6, pp. 2535 – 2549, 2010.

[82] A. L. Washburn, L. C. Gunn and R. C. Bailey, "Label-free quantitation of a cancer biomarker in complex media using silicon photonic microring resonators" *Anal. Chem.*, vol. 81, no. 22, pp. 9499 – 9506, 2009.

[83] B. Lewin, "Label-free quantitation of a cancer biomarker in complex media using silicon photonic microring resonators" *Genes VIII*, Pearson Prentice Hall, New Jersey, USA, 2004.

[84] F. W. Albert and L. Kruglyak, "The role of regulatory variation in complex traits and disease" *Nat. Rev. Genet.*, vol. 16, pp. 197 – 212, 2015.

[85] R. A. Sunde, "mRNA transcripts as molecular biomarkers in medicine and nutrition" *J. Nutr. Biochem.*, vol. 21, no. 8, pp. 665 – 670, 2010.

[86] R. C. Gupta, "Biomarkers in Toxicology" *Elsevier*, London, UK, 2014.

[87] L. S. Lin, Z. X. Cong, J. B. Cao, K. M. Ke, Q. L. Peng, J. Gao, H. H. Yang, G. Liu and X. Chen, "Multifunctional Fe_3O_4@polydopamine coreshell nanocomposites for intracellular mRNA detection and imaging-guided photothermal therapy" *ACS Nano*, vol. 8, no. 4, pp. 3876 – 3883, 2014.

[88] T. Chen, C. S. Wu, E. Jimenez, Z. Zhu, J. G. Dajac, M. You, D. Han, X. Zhang and W. Tan, "DNA micelle flares for intracellular mRNA imaging and gene therapy" *Angew. Chem., Int. Ed.*, vol. 125, no. 7, pp. 2066 – 2070, 2013.

[89] P. O. Brown and D. Botstein, "Exploring the new world of the genome with DNA microarrays" *Nat. Genet.*, vol. 21, pp. 33 – 37, 1999.

[90] J. J. Chen, "Key aspects of analyzing microarray gene-expression data" *Pharmacogenomics J.*, vol. 8, no. 5, pp. 473 – 482, 2007.

[91] T. Nolan, R. E. Hands and S. A. Bustin, "Quantification of mRNA using real-time RT-PCR" *Nat. Protoc.*, vol. 1, no. 3, pp. 1559 – 1582, 2006.

[92] H. D. VanGuilder, K. E. Vrana and W. M. Freeman, "Twenty-five years of quantitative PCR for gene expression analysis" *BioTechniques*, vol. 44, no. 5, pp. 619 – 626, 2008.

[93] J. Zhang, H. P. Lang, F. Huber, A. Bietsch, W. Grange, U. Certa, R. Mckendry, H. J. Gntherodt, M. Hegner and C. Gerber, "Rapid and label-free nanomechanical detection of biomarker transcripts in human RNA" *Nat. Nanotechnol.*, vol. 1, pp. 214 – 220, 2006.

[94] D. T. Ross et al., "Systematic variation in gene expression patterns in human cancer cell lines" *Nat. Genet.*, vol. 24, pp. 227 – 235, 2000.

[95] A. E. Prigodich, P. S. Randeria, W. E. Briley, N. J. Kim, W. L. Daniel, D. A. Giljohann and C. A. Mirkin, "Multiplexed nanoflares: mRNA detection in live cells" *Anal. Chem.*, vol. 84, no. 4, pp. 2062 – 2066, 2012.

[96] X. H. Peng, Z. H. Cao, J. T. Xia, G. W. Carlson, M. M. Lewis, W. C. Wood and L. Yang, "Real-time detection of gene expression in cancer cells using molecular beacon imaging: new Ssrategies for cancer research" *Cancer Res.*, vol. 65, no. 5, pp. 1909 – 1917, 2005.

[97] P. J. Santangelo, B. Nix, A. Tsourkas and G. Bao, "Dual FRET molecular beacons for mRNA detection in living cells" *Nucleic Acids Res.*, vol. 32, no. 6, pp. e57, 2004.

[98] A. Raj, P. van den Bogaard, S. A. Rifkin, A. van Oudenaarden and S. Tyagi, "Imaging individual mRNA molecules using multiple singly labeled probes" *Nat. Methods*, vol. 5, no. 10, pp. 877 – 879, 2008.

[99] A. C. Lee, Z. Dai, B. Chen, H. Wu, J. Wang, A. Zhang, L. Zhang, T. M. Lim and Y. Lin, "Electrochemical branched-DNA assay for polymerase chain reaction-free detection and quantification of oncogenes in messenger RNA" *Anal. Chem.*, vol. 80, no. 24, pp. 9402 – 9410, 2008.

[100] Z. Fang and S. O. Kelley, "Direct electrocatalytic mRNA detection using PNA-nanowire sensors," *Anal. Chem.*, vol. 81, no. 2, pp. 612 – 617, 2009.

[101] X. Chen, S. Roy, Y. Peng and Z. Gao, "Electrical sensor array for polymerase chain reaction-free messenger RNA expression profiling" *Anal. Chem.*, vol. 82, no. 14, pp. 5958 – 5964, 2010.

[102] M. S. Wu, G. S. Qian, J. J. Xu and H. Y. Chen, "Sensitive electrochemiluminescence detection of c-Myc mRNA in breast cancer cells on a wireless bipolar electrode" *Anal. Chem.*, vol. 84, no. 12, pp. 5407 – 5414, 2012.

[103] H. J. Lee, T. T. Goodrich and R. M. Corn, "SPR imaging measurements of 1-D and 2-D DNA microarrays created from microfluidic channels on gold thin films" *Anal. Chem.*, vol. 73, no. 22, pp. 5425 – 5531, 2001.

[104] T. K. Lim, M. Oyama, K. Ikebukuro and I. Karube, "Photocatalytic sensor for chemical oxygen demand determination based on oxygen electrode" *Anal. Chem.*, vol. 72, no. 14, pp. 2856 – 2860, 2000.

[105] J. T. Kindt and R. C. Bailey, "Chaperone probes and bead-based enhancement to improve the direct detection of mRNA using silicon photonic sensor arrays" *Anal. Chem.*, vol. 84, no. 18, pp. 8067 – 8074, 2012.

[106] J. O′Grady, S. Sedano-Balbás, M. Maher, T. Smith and T. Barry, "Rapid real-time PCR detection of Listeria monocytogenes in enriched food samples based on the ssrA gene, a novel diagnostic target" *Food Microbiol.*, vol. 25, no. 1, pp. 75 – 84, 2008.

[107] S. Y. Lee, S. C. Bailey and D. Apirion, "Small stable RNAs from *Escherichia coli*: evidence for the existence of new molecules and for a new ribonucleoprotein particle containing 6S RNA" *J. Bacteriol.*, vol. 133, no. 2, pp. 1015 – 1023, 1978.

[108] B. Felden, H. Himeno, A. Muto, J. P. McCutcheon, J. F. Atkins and R. F. Gesteland, "Probing the structure of the *Escherichia coli* 10Sa RNA (tmRNA)" *RNA*, vol. 3, pp. 89 – 103, 1997.

[109] S. D. Moore and R. T. Sauer, "The tmRNA system for translational surveillance and ribosome rescue" *Annu. Rev. Biochem.*, vol. 76, pp. 101 – 124, 2007.

[110] W. Schönhuber, G. Le Bourhis, J. Tremblay, R. Amann and S. Kulakauskas, "Utilization of tmRNA sequences for bacterial identification" *BMC Microbiol.*, vol. 1, no. 20, pp. 1 – 8, 2001.

[111] J. T. Keer and L. Birch, "Molecular methods for the assessment of bacterial viability" *J. Microbiol. Methods*, vol. 53, no. 2, pp. 175 – 183, 2003.

[112] J. H. Russell and K. C. Keiler, "Subcellular localization of a bacterial regulatory RNA" *Proc. Natl. Acad. Sci. U.S.A.*, vol. 106, no. 38, pp. 16405 – 16409, 2009.

[113] O. Scheler, L. Kaplinski, B. Glynn, P. Palta, S. Parkel, K. Toome, M. Maher, T. Barry, M. Remm and A. Kurg, "Subcellular localization of a bacterial regulatory RNA" *BMC Biotechnol.*, vol. 11, no. 17, pp. 1 – 7, 2011.

[114] S. McGuinness, T. Barry and J. O′Grady, "Development and preliminary validation of a real-time RT-PCR based method targeting tmRNA for the rapid and specific detection of *Salmonella*" *Food Res. Int.*, vol. 45, no. 2, pp. 989 – 992, 2012.

[115] O. Scheler, J. T. Kindt, A. J. Qavi, L. Kaplinski, B. Glynn, T. Barry, A. Kurg and R. C. Bailey, "Label-free, multiplexed detection of bacterial tmRNA using silicon photonic microring resonators" *Biosens. Bioelectron.*, vol. 36, no. 1, pp. 56 – 61, 2012.

[116] N. K. Navani and Y. F. Li, "Nucleic acid aptamers and enzymes as sensors" *Curr. Opin. Chem. Biol.*, vol. 10, no. 3, pp. 272 – 281, 2006.

[117] A. Sassolas, L. J. Blum and B. D. Leca-Bouvier, "Optical detection systems using immobilized aptamers" *Biosens. Bioelectron.*, vol. 26, no. 9, pp. 3725 – 3736, 2011.

[118] J. O. Lee, H. M. So, E. K. Jeon, H. Chang, K. Won and Y. H. Kim, "Aptamers as molecular recognition elements for electrical nanobiosensors" *Anal. Bioanal. Chem.*, vol. 390, no. 4, pp. 1023 – 1032, 2008.

[119] P. E. Nielsen, M. Egholm, R. H. Berg and O. Buchardt, "Sequence-selective recognition of DNA by strand displacement with a Thymine-substituted polyamide" *Science*, vol. 254, no. 5037, pp. 1497 – 1500, 1991.

[120] G. A. Rodriguez, S. Hu and S. M. Weiss, "Porous silicon ring resonator for compact, high sensitivity biosensing applications" *Opt. Express*, vol. 23, no. 6, pp. 7111 – 7119, 2015.

[121] Z. A. Weinberg, "Polysilicon recrystallization by CO_2 laser heating of SiO_2" *App. Phys. Lett.*, vol. 39, no. 5, pp. 421 – 422, 1981.

[122] J. W. Strutt, B. Rayleigh, "Theory of sound" *MacMillan*, vol. II, London, UK, 1894.

[123] B. Liedberg, C. Nylander, I. Lundstr/"om, "Surface-plasmon resonance for gas-detection and biosensing" *Sensor. Actuator.*, vol. 4, pp. 299 – 304, 1983.

[124] H. Muramatsu, J. M. Dicks, E. Tamiya, I. Karube, "Piezoelectric crystal biosensor modified with protein-a for determination of immunoglobulins" *Anal. Chem.*, vol. 59, no. 23, pp. 2760 – 2763, 1987.

[125] S. M. Spillane,T. J. Kippenberg, O. J. Painter, K. J. Vahala, "Ideality in a fiber-taper-coupled microresonator system for application to cavity quantum electrodynamics" *Phys. Rev. Lett.*, vol. 91, no. 4-25, pp. 043902, 2003.

[126] K. Srinivasan, M. Borselli, T. J. Johnson, P. E. Barclay, O. Painter, A. Stintz, S. Krishna, "Optical loss and lasing characteristics of high-quality-factor AlGaAs microdisk resonators with embedded quantum dots" *Appl. Phys. Lett.*, vol. 86, pp. 151106, 2005.

[127] Y. Takahashi, H. Hagino, Y. Tanaka, B. S. Song, T. Asano and S. Noda, "High-Q nanocavity with a 2-ns photon lifetime" *Opt. Express*, vol. 15, no. 25, pp. 17206 – 17213, 2007.

[128] J. C. Knight, G. Cheung, F. Jacques, T. A. Birks, "Phase-matched excitation of whispering-gallery-mode resonances by a fiber taper" *Opt. Lett.*, vol. 22, no. 15, pp. 1129 – 1131, 1997.

[129] M. L. Gorodetsky and V. S. Ilchenko, "High-Q optical whispering-gallery microresonators - precession approach for spherical mode analysis and emission patterns with prism couplers" *Opt. Commun.*, vol. 113, no. 1-3, pp. 133 – 143, 1994.

[130] F. Vollmer, S. Arnold, D. Braun, I. Teraoka and A. Libchaber, "Multiplexed DNA quantification by spectroscopic shift of two microsphere cavities" *Biophys. J.*, vol. 85, no. 3, pp. 1974 – 1979, 2003.

[131] F. Vollmer, S. Arnold and D. Keng, "Single virus detection from the reactive shift of a whispering-gallery mode" *Proc. Natl. Acad. Sci. U.S.A.*, vol. 105, no. 52, pp. 20701 – 20704, 2008.

[132] A. M. Armani, R. P. Kulkarni, S. E. Fraser, R. C. Flagan, K. Vahala, "Label-free, single-molecule detection with optical microcavities" *Science*, vol. 317, no. 5839, pp. 783 – 787, 2007.

[133] T. A. Birks, J. C. Knight and T. E. Dimmick, "High-resolution measurement of the fiber diameter variations using whispering gallery modes and no optical alignment" *IEEE Photonics Technol. Lett.*, vol. 12, no. 2, pp. 182 – 183, 2000.

[134] F. Vollmer, D. Braun, A. Libchaber, M. Khoshsima, I. Teraoka and S. Arnold, "Protein detection by optical shift of a resonant microcavity" *Appl. Phys. Lett.*, vol. 80, no. 21, pp. 4057 – 4059, 2002.

[135] M. Pöllinger, D. O'Shea, F. Warken and A. Rauschenbeutel, "Ultrahigh-Q tunable whispering-gallery-mode microresonator" *Phys. Rev. Lett.*, vol. 103, no. 5-31, pp. 053901, 2009.

[136] İ. Tosun, "Modelling in transport phenomena: a conceptual approach" *Elsevier*, Oxford, UK, 2002.

[137] G. T. Hermanson, "Bioconjugate techniques" *Elsevier Academic Press*, Amsterdam, Holland, 2008.

[138] J. R. Vig, "UV/ozone cleaning of surfaces" *J. Vac. Sci. Technol.*, vol. 3, no. 3, pp. 1027 – 1034, 1985.

[139] J. N. Pitts, G. S. Hammond, W. A. Noyes, "Advances in Photochemistry" *Interscience*, vol. 3, New York, USA, 1969.

[140] J. C. Love, L. A. Estroff, J. K. Kriebel, R. G. Nuzzo and G. M. Whitesides, "Self-assembled monolayers of thiolates on metals as a form of nanotechnology" *Chem. Rev.*, vol. 105, no. 4, pp. 1103 – 1170, 2005.

[141] E. T. Vandenberg, L. Bertilsson, B. Liedberg, K. Uvdal, R. Erlandsson, H. Elwing and I. Lundström, "Structure of 3-aminopropyl triethoxy silane on silicon oxide" *J. Colloid Interface Sci.*, vol. 147, no. 1, pp. 103 – 118, 1991.

[142] M. Malmsten, K. Emoto and J. M. Van Alstine, "Effect of chain density on inhibition of protein adsorption by poly(ethylene glycol) based coatings" *J. Colloid Interface Sci.*, vol. 202, no. 2, pp. 507 – 517, 1998.

[143] S. Herrwerth, W. Eck, S. Reinhardt and M. Grunze, "Factors that determine the protein resistance of oligoether self-assembled monolayers internal hydrophilicity, terminal hydrophilicity, and lateral packing density" *J. Am. Chem. Soc.*, vol. 125, no. 31, pp. 9359 – 517, 2003.

[144] D. Gerion, F. Pinaud, S. C. Williams, W. J. Parak, D. Zanchet, S. Weiss and A. P. Alivisatos, "Synthesis and properties of biocompatible water-soluble silica-coated CdSe/ZnS semiconductor quantum dots" *J. Phys. Chem. B*, vol. 105, no. 37, pp. 8861 – 8871, 2001.

[145] J. T. G. Pena, C. Sohn-Lee, S. H. Rouhanifard, J. Ludwig, M. Hafner, A. Mihailovic, C. Lim, D. Holoch, P. Berninger, M. Zavolan and T. Tuschl, "miRNA in situ hybridization in formaldehyde and EDCfixed tissues" *Nat. Methods*, vol. 6, pp. 139 – 141, 2009.

[146] C. D. Medley, S. Bamrungsap, W. H. Tan and J. E. Smith, "Aptamer-conjugated nanoparticles for cancer cell detection" *Anal. Chem.*, vol. 83, no. 3, pp. 727 – 734, 2011.

[147] E. Ozgur, P. Toren and M. Bayindir, "Phosphonate based organosilane modification of a simultaneously protein resistant and bioconjugable silica surface" *J. Mater. Chem. B*, vol. 2, no. 41, pp. 7118 – 7122, 2014.

[148] M. Kyo, K. U. Aoki and H. Koga, "Label-free detection of proteins in crude cell lysate with antibody arrays by a surface plasmon resonance imaging technique" *Anal. Chem.*, vol. 77, no. 22, pp. 7115 – 7121, 2005.

[149] A. Cattani-Scholz, D. Pedone, M. Dubey, S. Neppl, B. Nickel, P. Feulner, J. Schwartz, G. Abstreiter and M. Tornow, "Organophosphonate-based PNA-functionalization of silicon nanowires for label-free DNA detection" *ACS Nano*, vol. 2, no. 8, pp. 1653 – 1660, 2008.

[150] R. A. Shircliff, P. Stradins, H. Moutinho, J. Fennell, M. L. Ghirardi, S. W. Cowley, H. M. Branz and I. T. Martin, "Angle-resolved XPS analysis and characterization of monolayer and multilayer silane films for DNA coupling to silica" *Langmuir*, vol. 29, no. 12, pp. 4057 – 4067, 2013.

[151] P. H. T. Ngamou, J. P. Overbeek, H. M. van Veen, J. F. Vente, P. F. Cuperus and M. Creatore, "On the enhancement of pervaporation properties of plasma-deposited hybrid silica membranes" *RSC Adv.*, vol. 3, no. 34, pp. 14241 – 14244, 2013.

[152] A. Afzal, H. M. Siddiqi, S. Saeed and Z. Ahmad, "Exploring resin viscosity effects in solventless processing of nano-SiO_2/epoxy polymer hybrids" *RSC Adv.*, vol. 3, no. 12, pp. 3885 – 3892, 2013.

[153] X. N. Xie, M. Deng, H. Xu, S. W. Yang, D. C. Qi, X. Y. Gao, H. J. Chung, C. H. Sow, V. B. C. Tan and A. T. S. Wee, "Creating polymer structures of tunable electric functionality by nanoscale discharge-assisted cross-linking and oxygenation" *J. Am. Chem. Soc.*, vol. 128, no. 8, pp. 2738 – 2744, 2006.

[154] L. H. Wang, Y. Tian, H. Y. Ding and J. D. Li, "Microstructure and properties of organosoluble polyimide/silica hybrid films" *Eur. Polym. J.*, vol. 42, no. 11, pp. 2921 – 2930, 2006.

[155] R. G. Chapman, E. Ostuni, S. Takayama, R. E. Holmlin, L. Yan and G. M. Whitesides, "Surveying for surfaces that resist the adsorption of proteins" *J. Am. Chem. Soc.*, vol. 122, no. 34, pp. 8303 – 8304, 2000.

[156] J. H. Lee, J. Kopecek and J. D. Andrade, "Protein-resistant surfaces prepared by PEO-containing block copolymer surfactants" *J. Biomed. Mater. Res.*, vol. 23, no. 3, pp. 351 – 368, 1989.

[157] Y. Coffinier, N. Nguyen, H. Drobecq, O. Melnyk, V. Thomy and R. Boukherroub, "Affinity surface-assisted laser desorption/ionization mass spectrometry for peptide enrichment" *Analyst (Cambridge, U. K.)*, vol. 137, no. 23, pp. 5527 – 5532, 2012.

[158] I. Wilkening, G. del Signore and C. P. R. Hackenberger, "Synthesis of phosphonamidate peptides by Staudinger reactions of silylated phosphinic acids and esters" *Chem. Commun.*, vol. 47, no. 1, pp. 349 – 351, 2011.

[159] J. A. Howarter and J. P. Youngblood, "Optimization of silica silanization by 3-aminopropyltriethoxysilane" *Langmuir*, vol. 22, no. 26, pp. 11142 – 11147, 2006.

[160] M. Stenberg and H. Nygren, "The use of the isoscope ellipsometer in the study of adsorbed proteins and biospecific binding reactions" *J. Phys. Colloq.*, vol. 44, pp. C10-83 – C10-86, 1983.

[161] M. Q. Zhang, T. Desai and M. Ferrari, "Proteins and cells on PEG immobilized silicon surfaces" *Biomaterials*, vol. 19, no. 10, pp. 953 – 960, 1998.

[162] P. Tengvall, I. Lundstrom and B. Liedberg, "Protein adsorption studies on model organic surfaces: an ellipsometric and infrared spectroscopic approach" *Biomaterials*, vol. 19, no. 4-5, pp. 407 – 422, 1998.

[163] C. E. Soteropulos, K. M. Zurick, M. T. Bernards and H. K. Hunt, "Tailoring the protein adsorption properties of whispering gallery mode optical biosensors" *Langmuir*, vol. 28, no. 44, pp. 15743 – 15750, 2012.

[164] J. D. Watson and F. H. C. Crick, "Molecular structure of nucleic acids" *Nature*, vol. 171, no. 4356, pp. 737 – 738, 1953.

[165] R. Dawkins, "The selfish gene" *Oxford University Press*, Oxford, England, 1976.

[166] R. M. Hawk, M. V. Chistiakova and A. M. Armani, "Monitoring DNA hybridization using optical microcavities" *Opt. Lett.*, vol. 38, no. 22, pp. 4690 – 4693, 2013.

[167] R. F. McClure, P. Kaur, E. Pagel, P. D. Ouillette, C. E. Holtegaard, C. L. Treptow and P. J. Kurtin, "Validation of immunoglobulin gene rearrangement detection by PCR using commercially available Biomed-2 primers" *Leukemia*, vol. 20, pp. 176 – 179, 2006.

[168] D. J. Lockhart and E. A. Winzeler, "Genomics, gene expression and DNA arrays" *Nature*, vol. 405, pp. 827 – 836, 2000.

[169] L. G. Carrascosa, M. Moreno, M. Alvarez and L. M. Lechuga, "Nanomechanical biosensors: a new sensing tool" *TrAC Trends Anal. Chem.*, vol. 25, no. 3, pp. 196 – 206, 2006.

[170] L. G. Carrascosa, M. Moreno, M. Alvarez and L. M. Lechuga, "Electrochemical DNA sensors" *Nat. Biotechnol.*, vol. 21, no. 10, pp. 1192 – 1199, 2003.

[171] Q. He, S. Wu, Z. Yin and H. Zhang, "Graphene-based electronic sensors" *Chem. Sci.*, vol. 3, no. 6, pp. 1764 – 1772, 2012.

[172] G. Pelossof, R. Tel-Vered, X. Q. Liu and I. Willner, "Amplified surface plasmon resonance based DNA biosensors, aptasensors, and Hg^{2+} sensors using hemin/G-quadruplexes and Au nanoparticles" *Chem. Eur. J.*, vol. 17, no. 32, pp. 8904 – 8912, 2011.

[173] L. Matlock-Colangelo and A. J. Baeumner, "Recent progress in the design of nanofiber-based biosensing devices" *Lab Chip*, vol. 12, no. 15, pp. 2612 – 2620, 2012.

[174] Z. Li, Y. Chen, X. Li, T. I. Kamins, K. Nauka and R. S. Williams, "Sequence-specific label-free DNA sensors based on silicon nanowires" *Nano Lett.*, vol. 4, no. 2, pp. 245 – 247, 2004.

[175] Y. Wu, D. Y. Zhang, P. Yin and F. Vollmer, "Ultraspecific and highly sensitive nucleic acid detection by integrating a DNA catalytic network with a label-free microcavity" *Small*, vol. 10, no. 10, pp. 2067 – 2076, 2014.

[176] A. J. Qavi, T. M. Mysz and R. C. Bailey, "Isothermal discrimination of single-nucleotide polymorphisms via real-time kinetic desorption and label-free detection of DNA using silicon photonic microring resonator arrays" *Anal. Chem.*, vol. 83, no. 17, pp. 6827 – 6833, 2011.

[177] Y. Shin, A. P. Perera and M. K. Park, "Label-free DNA sensor for detection of bladder cancer biomarkers in urine" *Sens. Actuators B-Chem.*, vol. 178, pp. 200 – 206, 2013.

[178] V. R. Dantham, S. Holler, C. Barbre, D. Keng, V. Kolchenko and S. Arnold, "Label-free detection of single protein using a nanoplasmonic-photonic hybrid microcavity" *Nano Lett.*, vol. 13, no. 7, pp. 3347 – 3351, 2013.

[179] S. Eustis and M. A. El-Sayed, "Why gold nanoparticles are more precious than pretty gold: Noble metal surface plasmon resonance and its enhancement of the radiative and nonradiative properties of nanocrystals of different shapes" *Chem. Soc. Rev.*, vol. 35, no. 3, pp. 209 – 217, 2006.

[180] J. D. Suter and X. Fan, "Overview of the optofluidic ring resonator: a versatile platform for label-free biological and chemical sensing" *Conf. Proc. IEEE Eng. Med. Biol. Soc.*, Minneapolis, MN, USA, pp. 1042 – 1044, 2009.

[181] J. D. Suter, I. M. White, H. Zhu, H. Shi, C. W. Caldwell and X. Fan, "Label-free quantitative DNA detection using the liquid core optical ring resonator" *Biosens. Bioelectron.*, vol. 23, no. 7, pp. 1003 – 1009, 2008.

[182] M. S. Azam and J. M. Gibbs-Davis, "Monitoring DNA hybridization and thermal dissociation at the silica/water interface using resonantly enhanced second harmonic generation spectroscopy" *Anal. Chem.*, vol. 85, no. 17, pp. 8031 – 8038, 2013.

[183] Z. Guo, R. Guilfoyle, A. Thiel, R. Wang and L. Smith, "Direct fluorescence analysis of genetic polymorphisms by hybridization with oligonucleotide arrays on glass supports" *Nucleic Acids Res.*, vol. 22, no. 24, pp. 5456 – 5465, 1994.

[184] A. Peterson, L. Wolf and R. J. Georgiadis, "Hybridization of mismatched or partially matched DNA at surfaces" *J. Am. Chem. Soc.*, vol. 124, no. 49, pp. 14601 – 14607, 2002.

[185] E. Wong, E. Chow and J. Gooding, "DNA recognition interfaces: the influence of interfacial design on the efficiency and kinetics of hybridization" *Langmuir*, vol. 21, no. 15, pp. 6957 – 6965, 2005.

[186] H. Park, A. Germini, S. Sforza, R. Corradini, R. Marchelli and W. Knoll, "Effect of ionic strength on PNA-DNA hybridization on surfaces and in solution" *Biointerphases*, vol. 2, no. 2, pp. 80 – 88, 2007.

[187] L. Moiseev, M. Ünlu, A. Swan, B. Goldberg and C. Cantor, "DNA conformation on surfaces measured by fluorescence self-interference" *Proc. Natl. Acad. Sci. U. S. A.*, vol. 103, no. 8, pp. 2623 – 2628, 2006.

[188] M. Shchepinov, S. CaseGreen and E. Southern, "Steric factors influencing hybridisation of nucleic acids to oligonucleotide arrays" *Nucleic Acids Res.*, vol. 25, no. 6, pp. 1155 – 1161, 1997.

[189] T. Herne and M. J. Tarlov, "Characterization of DNA probes immobilized on gold surfaces" *J. Am. Chem. Soc.*, vol. 119, no. 38, pp. 8916 – 8920, 1997.

[190] A. Halperin, A. Buhot and E. Zhulina, "Hybridization at a surface: the role of spacers in DNA microarrays" *Langmuir*, vol. 22, no. 26, pp. 11290 – 11304, 2006.

[191] S. Schreiner, D. Shudy, A. Hatch, A. Opdahl, L. Whitman and D. Petrovykh, "Controlled and efficient hybridization achieved with DNA probes immobilized solely through preferential DNA-substrate interactions" *Anal. Chem.*, vol. 82, no. 7, pp. 2803 – 2810, 2010.

[192] N. Kamisetty, S. Pack, M. Nonogawa, K. Devarayapalli, T. Kodaki and K. Makino, "Additional alkylsilanization of aminosilane-modified glass slide: effect of alkylsilane structure for enhancing surface amine functionality" *Chem. Lett.*, vol. 36, no. 2, pp. 322 – 323, 2007.

[193] J. Brumbarov and J. Kunze-Liebhauser, "Silicon on conductive self-organized TiO_2 nanotubes - a high capacity anode material for Li-ion batteries" *J. Power Sources*, vol. 258, pp. 129 – 133, 2014.

[194] M. L. Miller and R. W. Linton, "X-ray photoelectron spectroscopy of thermally treated silica (SiO_2) surfaces" *Anal. Chem.*, vol. 57, no. 12, pp. 2314 – 2319, 1985.

[195] F. Pippig and A. Hollander, "Fluram labeling of high density NH_2 surfaces" *Appl. Surf. Sci.*, vol. 253, no. 16, pp. 6817 – 6823, 2007.

[196] H Min, P. Girard-Lauriault, T. Gross, A. Lippitz, P. Dietrich and W. Unger, "Ambient-ageing processes in amine self-assembled monolayers on microarray slides as studied by ToF-SIMS with principal component analysis, XPS, and NEXAFS spectroscopy" *Anal. Bioanal. Chem.*, vol. 403, no. 2, pp. 613 – 623, 2012.

[197] J. F. Zhao, P. Lemoine, Z. H. Liu, J. P. Quinn and J. A. McLaughlin, "The effects of Si incorporation on the microstructure and nanomechanical properties of DLC thin films" *J. Phys.: Condens. Matter*, vol. 12, no. 44, pp. 9201 – 9213, 2000.

[198] A. S. Maria Chong and X. S. Zhao, "Functionalization of SBA-15 with APTES and characterization of functionalized materials" *J. Phys. Chem. B*, vol. 107, no. 46, pp. 12650 – 12657, 2003.

[199] L. M. Demers, C. A. Mirkin, R. C. Mucic, R. A. Reynolds, R. L. Letsinger, R. Elghanian and G. Viswanadham, "A fluorescence-based method for determining the surface coverage and hybridization efficiency of thiol-capped oligonucleotides bound to gold thin films and nanoparticles" *Anal. Chem.*, vol. 72, no. 22, pp. 5535 – 5541, 2000.

[200] D. M. Hinckley, J. P. Lequieu and J. J. de Pablo, "Coarse-grained modeling of DNA oligomer hybridization: length, sequence, and salt effects" *J. Chem. Phys.*, vol. 141, pp. 035102, 2014.

[201] M. Hagan and A. Chakraborty, "Hybridization dynamics of surface immobilized DNA" *J. Chem. Phys.*, vol. 120, no. 22, pp. 4958 – 4968, 2004.

[202] J. Hannestad et al., "Hybridization dynamics of surface immobilized DNA" *ACS Nano*, vol. 7, no. 1, pp. 308 – 315, 2013.

[203] M. Livshits and A. Mirzabekov, "Theoretical analysis of the kinetics of DNA hybridization with gel-immobilized oligonucleotides" *Biophys. J.*, vol. 71, no. 5, pp. 2795 – 2801, 1996.

[204] A. Vainrub and B. Pettitt, "Surface electrostatic effects in oligonucleotide microarrays: control and optimization of binding thermodynamics" *Biopolymers*, vol. 68, no. 2, pp. 265 – 270, 2003.

[205] A. Vainrub and B. Pettitt, "Coulomb blockage of hybridization in two-dimensional DNA arrays" *Phys. Rev. E*, vol. 66, no. 4, pp. 041905, 2002.

[206] A. Yildirim, E. Ozgur and M. Bayindir, "Impact of mesoporous silica nanoparticle surface functionality on hemolytic activity, thrombogenicity and non-specific protein adsorption" *J. Mater. Chem. B*, vol. 1, no. 14, pp. 1909 – 1920, 2003.

[207] K. A. Spoonhower and P. B. Davis, "Epidemiology of cystic fibrosis, thrombogenicity and non-specific protein adsorption" *Clin. Chest. Med.*, vol. 37, no. 1, pp. 1 – 8, 2016.

[208] P. Toren, E. Ozgur and M. Bayindir, "Real-time and selective detection of single nucleotide DNA mutations using surface engineered microtoroids" *Anal. Chem.*, vol. 87, no. 21, pp. 10920 – 10926, 2015.

[209] A. W. Peterson, R. J. Heaton and R. Georgiadis, "Kinetic control of hybridization in surface immobilized DNA monolayer films" *J. Am. Chem. Soc.*, vol. 122, no. 32, pp. 7837 – 7838, 2000.

[210] D. A. Armbruster and T. Pry, "Limit of blank, limit of detection and limit of quantitation" *Clin. Biochem. Rev. (Ultimo, Aust.)*, vol. 29, no. Suppl(I), pp. S49 – S52, 2008.

[211] A. Khan and C. Cerniglia, "Detection of Pseudomonas aeruginosa from clinical and environmental samples by amplification of the exotoxin A gene using PCR" *Appl. Environ. Microbiol.*, vol. 60, no. 10, pp. 3739 – 3745, 1994.

[212] D. E. Woods and B. H. Iglewski, "Toxins of *Pseudomonas aeruginosa*: new perspectives" *Rev. Infect. Dis.*, vol. 5, no. Suppl(4), pp. S715 – S722, 1983.

[213] T. Yahr, J. Goranson and D. Frank, "Exoenzyme S of *Pseudomonas aeruginosa* is secreted by a type III pathway" *Mol. Microbiol.*, vol. 22, no. 5, pp. 991 – 1003, 1996.

[214] J. Hwang, D. J. Fitzgerald, S. Adhya and I. Pastan, "Functional domains of Pseudomonas exotoxin identified by deletion analysis of the gene expressed in E. coli" *Cell*, vol. 48, no. 1, pp. 129 – 136, 1987.

[215] G. W. Counts et al., "Evaluation of an immunofluorescent-antibody test for rapid identification of Pseudomonas aeruginosa in blood cultures" *J. Clin. Microbiol.*, vol. 26, no. 6, pp. 1161 – 1165, 1988.

[216] S. Fujita, A. Tonohata, T. Matsuoka, N. Okado and T. Hashimoto, "Identification of Pseudomonas aeruginosa by using a disk of phenanthroline and 9-chloro-9-[4-(diethylamino)phenyl]-9,10-dihydro-10-phenylacridine hydrochloride and by cell agglutination testing with monoclonal antibodies" *J. Clin. Microbiol.*, vol. 30, no. 10, pp. 2728 – 2729, 1992.

[217] Y. Chen, N. Cheng, Y. Xu, K. Huang, Y. Luoa and W. Xu, "Point-of-care and visual detection of *P. aeruginosa* and its toxin genes by multiple LAMP and lateral flow nucleic acid biosensor" *Biosens. Bioelectron*, vol. 81, pp. 317 – 323, 2016.

[218] P. Toren, E. Ozgur and M. Bayindir, "Label-free optical biodetection of pathogen virulence factors in complex media using microtoroids with multifunctional surface functionality" *Anal. Chem.*, under revision, 2016.

[219] S. D. Dinesh, " Artificial Sputum Medium" *Protoc. exch.*, 2010.

[220] X. Wang, Y. Wang, H. Xu, H. Shan and J. Lub, "Dynamic adsorption of monoclonal antibody layers on hydrophilic silica surface: a combined study by spectroscopic ellipsometry and AFM" *J. Colloid Interface Sci.*, vol. 323, no. 1, pp. 18 – 25, 2008.

[221] A. Toscano and M. Santore, "Fibrinogen adsorption on three silica-based surfaces: conformation and kinetics" *Langmuir*, vol. 22, no. 6, pp. 2588 – 2597, 2006.

[222] A. M. Armani, A. Srinivasan and K. J. Vahala, "Soft lithographic fabrication of high Q polymer microcavity arrays" *Nano Lett.*, vol. 7, no. 6, pp. 1823 – 1826, 2007.

[223] J. M. Goddard and J. H. Hotchkiss, "Polymer surface modification for the attachment of bioactive compounds" *Prog. Polym. Sci.*, vol. 32, no. 7, pp. 698 – 725, 2007.

[224] T. Wienhold et al., "All-polymer photonic sensing platform based on whispering-gallery mode microgoblet lasers" *Lab Chip*, vol. 15, no. 18, pp. 3800 – 3806, 2015.

[225] A. Giannetti et al., "Optical micro-bubble resonators as promising biosensors" *Proc. SPIE*, vol. 9506, pp. 950617, 2015.

[226] S. I. Shopova, R. Rajmangal, S. Holler and S. Arnold, "Plasmonic enhancement of a whispering-gallery-mode biosensor for single nanoparticle detection" *Appl. Phys. Lett.*, vol. 98, no. 24, pp. 243104, 2011.

[227] H. Nakagawa, I. Saito, T. Chinzei, Y. Nakaoki and Y. Iwata, "The merits/demerits of biochemical reaction measurements by SPR reflectance signal at a fixed angle" *Sens. Actuators B*, vol. 108, no. 1-2, pp. 772 – 777, 2005.

[228] M. Noto, D. Keng, I. Teraoka and S. Arnold, "Detection of protein orientation on the silica microsphere surface using transverse electric/transverse magnetic whispering gallery modes" *Biophys. J.*, vol. 92, no. 12, pp. 4466 – 4472, 2007.

[229] J. Topolancik and F. Vollmer, "Photoinduced transformations in bacteriorhodopsin membrane monitored with optical microcavities" *Biophys. J.*, vol. 92, no. 6, pp. 2223 – 2229, 2007.

[230] M. F. Fraga and M. Esteller, "DNA methylation: a profile of methods and applications" *BioTechniques*, vol. 33, no. 3, pp. 632 – 649, 2002.

Appendix A

Abbreviations for the Elements, Chemical and Biochemical Compounds

A

A: Adenine.

ABCR: 11 - Azidoundecyl triethoxysilane.

3 - APS: 3 - Aminopropyl - trimethoxysilane.

APTES: 3 - Aminopropyltriethoxysilane.

Ar: Argon.

B

BSA: Bovine serum albumin.

C

C: Carbon atom.

$\mathcal{C}$: Cytosine.

CH_2: Methylene.

CH_3: Methyl.

CH_3O_3P: Methylphosphonate.

CO_2: Carbon dioxide.

Cr: Chromium.

D

DCC: N - $N9'$ - dicyclohexylcarbodiimide.

DMF: Dimethylformamide.

DNA: Deoxyribonucleic acid.

DTPA: Diethylenetriaminepentaacetic acid.

E

EDC: N - (3 - Dimethylaminopropyl)- N′ - ethylcarbodiimide hydrochloride.

F

FBS: Fetal bovine serum.

FITC - BSA: Albumin - Fluorescein isothiocyanate conjugate.

G

G: Guanine.

GAD: Glutaraldehyde.

GFP: Green fluorescent protein.

GPTMS: 3 - Glycidoxypropylmethyldiethoxysilane.

H

H: Element hydrogen.

He: Helium.

HF: Hydrogen fluoride.

HMDS: Hexamethyldisilazane.

H_2O: Water.

H_2O_2: Hydrogen peroxide.

H_2SO_4: Sulfuric acid.

HyNic: 3 - N - ((6 - N' - isopropylidene hydrazino) nicotinamide) propyl triethoxy silane.

I

IL - 2: Interleukin - 2.

K

KCl: Potassium chloride.

KH_2PO_4: Monopotassium phosphate.

M

MES: 2 - Ethanesulfonic acid.

N

N_2: Nitrogen.

NaCl: Sodium chloride.

NaOH: Sodium hydroxide.

Ne: Neon.

NH_2: Amino.

NH_4F: Ammonium fluoride.

NHS: N - Hydroxysuccinimide.

O

O: Element oxygen.

O_2: Oxygen.

O_3: Ozone.

OH: Hydroxl.

P

P: Phosphorous element.

PBS: Phosphate buffered saline.

R

RNA: Ribonucleic acid.

S

SF_6: Isotropic sulfur hexafluoride.

S - 4FB: *N* - Succinimidyl - 4 - formylbenzamide.

S - HyNic: Succinimidyl 5 - hydrazinonicotinate acetone hydrazone.

Si: Silicon.

SiO_2: Silicon dioxide.

SPDP: Succinimidyl 3 - (2 - pyridyldithio) propionate.

T

T: Thymine.

THPMP: 3 - (Trihydroxysilyl) propyl methylphosphonate.

TMMS: Trimethylmethoxysilane.

Tris: Tris (hydroxymethyl) aminomethane.

Tris - HCl: Tris (hydroxymethyl) aminomethane hydrochloride.

Z

ZnSe: Zinc selenide.

Appendix B

Tables

Table B.1: The XPS data of the bare and THPMP coated SiO_2 surfaces.

	Peak binding energy (eV)	Peak fit FWHM (eV)	Atomic (%)
Bare silica			
P2p	-	-	0
Si2p	103.6	1.5	32.5
O1s	532.9	1.4	55.5
High C1s	284.8	1.5	11.1
Low C1s	286.5	1.3	0.9
THPMP coated silica			
P2p	133.2	2.0	2.8
High Si2p	103.6	1.6	24.8
Low Si2p	102.1	1.4	1.3
High O1s	532.9	1.4	47.0
Low O1s	531.1	1.5	4.1
High C1s	284.8	1.5	14.1
Low C1s	286.5	1.2	2.8
Na1s	1071.5	-	3.1

Table B.2: Ellipsometry data. NS_{1-3} : Non - specific adsorptions of BSAs onto Piranha cleaned SiO_2 surface. T_{1-3} : THPMP coated SiO_2 surface. TB_{1-3} : Non - specific adsorptions of BSAs onto THPMP coated SiO_2 surface.

	Thickness (nm)	Standard deviation	Mean - square - error	Average thickness (nm)	Protein adsorption (ng / cm^2)
NS_1	1.89	0.10	1.54		
NS_2	1.86	0.10	1.57	1.84 ± 0.07	242.30 ± 8.77
NS_3	1.76	0.09	1.73		
T_1	0.65	0.11	1.61		
T_2	0.64	0.09	1.41	0.65 ± 0.02	-
T_3	0.67	0.09	1.69		
TB_1	0.40	0.09	1.57		
TB_2	0.39	0.09	1.66	0.36 ± 0.07	47.50 ± 9.94
TB_3	0.28	0.15	2.34		